Influence of hygroscopic interior finishing on indoor comfort conditions

Amos Ronzino

POLITECNICO DI TORINO

A thesis presented in fulfilment of the requirements
for the Degree of Doctor of Philosophy
in Technological Innovation for the Built Environment

Supervisor: prof. Vincenzo Corrado

Department of Energy

May, 2014

Contents

iii

List of Figures

v

List of Tables

Nomenclature

Variables

A	surface area	[m^2]
b_m	moisture effusivity	[kg/(Pa m^2 s^{0,5})]
c_p	specific heat capacity	[J/(kg K)]
C_m	volumetric moisture capacity of room air	[kg/(Pa)]
C_r	imperfect mixing reduction coefficient	[-]
D	diameter	[m]
D_φ	liquid conduction coefficient	[kg/(m s)]
g	moisture uptake/release	[kg/m^2]
$\dot{g}$	density of moisture flux	[kg/(m^2 s)]
$\dot{g}_a$	density of air flux	[kg/(m^2 s)]
$\dot{g}_l$	density of liquid water flux	[kg/(m^2 s)]
$\dot{g}_v$	density of water vapour flux	[kg/(m^2 s)]
$\dot{G}$	moisture flux	[kg/s]
$\dot{G}_a$	air flux	[kg/s]
$\dot{G}_{diff}$	moisture flux to building components	[kg/s]
$\dot{G}_{vent}$	moisture flux through ventilation system	[kg/s]
$\dot{G}_{gen}$	moisture flux generation	[kg/s]
H	volumetric heat capacity	[J/(m^3 K)]
h	Fourier's harmonic function coefficient	[-]
h_m	convective mass transfer coefficient	[m/s]
h_c	convective heat transfer coefficient	[W/(m^2 K)]
h_v	evaporation enthalpy of water	[J/kg]

L	characteristic length	[m]
m	mass	[kg]
M	vapour permeance	[kg/(Pa m^2 s)]
p_a	air pressure	[Pa]
p_c	suction pressure	[Pa]
p_v	vapour pressure	[Pa]
$p_{v,s}$	vapour pressure at saturation	[Pa]
r	radius	[m]
R	thermal resistance	[(m^2 K)/W]
R_l	liquid water resistance	[(Pa m^2 s)/kg]
RH	relative humidity	[%]
s_d	equivalent air layer thickness	[m]
t	time	[s]
T	absolute temperature	[K]
u	moisture content by mass	[kg/kg]
v	velocity	[m/s]
$\dot{v}$	density of volumetric air flow rate	[m^3/(m^2 s)]
V	volume	[m^3]
$\dot{V}$	volumetric air flow rate	[m^3/s]
w	moisture content by volume	[kg/(m^3]
w_{cr}	critical moisture content	[kg/(m^3]
x	thickness	[m]
x_a	moisture content in air	[kg$_v$/kg$_a$]
Z_p	vapour resistance	[(Pa m^2 s)/kg]

Variables in Greek letters

α	fraction of time period	[-]
β	surface moisture trasnfer coefficient	[kg/(Pa m^2 s)]
δ_p	vapour permeability	[kg/(Pa m s)]
η	dynamic viscosity	[kg/(m s)]
θ	temperature	[°C]

λ	thermal conductivity	[W/(m K)]
λ_l	liquid conductivity	[s]
ρ_0	density of dry material	[kg/m^3)]
σ	surface tension of water	[N/m]
τ	moisture generation period	[h]
υ	kinematic viscosity	[m^2/s]
φ	relative humidity	[-]
ω	angular frequency of the cyclic load	[s^{0,5}]

Constants

$c_{p,a}$	specific heat capacity of dry air	1005 [J/(kg K)]
$c_{p,w}$	specific heat capacity of dry air	4186 [J/(kg K)]
e	Nepero's constant	2,718 [-]
g_n	standard gravity	9,78 [m/s^2]
Le	Lewis number	0,84 [-]
M_w	molecular weight of water	4,96$\cdot$10^{-50} [kg/mol]
P	standard barometric pressure	101325 [Pa]
R	universal gas constant	8,314 [J/(mol K)]
R_v	gas constant of water vapour	461,5 [J/(kg K)]
δ_a	vapour permeability of stagnant air	193$\cdot$10^{12} [kg/(Pa m s)]
ρ_a	density of dry air	1,205 [kg/m^3]
ρ_w	density of water	0,998 [kg/m^3]
π	Archimede's constant	3,142 [-]

Abbreviations

EMC	Equilibrium Moisture Content
HIR	Hygric Inertia of the Room

MBC	Moisture Buffer Capacity
MBV	Moisture Vuffer Value
TMT	Transient Moisture Transfer

Subscripts

ab	absorbed
de	desorbed
$diff$	diffusion
ext	external
gen	generated
i, j, k	node or surface index
int	internal
p	period
ref	reference value
$surf$	surface
sys	system
$vent$	ventilation

Extended abstract

Indoor humidity level is important for building performance and occupants. The durability of building components is directly related to the humidity condition and materials inside buildings can get damaged if they are persistently under high levels of moisture concentration. The indoor humidity level is related to the room factors including moisture gains and ventilation conditions and to the moisture ab/desorption capacity of hygroscopic materials for interior finishing or furnishing of the building.

The phenomenon of the indoor humidity level being dampened by the dynamic moisture interactive process between hygroscopic materials and indoor air is recognized as moisture buffering effect. The buffering effect and the moisture ab/desorption performance of hygroscopic materials under different room factors were studied in this thesis by means of numerical simulation. The transient state indoor environment influenced by room factors, taking into account the moisture interactive process between indoor air and enclosure, was investigated numerically in this thesis. The CFD technique was employed in the numerical investigation.

A literature review on the experimental and numerical investigations on moisture buffering and whole building indoor environment was carried out. This review showed that the moisture buffering effect of hygroscopic materials had been extensively studied at the material level, i.e. the characterization of the buffering property of materials. However, the hygroscopic properties of materials may not be representative of the buffering performance of the material at the room level because the indoor hygrothermal condition, room factors, and moisture buffering of hygroscopic materials influence each other.

The literature review also found that a CFD model in a single simulation

environment to study the HAM transport including the moisture interaction between the indoor air and the envelope is needed, but yet to be developed. Using this kind of CFD model, detailed information of the moisture transport in a building and inside its envelope could be obtained, and the indoor humidity level influenced by the room factors could be predicted by the simulation of the involved HAM transport processes.

In this thesis the following issues have been presented:

- the fundamental theories of the hygroscopic material properties, the governing equations describing HAM transport in the convection and diffusion processes and the analogy between mass and heat transfer

- the experimental measurement of hygroscopic properties of porous building material under transient conditions;

- the study of the moisture buffering effect at the room level through the numerical simulation of the HAM transport in the whole room and its enclosure;

- the coupling between CFD-HAM models in a single simulation environment to study the HAM transport, including the moisture interaction between the indoor air and the envelope.

To further study the buffering effect under different room factors, the buffering effect was evaluated by the indoor humidity level change with respect to a room factor variation. The study found that without the presence of the hygroscopic material (non-hygroscopic test) the average indoor relative humidity value increased by 11 % at the ventilation rate of 0.3 h^{-1} when the room factor of moisture generation rate is set at 80 g/h, with respect to the scenario with hygroscopic finishing (gypsum plaster).

These cases studied the influence of moisture loads, ventilation rates, and ventilation vents design on the indoor environmental changes and on the HAM-transport through the building component.

The fully coupled CFD model to simulate HAM transports in the simulation domains of test room and wall was established. This model was

built in COMSOL Multi-physics, a PDE basis simulation environment. The governing equations of the HAM-transport were coupled according to recent studies (Nusser and Teibinger, 2012). The coupling process of heat/moisture between the indoor air and gypsum plaster finishing were established by defining the CFD solution for indoor air.

The moisture buffering performance of gypsum plaster and wood fibre under dynamic conditions has been evaluated experimentally and compared to the steady-state measurements usually carried out according to the standards UNI EN ISO 12571 (2013) and UNI EN ISO 12572 (2006). The influence of uncertainty of measured data on the whole room numerical simulation was studied.

The nature of buffering effect caused by hygroscopic material under different room conditions has been explained and its values at room level have been obtained. The relationship of indoor environment, buffering effect, room factors has been elaborated through simulated data.

A CFD coupling model has been developed in a single simulation environment to overcome the limitations in existing coupling models. This new model can have application potential such as prediction of indoor environment hygroscopic conditions and evaluation of ventilation design.

Chapter 1

Introduction

1.1 Background

Moisture level inside buildings is a key factor influencing the durability of construction, indoor air quality, thermal comfort and energy consumption. Studies have shown that when relative humidity at surface reaches 70% or higher, the problems with mold, corrosion, decay and other moisture related deterioration occur (Lstiburek, 2002).

Water and moisture can cause structural damage, reduce the thermal resistance of building materials, change their physical properties and deform them (Kalamees et al., 2006). On the other hand, low humidity levels can cause static electricity, dry skin and hair, itching and chapping, increasing human discomfort and susceptibility to cold and respiratory illness. Keeping an appropriate room humidity level is important in maintaining a healthy indoor environment for both human comfort and building durability.

The indoor humidity level is the result of the dynamic moisture balance among the moisture gains, losses and storage inside buildings. There are many large and comprehensive projects at national and international level studying the moisture transport and its balance, both experimentally and numerically. Some of them, related to this thesis research, are briefly introduced.

Moisture Management for Exterior Wall Systems (MEWS) was a four-

year project that brought together researchers from IRC's Building Envelope and Structural Program and 11 industry partners. The MEWS methodology offered a way for stakeholders in the building envelope industry to evaluate the ability of building components and systems to manage moisture in any geographic location in North America. The research approach was three-fold: field characterization of wall assemblies, laboratory experimentation in materials and components, and numerical modeling for prediction if long-term performance under many sets of conditions (Kumaran et al., 2003). The hygrothermal properties of several building materials commonly used in North America were obtained by the project lab tests.

In the 1990s, moisture damages to the building envelope occurred in several dramatic envelope failure cases in the North America. In order to provide proper design guidelines to avoid these problems, the Collaborative Research and Development (CRD) project on the experimental evaluation of hygrothermal performance of building envelope systems was carried out at Concordia between 2003 and 2008 (Fazio et al., 2006; Alturkistani et al., 2008; Li et al., 2009). This research provided a uniform, measurable moisture source in the test, and its mapping methodology established the DEI (*Drying by Evaporation Index*) by identifying the correlation between the evaporation rate and the amount of moisture leaving the cavity. And advanced simulation tool, HAM-BE, was developed to investigate the hygrothermal performance of building envelopes tested in this experiment. This project established a new testing method for evaluating and ranking the performance of different envelope systems (Fazio et al., 2009).

In 2001, the European Commission initiated the project "HAMSTAD" (*Heat Air and Moisture Standard Development*) to focus in the development of draft standardization procedures in determination methods of moisture transfer properties and a draft methodology for certification of advanced moisture modeling codes (Adan et al., 2004). HAMSTAD included some of the comprehensive projects for developing numerical simulation of heat, air and moisture (HAM) transport in building envelopes. Some simulation tools such as DELPHIN, HAM-Tools and TRNSYS ITT were developed. Some of the partners who carried out this project later participated in the Annex 41

tasks of modeling and common exercises.

As moisture studies moved from components to whole building consideration, a better knowledge of the whole building HAM balance and its effect on the indoor environment, energy consumption for heating and cooling, air (de)humidification and construction durability was needed. This research for a better understanding of the HAM balance was the driving force behind the Annex 41 program of the International Energy Agency (IEA) from 2004 to 2008.

Annex 41 had two main objectives: 1) to carry out a detailed exploration of the complex physics involved in whole building HAM response; 2) to perform analyses on the effect of the whole building HAM response on the comfort, enclosures durability and energy consumption (Roels, 2008). In the research program of Annex 41, whole building HAM research methodologies in the modeling principles, experimental investigations, long term performance and technology transfer were proposed and developed.

1.2 Influence of hygroscopic materials on indoor comfort

The indoor environment is influenced by several factors, such as moisture and heat sources, ventilation conditions, and the existence of hygrothermal materials. In Annex 41, one important concept about the influence of the materials is the moisture buffer effect.

The moisture buffer effect of a room is the capacity of the materials within the room to moderate variations in the relative humidity (Rode et al., 2005). On one hand, moisture buffering provides a passive way to dampen the fluctuations of indoor humidity and temperature, which may be utilized as a way of adjusting indoor conditions and saving energy; on the other hand, the buffering phenomenon is a dynamic process of moisture absorbed/desorbed by the envelope materials between indoor and outdoor environment. This transport involves complex heat, air and moisture responses. The study of moisture buffering helps to understand the complex mechanisms involved in the durability of the building envelope and to provide solutions to failures.

Svennberg et al. (2007) stated that he interest in moisture buffering was not a new issue and they presented a review of such early studies on indoor surface materials from Germany and Sweden. However, it was Annex 41 that first systemically summarized and studied this phenomenon.

Rode et al. (2005) described the moisture buffer effects at the material, system and room levels. The material level was related to the traditional moisture properties, i.e. the slope of the sorption isotherm. The system level was about the *moisture buffering capacity*. The practical Moisture Buffer Value (MBV) was proposed to determine the buffer capacity of the material. This value was mainly, but not only, a property of the material, because the mass transfer coefficient at the boundary had to be considered. The MBV of several materials samples was measured by Round Robin tests conducted by four universities and research institutes that participated in Annex 41. Agreements in MBVs of some materials were obtained. The room level included the buffering effect caused by the building and furnishing materials

exposed to the indoor air and the room factors such as moisture load, ventilation rate and indoor climate.

A number of whole-building HAM tools were evaluated and benchmarked during Annex 41. BSim, Clim2000, DELPHIN4, Energy Plus, ESP-r, HAM-Lab, TRANSYS and WUFI Plus were well known software for the analysis of indoor climate, energy consumption, humidity balance and/or moisture airborne transport, condensation and evaporation. Even though some of these existing tools included vapor advection in the air, they did not take into account the vapor mass transfer at the interface between air and building envelope (Woloszyn and Rode, 2008b).

To obtain detailed information of air flows in buildings and hygrothermal transport through building components, CFD has been combined with the HAM response simulation. Erriguible et al. (2006) modeled 2D convective drying of a porous material with the air flow at the material boundary calculated by a CFD model. Neale (2007) developed a coupled numerical model using CFD simulation in Fluent to determine the heat and moisture transfer coefficients between air and porous materials for the HAM simulation in MatLab. Steeman et al. (2009) coupled CFD and effective penetration depth (EPD) model to investigate the effect of the assumption of the well-mixed air on the prediction of indoor temperature and relative humidity and on the hygrothermal behavior of the walls.

Anyway, the coupling between two different simulation environment is very time-consuming and still represents a target to reach.

1.3   Objectives of the research

The indoor environment study is the fundamental of "whole building" research for the purpose of establishing sustainable buildings and communities. The increasing climate change concern requires building engineers to find ways to reduce energy consumption and green house gas emissions associated with the use of active HVAC systems while keeping appropriate indoor conditions.

Among the material tested experimentally the research focuses on the influence of gypsum plaster on hygrothermal environmental conditions. In particular the plaster under investigation is a product Gyproc Saint-Gobain, company financing the PhD grant.

The moisture buffering effects of interior finishing materials in building envelopes have been recognized as a passive way to assist in moderating indoor conditions. In many residential buildings, where only the natural ventilation is available, moisture buffering is an important factor in affecting indoor comfort change. In order to predict and utilize the moisture buffering effect, hygroscopic performance of porous materials within buildings at room level must be known.

The material's buffering properties at material level have been measured and calculated in experimental studies. However, apart from the lack of good benchmark cases also performing a reliable fitting of material properties remains difficult; although experimental data are available from literature, only carefully planned measurements are best suited for HAM models validation. Moreover there's not enough information and testing standards for evaluating the material buffering performance at room level.

Meanwhile, the hygroscopic properties may not be directly representative of the material buffering performance at room level because the (de)sorption process is influenced by room factors such as ventilation conditions, indoor humidity and temperature profiles and environmental initial conditions.

To predict reliably the buffering performance through numerical models, the real link between material level and room level must be found taking into account even those aspects or habits such as coating the finishing materials. In the aspect of simulation, numerical studies have advanced the state of the art in whole building heat, air and moisture response. CFD has the advantage to investigate indoor air movements, the local information of the temperature and moisture distribution. But currently, the HAM simulation of CFD taking into account the moisture interaction between indoor air and envelope is achieved through the third party programming. This may limit the application of CFD modeling due to the simulation conditions.

To simulate the indoor environment change under given moisture loads and to explain how the air movement caused by buoyancy forces and ventilation influences indoor temperature and humidity levels, a CFD modeling able to couple the momentum, heat and moisture in whole building domain, including indoor air and wall systems, is highly desirable.

The aim of this thesis is obtaining a better understanding of the nature of moisture buffering at room level, in order to predict in a better way how this effect affects the indoor comfort, and how to maximally use it in certain design conditions. The research also focuses on the influence of different ventilation strategies on the indoor environment. The main objectives are:

- **Analysis of reliability of measured data and their influence on numerical simulation**. The reliability of measured material properties, such as vapour permeability and sorption isotherm, is analyzed by means of statistical analysis for tested products. The correlation between measured and simulated data is carried out, focussing on uncertainty of measuring data, and on its influence on simulation results through a sensitivity analysis. The hysteresis influence on the hygroscopic performance of buffer materials is evaluated;

- **Influence of boundary conditions on the hygroscopic behaviour of finishing materials**. Aim of this part is to find out the main factors dominating the heat and moisture fluxes in the wall system through the numerical investigation. The coatings influence on material properties is investigated and the Moisture Buffer Value (MBV) for finishing products is evaluated and compared to results from literature. A special attention is given to the ventilation topic. Results from the lumped HAM model are compared to those from CFD: the effect of the air velocity distribution on the hygrothermal performance of finishing materials at room level is studied;

- **Implementation and calibration of a lumped numerical model**. Involves the identification of dead zones not involved in the moisture

buffering process and enhancement of a correction factor for the Hygric Inertia Index $I_{h,d}$ (Ramos et al., 2012) for relative humidity level classification in building design. This part considers: 1) different ventilation rates and air velocity distributions; 2) different vents position for mechanical ventilation systems.

A combination of experimental measurements, calculations and numerical simulations are utilized as an approach to accomplish the above goals set for this thesis.

The experimental investigation on the hygroscopic properties of the tested materials was carried out at the *Technische Universität* of Wien by taking advantage of a special climate chamber especially built for this purpose, of the data acquisition system, installed sensors and their calibration for the measuring device. A second climate chamber was built afterwards in order to measure the properties of two specimens during the same transient conditions, and compare the results.

To study the influence of moisture loads and different ventilation strategies on indoor environment with the heat and moisture interaction between indoor air and the considered finishing material, the numerical coupling between the indoor conditions obtained by CFD calculations and HAM transport inside porous media described by diffusion equations was used. In this thesis, the conservation equations of momentum, heat and mass were described in a single simulation environment (COMSOL) and transient conditions were considered in the numerical simulation.

Chapter 2

Literature review

This chapter presents a literature review of current studies on the moisture buffering phenomenon and HAM transport in buildings. The existing efforts in defining and describing the buffering effects are reviewed. The overall review about impacts of moisture buffering on the indoor environment, energy consumption as well as its calculation by numerical simulation in whole building follows.

2.1 Definition and measuring of the moisture buffering

2.1.1 The *Moisture Buffer Value*

The hygroscopic materials used in building enclosures are able to dampen the peaks of humidity levels in indoor environments when rooms are subjected to moisture load changes. This phenomenon has been investigated in some earlier studies and has been recognized as the moisture buffering effect (Padfield, 1999; Karagiozis and Salonvaara, 2001; Rode et al., 2002, 2003, 2004; Salonvaara et al., 2004).

The traditional material properties such as moisture capacity, vapor permeability, density and moisture sorption isotherm, which are measured in the steady state conditions, can be used to describe this phenomenon.

In the NORDTEST Project (Rode et al., 2005), the concept called Moisture Buffer Value (MBV) and its theory were developed. Based on the heat/moisture transfer analogy, the moisture flux $\dot{g}$ [kg/(m²s)] on the surface of a hygroscopic material under rectangular signal loads (e.g. 8 hours of high moisture load, followed by 16 hours of low load) can be calculated by the Fourier transform method. The accumulated moisture uptake and moisture release $g(t)$ [kg/m²] is expressed as:

$$g(t) = \int_0^t \dot{g} \cdot dt = b_m \cdot \Delta p_v \cdot h(\alpha) \cdot \sqrt{\frac{t_p}{\pi}} \tag{2.1}$$

where b_m [kg/(m²s$^{1/2}$Pa)] is the moisture effusivity, Δp_v [Pa] is the vapor pressure difference, t_p [s] is the time period and the harmonic function coefficient $h(\alpha)$ depends on the moisture load scheme and is expressed as:

$$h(\alpha) = \frac{2}{\pi} \sum_{n=1}^{\infty} \frac{sin(n \cdot \alpha \cdot \pi)}{n^{3/2}} \approx 2,252 \cdot [\alpha(1-\alpha)]^{0,535} \tag{2.2}$$

For the 8-16 hours scheme, $\alpha = 1/3$ and $h(\alpha) = 1,007$. The accumulated moisture uptake is then reduced to:

$$g(t) \approx 0,568 \cdot b_m \cdot \Delta p_v \cdot \sqrt{t_p} \tag{2.3}$$

The Ideal Moisture Buffer Value (MBV$_\text{ideal}$) is defined as the moisture exchange $g(t)$ normalized by the change in the surface relative humidity ΔRH:

$$MBV_{ideal} \approx \frac{g(t))}{\Delta RH} = 0,00568 \cdot b_m \cdot \Delta p_v \cdot \sqrt{t_p} \tag{2.4}$$

To measure the MBV of hygroscopic materials, the concept of the Practical MBV, as well as the experimental measurements condition and set up, is proposed in the project and later is standardized as (Rode and Grau, 2008):

> *The standardized Moisture Buffer Value (MBV) indicates the amount of water that is transported in or out of a material per open surface area, during a prescribed period of time, when is subjected to specific variations in relative humidity of the surrounding air with a specified velocity. When the moisture exchange during the period is reported per open surface area and per %RH variation, the result is the MBV. Standardized exposure is 8 h of 75% RH, and 16 h of 33% RH. The unit for MBV is [kg/(m² %RH)].*

The *Ideal MBV* is derived from material hygroscopic properties and belongs to the material level definition as stated in Section 1.2, while the *Practical MBV* measured from experiments includes the effect of the vapor resistance of the surface air film and is a system level definition. The surface resistance is assumed as zero in the MBV_{ideal} calculation formula. With this assumption, the calculated MBVs of some materials are about three times higher than the measured values presented in the NORDTEST Project report (Abadie and Mendonça, 2009).

2.1.2 The moisture transfer coefficient

A key factor in evaluating the moisture buffer capacity of a hygroscopic material is the amount of water it can absorb and release in the different load conditions. This amount of water is significantly affected by the surface transfer coefficient, although this term is usually neglected in academic studies on vapour diffusion. The theory of mass transfer coefficient is analogized to heat transfer as:

$$h_m = \frac{h_c}{\rho_a \cdot c_{p,a} \cdot Le^{2/3}} \tag{2.5}$$

where h_m [m/s] is the convective mass transfer coefficient, h_c [W/(m²K)] the convective heat transfer coefficient, ρ_a [kg/m³] the air density, $c_{p,a}$ [J/(kg K)] is the specific heat capacity, Le [-] is the Lewis number. This equation, relating convective heat and mass transfer, is the well-known Chilton-Colburn analogy. The analogy itself has been the subject of many research projects that proved or disproved the accuracy of the results for a variety of conditions (Neale, 2007) as, for example, when radiation and heat or moisture sources are included.

Rode et al. (2005) summarized the convective moisture transfer coefficient β_{int} [kg/(Pa m²s)] and the surface resistance $Z_{p,surf}$ [(Pa m²s)/ kg], by using the Lewis relation and choosing exponent 3/4 recommended for interior surfaces in building as:

$$Z_{p,surf} = \frac{1}{\beta_{int}} = \frac{\rho_a \cdot c_{p,a} \cdot R_v \cdot T}{h_c} \cdot Le^{3/4} \qquad (2.6)$$

where ρ_a [kg/m³] is the air density at 20 °C, $c_{p,a}$ [J/(kg K)] the specific heat capacity of air at constant pressure, R_v [J/(kg K)] the gas constant for water vapor, T [K] the temperature, Le [-] the Lewis number. The general moisture transfer resistance in a building can be assumed to be $Z_{p,surf} = 5 \cdot 10^7$ (m² s Pa)/kg.

Osanyintola and Simonson (2006) used the Transient Moisture Trasnfer (TMT) facility to measure the moisture buffering performance of spruce plywood under three different Reynolds numbers: $Re = 1000$ - 2000 - 4000, which correspond to the convective heat transfer coefficients $h_c = 2,5$ - 3,5 - 8,1 W/(m² K) respectively and to the convective mass transfer coefficients $h_m = 0,0021$ - 0,0029 - 0,0067 m/s respectively.

Simonson et al. (2005) performed a numerical simulation to study the influence of the surface film resistance on MBVs of four hygroscopic materials. The simulation results are presented in Table 2.1. Different materials had different MBV changes for a change surface resistance, and a sudden drop of MBV was observed for wood fiber board when increasing the surface film resistance from $1 \cdot 10^7$ to $3,3 \cdot 10^8$ (m^2 s Pa)/kg.

Table 2.1: Influence of the surface film resistance on the obtained MBV [g/(m^2 %RH)] for the four material investigated (WFB = wood fiber board, PW = plywood, ACC = aerated cellular concrete, GP = gypsum plaster).

Surface Resistance x 10^7 [(m^{2}s Pa)/kg]	WFB	PW	ACC	GP
33	0,55	0,47	0,56	0,61
10	1,55	0,64	0,75	0,86
5	1,86	0,69	0,82	0,94
3,3	1,99	0,71	0,83	0,97
1	2,20	0,74	0,86	1,01
Negligible (0,0033)	2,31	0,76	0,89	1,03

A study of local surface water vapor transfer coefficient in a ventilated test room based on a coupled CFD-EPD model was performed by Steeman et al. (2009). Since the commercially available CFD packages do not allow to simulate the coupled heat and moisture transport in porous media, the Effective Penetration Depth (EPD) model to simulate the hygrothermal behavior of the wall was combined into the CFD package. To couple the CFD and the EPD models, the water vapor mass fraction at the surface of the wall for a given time step was obtained from the previous step results of the EPD model; then the water vapor flux from the air to the wall at this time step was calculated by the CFD model and input into EPD to generate the next step's mass fraction value on the wall surface. The coupled CFD-EPD model was first validated by a non-hygroscopic wall configuration test with 8 hours moisture load from the inlet, and then applied to the hygroscopic wall configuration.

The local surface moisture transfer coefficient β_{local} and the average moisture transfer coefficient $\bar{\beta}$ in Steeman et al. (2009) were defined as:

$$\beta_{local} = \frac{\dot{g}}{p_{v,surf} - p_{p,ref}} \tag{2.7}$$

$$\bar{\beta} = \frac{\bar{g}}{\bar{p}_{v,surf} - \bar{p}_{v,int}} = \frac{\frac{1}{A} \int \dot{g} dA}{\frac{1}{A} \int p_{v,surf} dA - \bar{p}_{v,int}} \tag{2.8}$$

where $p_{v,ref}$ is the reference water vapor pressure - also called free stream water vapor pressure - and is defined as the average indoor vapor pressure inside the considered air volume V [m^3]:

$$p_{v,ref} = \bar{p}_{v,int} = \frac{\int p_{v,int} dV}{V} \tag{2.9}$$

The simulation results of Steeman et al. (2009) showed that the local surface moisture transfer coefficient was not constant over the surface area and varied between $0,8 \cdot 10^{-8} < \beta_{local} < 3,0 \cdot 10^{-8}$ s/m in the first hour of the moisture generation and decreased to $1,8 \cdot 10^{-8}$ s/m after 8 hours. Anyway, the average surface moisture transfer coefficient remains constant during the whole period of testing.

2.1.3 Other moisture buffering measurements

Another notable standard for characterizing building materials with respect to the moisture buffering is the Test method of ad/desorption performance of building materials to regulate indoor humidity, the Japanese Industrial Standard JIS A 1470-1:2002. With the similar objectives and measurement principles as the NORDTEST protocol, this test standard used a square wave signal with 24 h high RH followed by 24 h with low RH. Three humidity levels, 33 to 53%, 53 to 75% and 75 to 93%, were chosen as the load signal.

The specimen thickness was equal to the product thickness. The surface film resistance was set to $4, 8 \cdot 10^7 \pm 0, 1$ (m² s Pa)/kg. The test results were reported as moisture masses absorbed and released by the test materials as well as the moisture content profiles with respect to time.

Wu et al. (2008) measured the moisture buffering capacities of five building materials commonly used in North America: gypsum board, plywood, OSB (Oriented Strand Board), fiberboard and stucco. The test conditions were the same as the NORDTEST ones: 8 hours at 75% RH and 16 hours at 33% RH, with a constant temperature of 23 °C. The MBV values were calculated, the absorption and desorption curves were plotted and the fitting equations were calculated for the tested materials.

Highly absorbing materials, such as sodium polyacrylate and cellulose-based materials, are super-absorbent polymers and combination of cellulose and super-absorbent polymers respectively and are used in several industrial sectors ranging from personal hygiene to medical field. The moisture buffering capacities of these materials were investigated by Cerolini et al. (2009). In their test the materials were wound in a nonwoven fabric and then placed in a non absorbing plastic container to facilitate the weighing procedure. The container was covered with a perforated metal sheet to simulate the presence of a surface closure and sealed with aluminum adhesive tape. The same moisture load scheme as NORDTEST project was applied.

Comparing the moisture buffering results of gypsum to perlite materials, this study found out that the super absorbent polymer reacted more quickly than the other materials to RH changes in both the absorption and desorption phases. However polyacrylate showed a hysteretic behavior that may cause the loss of its sorption properties. Therefore the cellulose-based material seemed to be the most suitable for moisture buffer applications.

Svennberg et al. (2004) studied the moisture buffering of furniture in the indoor environment. In one project, two bed systems, one of a homogenous mattress and the other of a multilayer type, were tested in a Swedish house subjected to diurnal temperature and RH variations. The systems were

15

mathematically analyzed and the noticeable differences of microclimatic conditions in the two systems had been observed. The moisture uptake in a chair seat as a response to daily RH variations was studied in another project. The comparison between chair measurements and analytical solution showed that the latter provided a good representation of the moisture uptake. An addition of internal resistance in the analytical solution and using truer boundary conditions would further improve the agreement.

There were also some large scale experimental studies on the moisture buffering. However, these studies were mostly focusing on the moisture buffering impact on indoor room conditions instead of on its measurement. This subject, as well as the influence of the moisture buffering on energy consumption are reviewed in the next section.

2.2 Moisture buffering in the whole building

The moisture buffering phenomenon, as stated in Chapter 1 and reviewed in the previous section, is a dynamic process that the hygroscopic materials inside buildings dampen the peaks of indoor humidity levels. One goal of studying the moisture buffering is to predict how to use it to control the indoor environment and to achieve energy saving. In this section, the existing studies on the impact of moisture buffering on indoor environments and energy consumption are reviewed, and the current numerical simulation for the whole building moisture response studies are also presented.

2.2.1 The moisture buffering effect on indoor environment

Indoor humidity is an important factor in keeping human body in a healthy condition. Toftum et al. (1998) studied the influence of the indoor humidity level on the human skin humidity and respiratory comfort. Fang et al. (1998) investigated the indoor air quality related to the humidity conditions, while

Bornehag et al. (2004) found that the appropriate indoor humidity could prevent mould growth and reduce health risks due to sick building syndromes such as asthma, allergic symptoms and airway infections.

Several large-scale, lab and field experiments on moisture buffering effects have been performed by several authors (Simonson et al., 2004; Ojanen and Salonvaara, 2004; Satio, 2005; Svennberg et al., 2007; Holm and Lengsfeld, 2007; Yang et al., 2007, 2009; Yang, 2010; Yang et al., 2012). Different hygrothermal materials including plywood, coated and uncoated gypsum board, cellular concrete, unpainted wood, as well as the furnished room with desk, table, books, chair and carpet were used as moisture buffering objects to dampen the indoor environment variations of temperature and relative humidity, especially for the latter changes. Different moisture load schemes ranging from simple square wave at constant generation rates at different time periods had been used in these experiments. The studies found that the buffering effects of the hygroscopic materials depended on many factors, including the type and area of the buffering objects exposed to the moisture, the ventilation rate, the moisture generation rate and the outdoor climate conditions.

A method of comparative testing with the ceiling, floor and walls of a testing house located in Helsinki, covered by plastic sheets in one case and not covered in the other, was adopted by Simonson et al. (2004). the indoor humidity ratios as a function of time for different ventilation rates, with and without a plastic vapor retarder, were measured. A reduction of the moisture buffering effect as the ventilation rate increased was observed.

The fact that moisture buffering effects have significant impacts on indoor environment, especially on the humidity change, has been recognized and verified. Being a passive way to save energy consumption is one of its applications. Atthajariyakul and Leephakpreeda (2004) proposed a systematic approach to determine the optimal indoor-air condition by simultaneously setting the time-dependent variables to appropriate reference values for real-time control implementation of the HVAC system. This HVAC control methodology used RH as one of the control parameters and the results

17

showed that the buildings with this control strategy consumed less energy than the traditional approach while providing desired thermal comfort and air quality.

Barbosa and Mendes (2008) combined heat, vapor and liquid transfer in porous media and the HVAC systems, building and integrated model for both the conditioning system and the multi-zone building hygrothermal simulation. The simulation results showed that the monthly peak load could be 13% lower when moisture was taken into account, as compared with the situation disregarding the presence of moisture. Therefore, they concluded that when moisture within the construction was neglected, HVAC systems might be oversized.

Osanyintola and Simonson (2006) studied the effect of hygroscopic materials on energy consumption in buildings by dividing the potential energy savings into direct, which means the energy required for the heating and cooling of a building, and indirect, which means the possible savings due to a lower ventilation rate, a higher indoor temperature during wintertime and lower during summertime. The results showed that it may be possible to reduce heating and cooling energy consumption by up to 5% and 30%, respectively, when applying hygroscopic materials with well-controlled HVAC systems.

To utilize the moisture buffering effects, a reasonably accurate prediction of the buffering performance of the hygroscopic material in the building is required. The measurements of the material properties and the room factors must be combined together to achieve this prediction. Abadie and Mendonça (2009) summarized this combination and the contribution of their work is shown in Figure 2.3. There was an effort to derive and use a single-element to characterize the moisture buffering performance of interior elements, getting to the hygric inertia of a room.

Roels and Janssen (2006) found the MBV to be a good indicator of the buffering capacities of a finishing material as long as there is a close agreement between indoor conditions in the room and the imposed conditions in the test protocol. Mainly the loading protocol, the specimen thickness and the surface

film conditions were found to be crucial. This strongly restricts the practical applicability of the MBV as currently defined in the NORDTEST protocol.

Furthermore, in a real building zone a combination of hygric buffering materials are present. Ramos et al. (2005) proposed to characterize the hygroscopic inertia of a room (HIR) as a function of the MBV of the finishing materials and furnishing in the room:

$$HIR = \frac{\sum_{i=1}^{n} A_i \cdot MBV_i + \sum_{j=1}^{m} MBV'_j}{V} \qquad (2.10)$$

where HIR [kg/(m^3 %RH)] is the hygric inertia per cubic meter of room volume, MBV_i [kg/(m^2 %RH)] and A_i [m^2] respectively the moisture buffer value and area of finishing material i, MBV'_j [kg/%RH] the equivalent moisture buffer value of element j and V [m^3] the volume of the room.

Janssen et al. (2007) demonstrated that the MBV only reliably assesses the hygric buffering of building materials when the measurement protocol corresponds closely with the real production regime concerned. This implies that just one MBV-value is not sufficient to describe the overall hygric buffering of building materials. As it is impractical to characterize building materials by a multitude of MBVs, for every possible production regime, a weighted-average value is proposed to be used in Eq. 2.10:

$$MBV'' = \alpha \cdot MBV_{8h} + (1 - \alpha) \cdot MBV_{1h} \qquad (2.11)$$

where MBV'' is the Moisture Buffer Value adapted to the real production regime, $MBV_{8h/1h}$ the measured MBVs, and α is a weighting factor.

The newly introduced MBV_{1h} involves no extra measurement effort, but is an additional result from the traditional MBV_{8h} measurement protocol. The MBV$_{8h}$ is derived from the absorbed moisture after eight hour at high RH. Likewise the MBV$_{1h}$ is derived from the absorbed moisture after just

one hour at high RH, within the traditional 8/16 h measurement protocol.

The following values are proposed for the weighting factor α:

- 0 hour < production regime $\leq$ 2 hour: $\alpha = 0{,}0$

- 2 hour < production regime $\leq$ 6 hour: $\alpha = 0{,}5$

- 6 hour < production regime $\leq$ 24 hour: $\alpha = 1{,}0$

Starting from the definition of the HIR, Delgado et al. (2010) implemented a daily Hygroscopic Inertia Index, $I_{h,d}$ [kg/m³ %RH], which can be considered as the room MBV normalized to air renovation conditions and to the moisture generation period:

$$I_{h,d} = \frac{\sum_{i=1}^{n} A_i \cdot MBV_i + \sum_{j=1}^{m} MBV_j'}{n \cdot V \cdot \tau} \tag{2.12}$$

where n [h^{-1}] are the air change per hour and τ [h] the moisture generation period.

Ramos et al. (2012) then focused on the air-flow pattern, comparing experimental measurements results to theoretical ones. An appreciable difference between the measured hygroscopic inertia and the calculated $I_{h,d}$ was found due to the air velocity field which caused the development of several dead zones inside the test chamber. This meant that the perfect mixing of the room air, a simplification commonly assumed in HAM simulations, has a clear impact on the results of this kind of problem. If perfect mixing is assumed, all the hygroscopic surfaces would be fully active; but since this is not true, the flux chamber simulations overestimated the moisture buffering effect.

The confirmation of the chamber's air imperfect mixing was found in some positions of the sensors, between which the pressure difference reached 400 Pa in certain periods. The coefficient for imperfect mixing of air C_r was introduced as correction factor in the Hygric Inertia Index:

$$I_{h,d} = \frac{\sum_{i=1}^{n} A_i \cdot C_{r,i} \cdot MBV_i + \sum_{j=1}^{m} C_{r,j} \cdot MBV_j'}{n \cdot V \cdot \tau} \qquad (2.13)$$

2.2.2 The moisture transport in the whole building

A common way to evaluate the moisture amount absorbed and released by the hygroscopic enclosure is by calculating the moisture distribution in each part of the building according to the transport mechanism.

Example of this method can be seen from Yang et al. (2012), in which the moisture buffering amount was calculated by the total moisture generation in the test room subtracting the moisture taken away by ventilation, air leakages and diffusion through the wall system.

With a numerical simulation approach, a complicated interacting mechanism among these building components was modeled by Zhang (2005).

There are several models with different degrees of complexity for predicting HAM transfers in the building envelope systems.

Chen and Shi (2005) established a phenomenological equation with the determination of the coefficients of heat and moisture transfer to describe the migration process of heat and mass in unsaturated porous building materials. Qin et al. (2006) provided an analytical approach to calculate the coupled heat and moisture transfer in the porous building materials. The coupled system was solved by using the Laplace transform. Janssen et al. (2007) investigated the hygrothermal responses of the building components under atmospheric excitation. Abadie and Mendes (2006) compared the analysis of response-factor and finite-volume methods for predicting the heat and moisture transfer through porous media.

Straube and Burnett (2001) summarized 5 factor in performing the building envelope simulation including:

- Geometry of the enclosure with all macro building details;

- Interior and exterior boundary conditions;

- Material properties and their variation with temperature, moisture content and age, as well as their chemical interaction with other materials;

- Physics, chemistry, thermodynamics and mathematics of combined HAM transport;

- Performance thresholds, i.e. the conditions under which a material or assembly will cease to perform as intended.

The room models which focus on the resolution of the spatial distribution of temperature, humidity and air flow profiles inside a room had been built mostly by using the computational fluid dynamics (CFD) techniques.

Liu et al. (2003) studied the airflow and moisture distribution inside a ventilated test room by using a standard $\kappa - \varepsilon$ turbulent model, and a good agreement was obtained between the modeling simulation and experimental results. Teodosiu et al. (2003) investigated the uncertainties influenced by boundary conditions by performing a numerical simulation on a full-scale test room with mixed ventilation.

The integration of all the sub-models into a whole building simulation poses a great challenge, and it was a main subtask of Annex 41. The Annex report summarized the current integration efforts in coupling these models into a whole building simulation tool.

In order to develop numerical codes to couple the transfer of water vapor between the air and the material surface, the moisture transfer and the moisture storage within the material, simplified coupling methods were often adopted. In these models the moisture balance for the indoor air in a room was described by the so-called multi-zone models, with the assumption of well-mixed air properties.

The governing equation can be described as follows (Woloszyn and Rode, 2008a):

$$\dot{G}_{gen} + \dot{G}_{sys} + \frac{\dot{V}_{ext}}{R_v T_i} \cdot (p_{v,ext} - p_{v,int}) = \frac{V}{R_v T_i} \cdot \frac{dp_{v,i}}{dt} + \sum_{j=1}^{n} A_j h_m (p_{v,int} - p_{v,surf,j})$$

(2.14)

where $\dot{G}_{gen}$ [kg/s] is the indoor vapor generation, $\dot{G}_{sys}$ [kg/s] is the vapor added/removed by HVAC systems, $\dot{V}_{ext}$ [m³/s] is the volumetric flow rate of outside air, V [m³] is the room air volume and h_m [m/s] the convective mass transfer coefficient.

Woloszyn and Rode (2008b) also provided in Annex 41 a summary of these models in simulating the whole building HAM-transfer. In many cases, the moisture transfer coefficient between the air in the room and wall was assumed or defined by the users.

One of the popular model based on the simplified lumped approach is the Effective Moisture Penetration Depth (EMPD) model. It has been used to simulate moisture absorption and desorption in the building material. With the assumption of different material properties, several codes have been developed in this model.

For example in EnergyPlus non-isothermal conditions are assumed, where the temperature used in the EMPD model comes from the solution of the energy conservation equations and the moisture capacity of the material is not constant but a function of the layer relative humidity; in TRNSYS the isothermal conditions are assumed, and the moisture capacity is constant.

The advances in 3D airflow modeling by using CFD to determine the local moisture transfer coefficient has not been widely applied in the coupled simulations, due to two main limitations. The first one is the computational time, as the whole building annual simulation by CFD are beyond the capacity of the current computational resources. The second one is the problem of validation, as only few simulation studies took this approach.

Steeman et al. (2009) coupled an EMPD model with a CFD one in Fluent, so that the CFD code could be used to solve the moisture transfer within the material. Neale (2007) solved the heat and mass transfer for boundary layers close to a wall by implementing vapor transfer equations in MATLAB and coupled it with Fluent. This approach was validated and compared with the experimental data, but the post-processing was complicated due to the

23

non-single simulation environment.

Chapter 3

Modelling HAM (*Heat, Air and Moisture*) transfer in building components

In this chapter the following topics will be reviewed:

- The building materials hygroscopic properties and relative concepts, such as sorption isotherm, moisture effusivity and penetration depth;

- The principles of moisture transport, as well as the fundamental governing equations and dimensionless numbers used in fluid flow, heat and mass transfer;

- The moisture balance in the room and enclosures.

3.1 Hygroscopic properties of materials

In this section material properties are introduced. For the experimental and numerical study about the properties measurement and determination one can refer to Carmeliet and Roels (2001) or to standards UNI EN ISO 12571 (2013) and UNI EN ISO 12572 (2006).

Moisture transfer in porous media involves a complex interaction of different transport mechanisms, their driving forces and the effect of available

capacity and temperature gradients. This Chapter points out those parts of the accepted theory that are both essential and interesting for this research. The focus in this study concerns the dynamics of moisture transfer in the hygroscopic range.

3.1.1 Moisture sorption isotherm

The moisture sorption isotherm, which is usually represented by a regression curve, also called retention curve, describes the relationship between water content and the equilibrium humidity of a material at constant temperature.
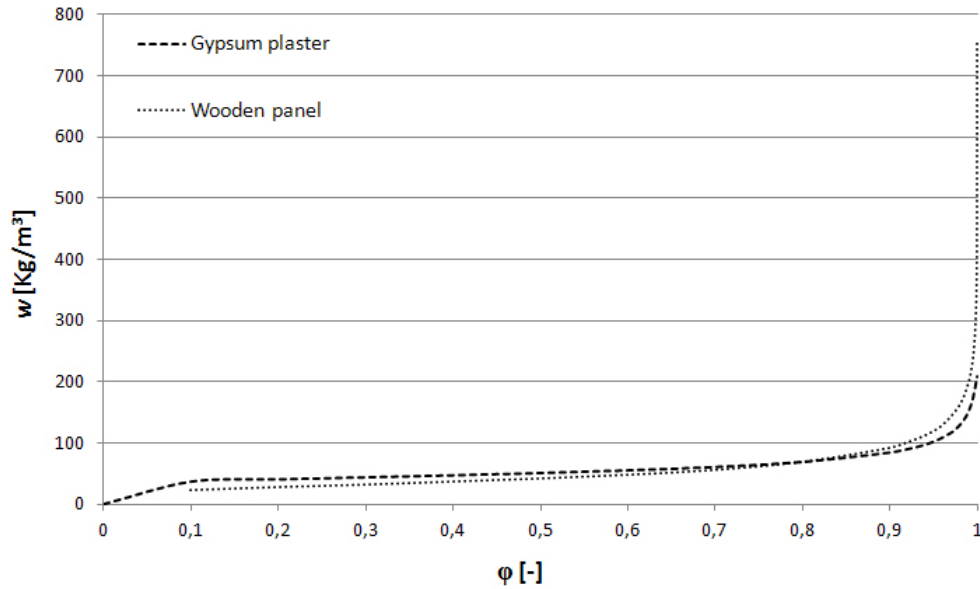
Figure 3.1: Sorption isotherm of wood panel and gypsum plaster. Material data from IEA Annex 23.

Moisture can be adsorbed to the surface of the pores within hygroscopic materials, physically fixed in pores, present as free water or chemically bound with the material itself. The amount of hygroscopic moisture depends on relative humidity of the air [-] within the pore.

Moisture content can be given by mass u [kg/kg] or by volume w [kg/m^3] and expressed as:

$$u = \frac{m - m_0}{m_0} \tag{3.1}$$

$$w = \frac{m - m_0}{V} = \rho_0 \cdot u \tag{3.2}$$

where m [kg] is the mass of the moist sample, m_0 [kg] is the mass of the dry sample, V [m^3] is its volume and ρ_0 [kg/m^3] its dry density.

For very low relative humidities, just a single layer of water molecules forms on the inner surfaces of the material pores. The fixation of these molecules by hydrogen binding, based on dipole moment of water molecules, is very strong. When the relative humidity increases, additional layers of molecules are added to the surfaces, and their binding force decreases until water molecule layers in very small pores combine and capillary condensation starts. Capillary condensation depends on the suction pressure p_c [Pa], defined as the difference between the total pressure p_a and the pressure of the liquid under a meniscus p_l [Pa] according to Laplace equation:

$$p_c = p_a - p_l = \frac{2\sigma}{r} \tag{3.3}$$

where σ [N/m] is the surface tension of water and r [m] is the pore radius.

There is a connection between relative humidity of the air in the pores and the suction pressure within the pores subjected to capillary condensation, given by Kelvin equation:

$$\ln(\varphi) = -\frac{p_c M_w}{\rho_w \cdot R \cdot T} \tag{3.4}$$

where M_w [kg/mol] is the molar weight of water, ρ_w [kg/m^3] the density of water and R [J/(mol K)] the universal gas constant.

The equilibrium moisture content (EMC) is a function of relative humidity, and together with the point where the capillary condensation starts are very material-specific, depending on the size of the inner surface available for adsorption and on the pore volume suitable for the condensation itself.

In the hygroscopic range ($\varphi < 0, 98$) the retention curve is given by the sorption isotherm, while in the over-hygroscopic range ($\varphi > 0, 98$) the EMC is expressed as a function of suction pressure p_c. At a certain RH level the liquid phase just become continuous.
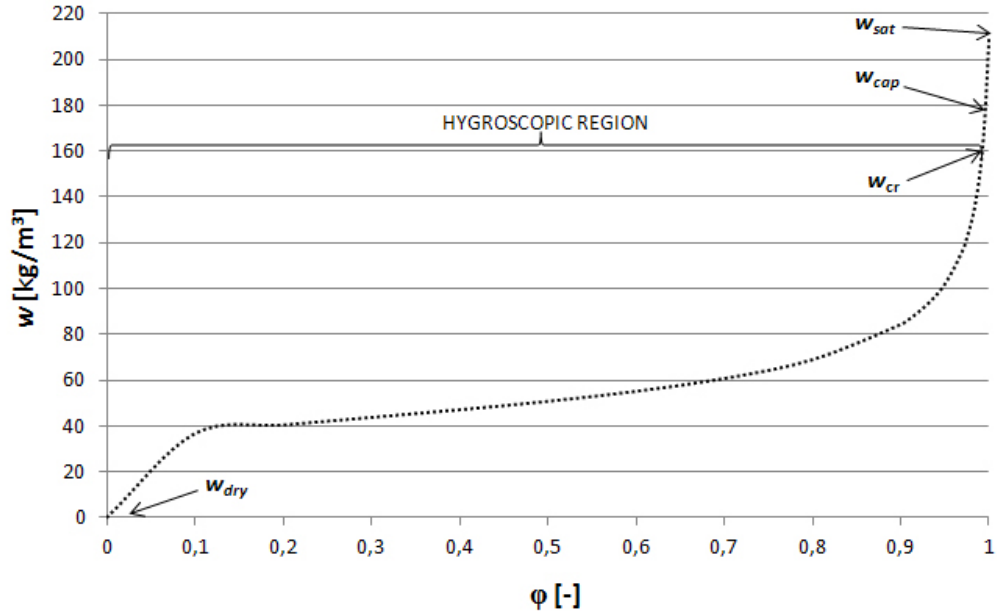
Figure 3.2: The hygroscopic range of gypsum plaster.

Critical moisture content w_{cr} [kg/m³] is defined as the moisture content where this level is reached; after it, a higher moisture content can be achieved during wetting, denoted as w_{cap}; the maximum moisture content w_{sat} can be reached if the material is exposed to the wetting long enough, so the air trapped in pores can dissolute in water.

A very important distinction exists between moisture uptake and release, described by sorption and desorption isotherms. The deviation between these two curves is given by the hysteresis effect, where the desorption isotherm always gives an higher EMC than absorption for a given relative humidity.

The hysteresis effect, due to a ink-bottle-effect, is still not totally understood and its numerical modeling is a big challenge.

3.1.2   Moisture capacity

A porous material's ability to store moisture is described by the retention curve. The moisture capacity of a material is defined as its ability for adsorption and desorption, when environmental moisture conditions are changed. Mathematically the moisture capacity ξ [kg/kg] is defined by the slope of the sorption isotherm:

$$\xi = \frac{\partial w}{\partial \varphi} \tag{3.5}$$

This definition is valid under equilibrium conditions. The existence of hysteresis also influences moisture capacity, i.e. ξ will differ, depending on whether the material is drying or wetting.

The moisture storage capacity of a material is also a function of temperature.

3.1.3   Water vapor permeability

In building science, water vapor permeability, δ_p [kg/(m s Pa)], describes the ability of a material to transmit the water vapor. It is defined in Fick's first law equation:

$$\dot{g}_v = -\delta_p \frac{\partial p_v}{\partial x} \tag{3.6}$$

where $\dot{g}_v$ [kg/(m²s)] is the density of water vapor flow, ∂p_v [Pa] is the vapor pressure difference between the material surfaces, ∂x [m] is the specimen total

thickness.

The ratio between the permeability of stagnant air δ_a and the permeability of the material defines the water vapor resistance factor μ [-]:

$$\mu = \frac{\delta_a}{\delta_p} \tag{3.7}$$

where δ_a is calculated by the Schirmer equation as:

$$\delta_a = \frac{0,083 \cdot P}{R_v \cdot T \cdot p_a} \left(\frac{T}{273}\right)^{1,81} \tag{3.8}$$

3.1.4 Moisture diffusivity

The moisture diffusivity D_w [m^2/s] combines the transport and retention properties into one property. It describes how fast the moisture potential propagates through the material (Rode and Grau, 2008) as:

$$D_w = \frac{\delta_p \cdot p_{v,s}}{\rho_0 \cdot \xi} \tag{3.9}$$

where $p_{v,s}$ [Pa] is the saturation vapor pressure. The moisture diffusivity has the same unit with thermal diffusivity α and kinematic viscosity ν.

3.1.5 Moisture effusivity

In thermodynamics, the thermal effusivity b [J/(m^{2}K s^{0,5})] of a material is defined as the square root of the product of the material's thermal conductivity and its volumetric heat capacity.

$$b = \sqrt{\lambda \cdot \rho_0 c_p} = \frac{\lambda}{\sqrt{\alpha}} \tag{3.10}$$

where λ [W/(m K)] is the thermal conductivity, ρ_0 [kg/m³] is the density of the material, c_p [J/(kg K)] is the specific heat capacity of the material and α [m²/s] is the thermal diffusivity. The product of ρ_0 and c_p is known as the volumetric heat capacity. A material's thermal effusivity is a measure of its ability to exchange thermal energy with its surroundings.

Analogue to this definition, Rode et al. (2005) described moisture buffering capacity by the moisture effusivity b_m [kg/(m² Pa s^{0,5})] as:

$$b_m = \sqrt{\frac{\rho_o \cdot \delta_p \cdot \xi}{p_{v,s}}} \tag{3.11}$$

3.1.6 Moisture penetration depth

Cunningham (1992) obtained the analytical solution for the effective moisture penetration depth d_m [m] for the semi-infinite material in one-sided case which is subjected to cyclic moisture concentration load. For a constant vapor diffusion coefficient and under isothermal conditions, the effective moisture penetration depth is equal to:

$$d_m = \sqrt{\frac{D_w}{\omega}} \tag{3.12}$$

where ω is the angular frequency of the cyclic load $[\sqrt{s^{-1}}]$.

Eq. 3.13 is obtained by substituting (3.9) into (3.12):

$$d_m = \sqrt{\frac{\delta_p \cdot p_{v,s} \cdot t_p}{\rho_0 \cdot \xi \cdot \pi}} \tag{3.13}$$

where t_p is the time period of the cyclic variation [s].

3.2 Principles of moisture transfer

The previous section provided a description of the material properties related to moisture transport. In this section a brief description of the theories of HAM transport, including characterizing fluid low, heat and mass diffusion and analogy of heat and mass transfer in building science, are reviewed.

3.2.1 Convective flow characterization

The governing equations of a convective fluid flow are derived from the principles of conservation of mass, momentum, and energy. They describe the convection of fluid flow within porous media and air as well. As for the compressible and incompressible are highly non-linear, and the analytical solutions for complex boundary conditions cannot be obtained, these equations must be solved numerically.

Different numerical models are available to describe the fluid flow based on the flow characteristics, and the dimensional analysis plays an important role in characterizing the flows. In this section, some dimensionless numbers are introduced (Li, 2011), which are relevant in identifying the flow characteristics.

Nusselt number, Nu

The Nusselt number is the ratio of convective to conductive heat transfer across (normal to) the boundary. A large Nusselt number means an efficient convective heat transfer. The Nusselt number is defined as:

$$Nu = \frac{h_c L}{\lambda_f} \tag{3.14}$$

where h_c [W/(m^2 K)] is the convective heat transfer coefficient, λ_f [W/(m K)] is the thermal conductivity of the fluid and L [m] the characteristic length.

Reynolds number, Re

The Reynolds number is defined as the ratio of inertial forces ($\rho \cdot v$) to viscous forces (μ/L) and consequently quantifies the relative importance of these two types of forces for given flow conditions. Reynolds numbers are used to characterize different flow regimes within a similar fluid, such as laminar or turbulent flow: laminar flow occurs at low Reynolds numbers ($Re < 2300$), where viscous forces are dominant, and is characterized by smooth, constant fluid motion; turbulent flow occurs at high Reynolds numbers ($Re > 4000$) and is dominated by inertial forces, which tend to produce chaotic eddies, vortices and other flow instabilities. It's defined as:

$$Re = \frac{\rho \cdot v \cdot L}{\eta} = \frac{v \cdot L}{\nu} \tag{3.15}$$

where v [m/s] is the mean velocity of the object relative to the fluid, η [kg/(m s)] is the dynamic viscosity of the fluid, ν [m^2/s] is the kinematic viscosity.

Grashof number, Gr

The Grashof number approximates the ratio of the buoyancy to viscous force acting on a fluid in fluid dynamics and heat transfer. It frequently arises in the study of situations involving natural convection and for vertical flat plates is expressed as:

$$Gr = \frac{g_n \gamma (T_{surf} - T_\infty) L^3}{\nu^2} \tag{3.16}$$

where g_n [m/s^2] is the acceleration due to Earth's gravity, γ [K^{-1}] is the

volumetric thermal expansion coefficient (equal to approximately 1/T, for ideal fluids), T_{surf} and T_∞ [K] are the surface temperature and the bulk temperature respectively.

Prandtl number, Pr

The Prandtl number Pr is a dimensionless number approximating the ratio of momentum diffusivity (kinematic viscosity ν) and thermal diffusivity α as:

$$Pr = \frac{\nu}{\alpha} = \frac{\eta c_p}{\lambda} \tag{3.17}$$

where c_p [J/(kg K)] is the specific heat capacity. Note that whereas the Reynolds number and Grashof number are subscripted with a length scale variable, the Prandtl number contains no such length scale in its definition and is dependent only on the fluid and the fluid state. As such, the Prandtl number is often found in property tables alongside other properties such as viscosity and thermal conductivity.

Eckert number, Ec

Eckert number Ec expresses the relationship between a flow's kinetic energy and enthalpy, and is used to characterize dissipation.

$$Ec = \frac{v^2}{c_p \Delta T} \tag{3.18}$$

If the Eckert number $Ec \ll 1$, then the dissipation is negligible. For the free convection, substituting the v in Ec number by the velocity $(g_n \gamma \Delta T L)^{1/2}$, the Eckert number is with the form of:

$$Ec = \frac{v^2}{c_p \Delta T} = \frac{g_n \gamma \Delta T L}{c_p \Delta T} = \frac{g_n \gamma L}{c_p} = \frac{L}{c_p / (g_n \gamma)} \tag{3.19}$$

The scale $c_p/(g_n\gamma)$ is equal to 30 and 2030 km for the air and water respectively. So the vertical length scale L in most cases is much smaller than $c_p/(g_n\gamma)$ and $Ec \ll 1$. This is the reason why most CFD software neglect the dissipation when perform natural convection analysis.

3.2.2   Mechanisms of moisture transfer

In building physics the transport of water vapour is a transport of gas in the pores of any porous material.

In isothermal conditions, the theory on moisture transport in porous materials is originally based on Fick's law of diffusion of water vapor (see Eq. 3.6).

As already discussed (see Chapter 3.1.1) it is generally assumed that liquid transfer begins at the critical moisture content w_{cr}, which is determined by the existence of a continuous liquid phase. Pure water vapour transfer decreases from this point with increasing moisture content until vapour transfer becomes zero at saturation. The vapour-liquid-vapour series transport, where liquid islands act as short circuits for transfer of vapour, is normally treated as vapour transport. One reason to distinguish between vapour and liquid transport is that the transfer of soluble salts under thermal gradients takes place in the liquid phase.

Using Darcy's law, the liquid moisture transport can be expressed as the liquid moisture flux density $\dot{g}_l$ [kg/(m²s)] with the suction pressure p_c [Pa] as driving force:

$$\dot{g}_l = -\lambda_l \cdot \frac{\partial p_c}{\partial x} \tag{3.20}$$

where λ_l [kg/(Pa m s)] is the liquid conductivity.

For $w < w_{cr}$ most of the moisture transport can be regarded as water vapour diffusion. Above this level, liquid transport exists as capillary suction. However some liquid transport will already exist locally at quite low moisture contents. Furthermore, the limit where the liquid transport starts, is difficult to determine and it is obviously dependent on the pore structure of the different materials. Philip and De Vries (1957) explained how liquid transfer already exists at very low humidity levels by vapour/liquid/vapour transport in series. Total moisture transport increases with increasing moisture content, because hydraulic conductivity in small pores is larger than water vapour permeability (Pedersen, 1990).

In stationary and isothermal conditions the total moisture flux $\dot{g}$ [kg/(m²s)] can be expressed as:

$$\dot{g} = \dot{g}_v + \dot{g}_l = -\delta_p \frac{\partial p_v}{\partial x} - \lambda_l \frac{\partial p_c}{\partial x} \qquad (3.21)$$

Surface diffusion involves the transport of liquid water. When the moisture content exceeds a certain value, i.e. where there exists more moisture on the inner pore surfaces than just multi-molecular layers, the moisture becomes mobile. The binding forces of these outer molecules are not as strong as those bound to the pore wall.

This transport takes place when the moisture content is less than that for capillary saturation, where capillary pores (radius $r < 10^{-7}m$) start to be filled and actual liquid transport takes over.

When looking at moisture transport in porous materials on a microscopic scale, a temperature gradient across a pore with a liquid island (see Fig. **??**) makes the vapour condensate on the warm side of the liquid island (= cold side of the air filled pore) and to evaporate from the cold side of the liquid island (= warm side of the next air filled pore). In this way, the temperature gradient induces moisture transport in the direction of the temperature

gradient (also in the direction of vapour pressure gradient), until there is an equilibrium in the liquid capillary flow due to the different curvatures.

For isothermal cases, these two mechanisms will work in the same direction, i.e. higher water vapour pressure on one side will result in a higher relative humidity, which again gives a higher moisture content and a thicker sorbate layer. When introducing a temperature gradient, these potentials usually become opposite. In winter, in cold climates, there is usually an inward relative humidity gradient in the building envelopes, while the vapour pressure gradient is outwards. When considering only moisture transport driven by the water vapour pressure difference, therefore, the moisture flux is usually outwards in cold climates.

3.2.3 Governing equations for dynamic moisture transport

When setting up the theoretical model to be able to analyse the dynamic moisture transport, the governing equation for conservation of mass in a building component can be expressed by Fick's second law equation regarding only one dimensional transport as:

$$\frac{\partial w}{\partial t} = -\frac{\partial}{\partial x}\left(\lambda_l \frac{\partial p_c}{\partial x} - \delta_p \frac{\partial p_v}{\partial x} + \dot{g}_a u\right) \tag{3.22}$$

where $\dot{g}_a$ [kg/(m^{2}s)] is the air flux density and u [kg/kg] is the equilibrium moisture content.

For the adopted model the moisture balance equation for the room reads:

$$C_m \cdot \frac{\partial p_{v,int}}{\partial t} = \dot{G}_{diff} + \dot{G}_{vent} + \dot{G}_{gen} \tag{3.23}$$

where C_m [kg/Pa] is the volumetric moisture capacity of room air:

$$C_m = 0,621 \cdot 10^{-6} \cdot \rho_a \cdot V \qquad (3.24)$$

$\dot{G}_{diff}$ [kg/s] is the moistrue diffusion through the building envelope:

$$\dot{G}_{diff} = \sum_{i=1}^{n} \frac{A_i(p_{v,int} - p_{v,surf,i})}{Z_{p,i}} \qquad (3.25)$$

$\dot{G}_{vent}$ [kg/s] is the moisture flux through the ventilation system:

$$\dot{G}_{vent} = 6,21 \cdot 10^{-6} \cdot \rho_a \sum_{k=1}^{m} \dot{V} \cdot (p_{v,ext,k} - p_{v,int}) \qquad (3.26)$$

and $\dot{G}_{gen}$ [kg/s] is the moisture generation rate.

Eq. 3.23 is the differential equation stating that the indoor humidity level is the result of the moisture balance of moisture generation inside the room, moisture gains/losses from the ventilation, moisture diffusion through the walls.

As this research aims at deepening the moisture interaction between indoor air and interior finishings in living spaces such as residential buildings and offices, only the hygroscopic range, i.e. $\varphi < 0,98$, will be taken into account in the next sections, neglecting the liquid transport in saturation conditions.

Chapter 4

Analysis of the simulation tool

4.1 HAM-Tools

HAM-Tools is a building simulation software implemented on the Simulink-Matlab platform by the Chalmers University of Technology (Gotheborg, Sweden) and the Technical University of Denmark (Lygby, Denmark) during the Annex 41 (Sasic Kalagasidis, 2002, 2003, 2004).

"HAM" stands for *Heat, Air and Moisture* transport processes in a building and its envelope that can be simulated by this program, and "Tools" describes its modular structure. The main objective of this tool is to obtain simulations of transfer processes related to building physics, i.e. heat and mass transport in buildings and building components in operating conditions. The tool is to be used as a research and educational tool for the investigation of the mechanism of above mentioned processes and of the degree of their correlation when they are coupled.

The scope of the simulation is to obtain transient HAM states of a building enclosure and indoor air, as a result of a building usage in specified operating conditions. This knowledge enables further analyses such as calculation of energy consumption of the building, indoor comfort assessment, risk analyses regarding moisture content levels in building construction and indoor air, functionality of HVAC systems, air flow distribution through openings

on building enclosure, etc.

The library is the part of IBPT - International Building Physics Toolbox, and available for free downloading on www.ibpt.org.

Five interacting systems may be identified: building construction, environment, indoor air, building services and occupants. These represent main subsystems in HAM-Tools simulations and they are named such as: *Construction, Weather, Zone, HVAC* and *Gains.* Some possible relations between them are illustrated in Figure **??**.

The *Construction* system represents a building enclosure composed of walls, windows, etc. The *Weather* system defines external climate load, i.e. outdoor operating conditions based on building position in space. The *Zone* refers to an air volume of a room. The *HVAC* system is a technical system which provides desired indoor climate through a certain input of heat, air and/or moisture. The *Gains* system gives casual HAM inputs to the zone, which result from the building occupancy (from people living or working inside, appliances, etc). As it is indicated in Figure **??**, physical properties of building materials should be known; the same is valid for the weather data which may be given in a form of a reference or a real (measured) climate for a specific location.

The systems interact in different ways. They "meet" or "communicate" with each other by exchanging data about present states. The way and degree of their coupling determine the data flow between them. For example, the HAM response of the Zone is governed by the magnitude of gains coming from the Construction, HVAC and Gains systems. Changes in HAM states of the Zone is registered by the HVAC system, which adjusts its next input, end so on.

HAM-Tools program is constructed using a software package Simulink (MathWorks). Simulink is a graphical programming language, built on top of mathematical software package Matlab (MathWorks), for modelling, simulating and analysing dynamic systems. The reason for choosing Simulink as a development environment was a large degree of flexibility, modular structure,

40

transparency of the models and ease of use in the modelling process. Models in Simulink are built as block diagrams, in the same way as it would be done on paper. Modelling in Simulink is a process of assembling more complex blocks from the standard ones. A library of predefined blocks, which covers a variety of arithmetical functions, sinks, sources, linear and non-linear components and connectors, is provided in the package. As a part of the Matlab package, Simulink has built-in state-of-the-art ordinary differential equation (ODE) solvers, which are automatically configured at run-time of the model. Therefore, only a physical model needs to be implemented, and not the solver. This wide variety of modelling possibilities ensures that an optimal choice can always be made with respect to the task.

HAM-Tools is also a library of predefined elements, designed to serve as building physics calculation tools. Tools are grouped according to their functionality into five categories:

Constructions	(external / internal walls and windows)
Zones	(air volume of the room, air cavity in a wall)
Systems	(HVAC sytems)
Helpers	(handling of weather data and other basic blocks)
Gains	(internal heat and moisture gains)

In the Simulink graphical approach, the HAM-Tools library appears as it is shown in Figure 4.1, where the five subsystems appear as separate folders. Input and output connection ports that appear on the blocks are named according the signals they accept.

All models, including the ones presented, are hierarchical and open on every level. This means that each of the block diagrams may hide many other subsystems. This modular structure in Simulink - using systems and subsystems and the graphical approach, facilitate handling and control of a very complex interaction between different parts of the model.

There are two main blocks, representing the most frequent objects of interest: a building envelope *construction* (walls, windows), as a layered structure of different building materials, and a *thermal zone* (ventilated space),
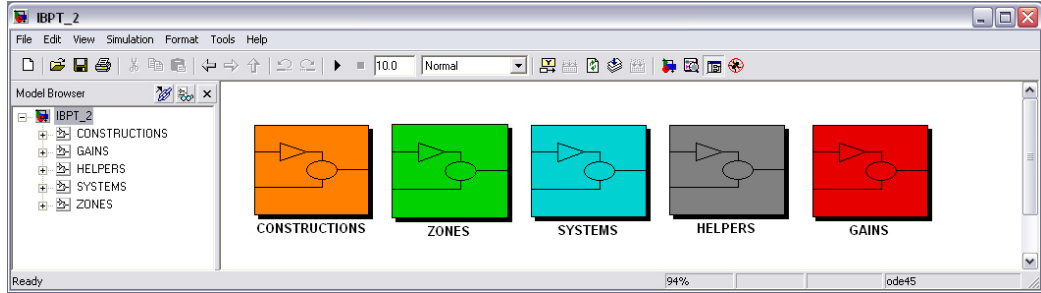
Figure 4.1: HAM-Tools library in Simulink.

which is enclosed by the building envelope. Component models provide detailed calculations of the hygro-thermal state of each subcomponent in the structure, according to the surrounding conditions to which it is exposed. The hygro-thermal state of the zone is determined by the heat, air and moisture gains through the building envelope, (HVAC) *systems* and internal *gains*, additional components presented by the model of the same name. Direct coupling between building envelope and surrounding air (outdoors/indoors climate, ventilated space) is accomplished by *outdoor and indoor surface conditions* - models for heat balance at the wall boundaries.

Material properties

The building components must be characterized by a number of material data. The following list gives an overview of necessary material properties:

Physical properties

- Density of the dry material, ρ_0, [kg/m^3];

- open porosity, ϵ , [-];

Thermal properties

- Specific heat capacity of the dry material, c_0, [J/(kg K)];

- Thermal conductivity, λ, [W/(m K)];

42

Hygroscopic properties

- Sorption isotherm $w(\varphi)$, according to Equations 3.1 and 3.2;

- Moisture capacity ξ [kg/m^3], according to Equation 3.5;

- Water vapor permeability, δ, [kg/(m s Pa)] according to Equation 3.6;

- Liquid water conductivity, δ_l, [kg/(m s Pa)] according to Equation 3.20;

Liquid water conductivity and vapour diffusivity have been introduced in phase-divided manner, i.e. they describe liquid water flux and water vapour diffusion separately (see Chapter 2). However these coefficients are not directly measurable. Experimental determination of the vapour diffusivity is usually affected by liquid water transport, as well as the determination of the liquid water conductivity is affected by vapour transport. Therefore a phase dividing function is introduced to describe the percentage of liquid and vapour flux as a part of the total moisture flux.

Material data file

Material properties are placed in the special data file, so called *material database.* The file should be loaded on Matlab workspace before simulation starts. Data are organized in the form of Matlab structures. Each structure represents the place in the file occupied with the data for one material; they are numbered in acceding order, as they have been added to the file. The number of structure is not limited.

Structures can contain data of different kind and length: either a string or a constant, or an array of values. The structure format, or here a data array with material properties, should be the same for each material within the same file, as the example shown in Figure 4.2.

Each material property has its own name, for example "`dry_density`". These names act as the personal name of the properties. It is important to remember that they are unique and reserved. The complete list of the names can be found in the IBPT General report.

```
CTHmaterial(2)=struct(...
'index',2,...
'name','Plaster',...
'dry_density',790,...
'lambda_dry',0.2,...
'lambda_T',0,...
'lambda_W',0.0045,...
'heat_capacity',870,...
'emissivity',0.9,...
'transmittance',0,...
'absorptivity',0.9,...
'porosity',0.209,...
'W_capillary',208.9,...
'WAC',0,...
'sorption_RH',[0 0.1 0.2 0.3 ...  0.975 0.98 0.985 0.99 0.995 1],...
'sorption_W',[0 36.78 40.51 ... 138.28 151.36 172.42 209],...
'delta_W',[ 0 36.78 40.51 ... 138.28 151.36 172.42 209],...
'delta_p_W',[6.37e-11 6.31e-11 6.29e-11  ... 3.31e-11 2.19e-11 0],...
'hyd_cond_W',[ 0 36.78 40.51 ... 138.28 151.36 172.42 209],...
'hyd_cond_K',[6.52e-31 9.77e-26 ...  1.61e-14 3.77e-14 2.02e-13 6.2e-9],...
'air_permeability',0,...
'slope_sorption_RH',[],...
'slope_sorption_ksi',[])'
```

Figure 4.2: The material data array for gypsum plaster.

The *family name* of the material is given in a beginning of the structure, like "CTHmaterial(2)". While the personal names are unique, the family name can be defined by the creator of the material database. When the file is loaded, this name appears in the Matlab workspace, identifying the whole library. It is useful then to give some associative name, although more than one material library can be used at the same time. The number in the brackets (here number "2"), says that this particular material is placed as the second material in the data file-

To reach a certain property for a certain material, both the family and personal name must be specified:

```
CTHmaterial(2).sorption_RH
```

which gives the following array:

```
[0 0.1 0.2 0.3 ... 0.975 0.98 0.985 0.99 0.995 1]
```

The Simulink model for the Material data block is shown, modelled ac-

cording to the described mathematical model within the *Moisture Balance* block.
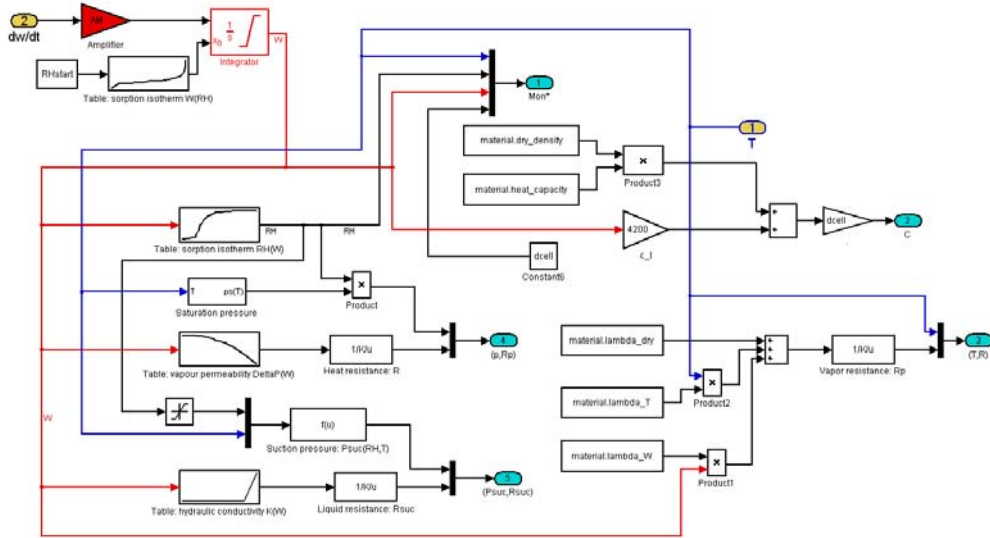
Figure 4.3: Simulink model for the Material data block.

The *One Node* block represents one layer (one control volume) of the certain material in the wall construction. It calculates the temperature and moisture content of the node placed in the middle of the layer, accounting for the heat, moisture and air loads.
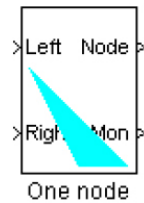
Figure 4.4: The *One Node* block diagram in Simulink.

In the *Block Mask* the user inputs to the block are: material type, thickness of the layer, initial temperature and relative humidity of the layer and time amplifier. Amplifier gains time steps of climate data. If the time scale

45

is one hour (hours of the year), the value of 3600 should be specified (1 h = 3600 s), or 1 if the time scale is one second.

4.1.1   HAM: numerical model

The numerical model is based on a control volume method and applies the governing equations shown in Chapter 3 for the moisture balance in building components (Eq. 3.22) and in the room air volume (Eq. 3.23).

It is assumed that lumped thermal capacity C of the volume is localized in the middle.

The thermal (vapour, liquid) resistance between the node and the surface of the volume (corresponds to one half of the total thickness d) are defined as:

$$R = \frac{d/2}{\lambda}, Z_p = \frac{d/2}{\delta_p}, R_l = \frac{d/2}{\lambda_l} \tag{4.1}$$

The specified node position is denoted with an indice i, and positions of the preceding and following one nodes are denoted with $i - 1$ and $i + 1$ respectively (Figure 4.5).

Figure 4.6 shows the first subsystem of the *One Node* block in HAM-Tools, while in the *Moisture Balance* block (Figure 4.7) the flow division method - vapour and liquid phase - is visible.
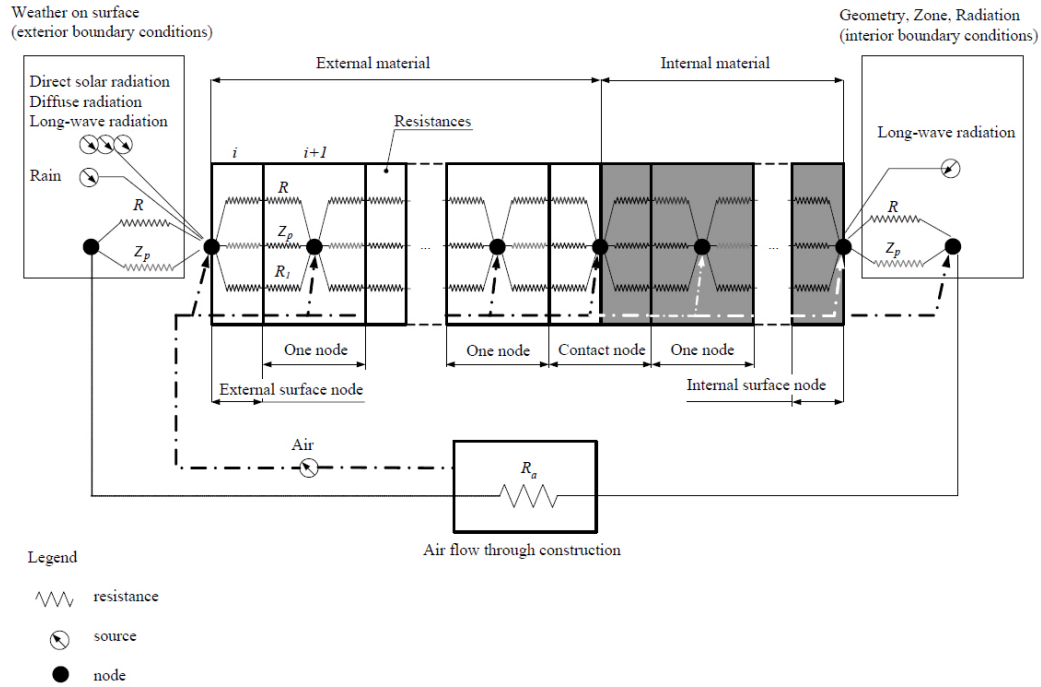
Figure 4.5: The numerical model.
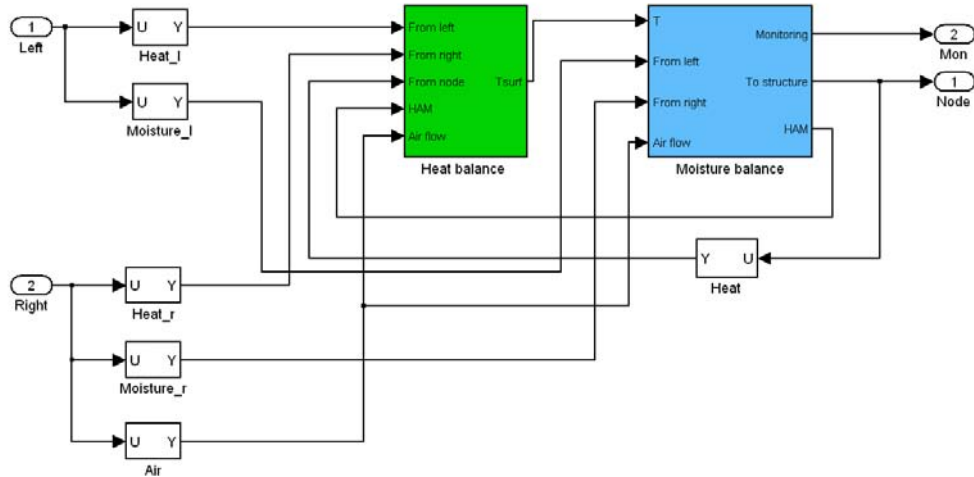
Figure 4.6: The first subsystem of the *One node* block.

47
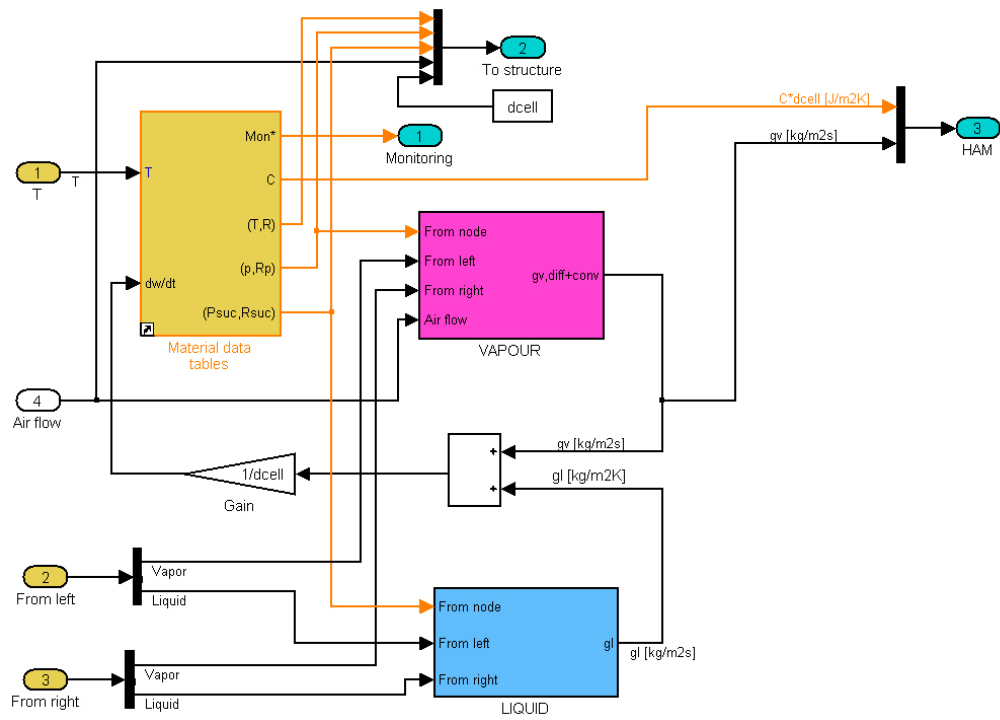
Figure 4.7: Subsystem *Moisture balance*.
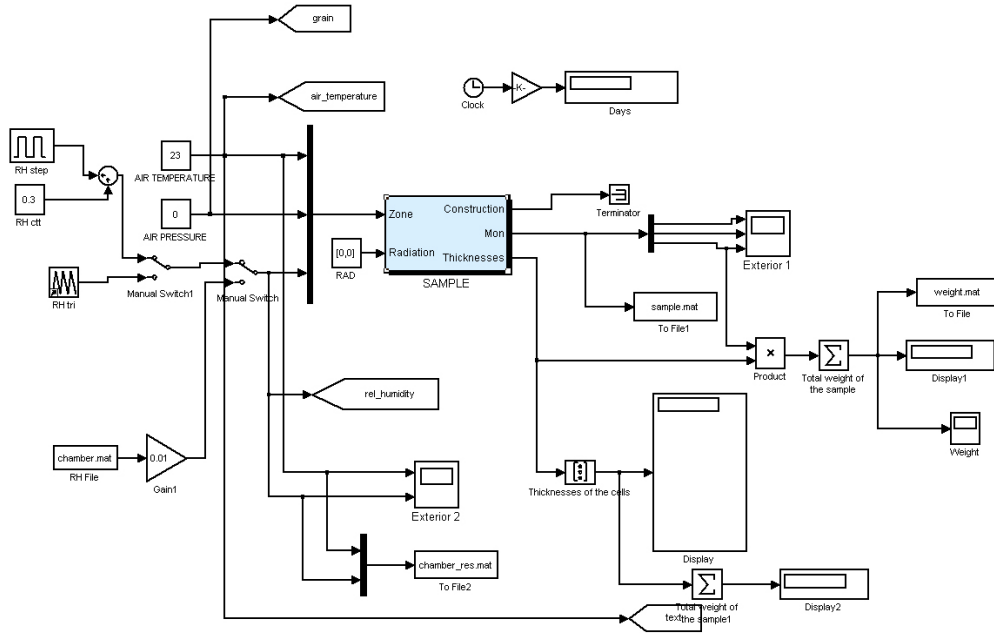
Figure 4.8: the specific arrangement of HAM-Tools modules *MBVsim*.

4.1.2 MBVsim

In Ramos et al. (2012) the Simulink model was subject to small yet decisive adaptations in order to simulate a climate chamber environment for reproducing the MBV test conditions, as will be explained in Chapter 5. The simulation of MBV tests used the specific arrangement of HAM-Tools modules (Figure 4.8).

The applied conditions of temperature and RH are simulated by means of a step function, but one can also input the conditions applied to the samples in the laboratory tests, which can be registered continuously and used in the simulations.

The specific problem related to the MBV test is very sensitive to the behaviour of layers in contact with air, especially the case of coatings. For this reason a higher number of nodes has been modelled to increase the accuracy of results, but while in Ramos et al. (2012) several techniques were applied for the simulation of the paints effect, in Chapter 5 MBVsim will be used to simulate the coated elements without modelling the single paint

49

layer, but comparing the naked specimen behaviour with the coated one.

4.1.3   Limits of the lumped model: air balance

The HAM-Tools model for 1D heat, air and moisture transfer through the construction element has following limitations (Sasic Kalagasidis, 2002):

- temperature should be in the range of - 30 °C to + 80 °C;

- effects associated with phase change, liquid to ice, are neglected;

- climatic load due to driving rain is simplified;

- no hysteresis is accounted for;

- no gravity effects;

- no chemical reactions are considered;

- no drainage between material layers;

- ageing effects or changes in the geometrical dimensions are neglected;

- 2D and 3D effect (like thermal bridges) are not considered.

The lumped model considers a node in the middle of the thermal zone to solve the HAM balance of the air volume.

Air flow through the structure is driven by the air pressure differences across the structure. The mass airflow rate, g_a, is assumed constant through the whole structure, allowing for variations in time.

$$\dot{g}_a = \rho_a \cdot \dot{v}_a \tag{4.2}$$

where $\dot{v}_a$ [m^3/m^2 s] is the density of volumetric air flow rate and is a function of the air pressure difference, Δp_a. The air flow is positive when it is directed towards interior

The vapour flow in building components consists of a diffusive and a convective part:

$$\dot{g}_v = -\delta_p \frac{\partial p_v}{\partial x} + \dot{g}_a \cdot x_a \qquad (4.3)$$

The diffusive part is proportional to the gradient of the water vapour partial pressure (Fickian diffusion); the convective part only exists if the air flow is taken into account, in which case the moisture content in air x_a [kg_v/kg_a] is approximated by the following equation:

$$x_a = \frac{0,621 \cdot p_v}{p_a - 0,379 \cdot p_v} \approx 6,21 \cdot 10^{-6} \cdot p_v \qquad (4.4)$$

The moisture flow $\dot{g}_v$ to the interior surface reads:

$$\dot{g}_v = \beta_{int} \cdot (p_{v,int} - p_{v,surf}) + \begin{cases} \dot{g}_a \cdot x_{a,surf}, & g_a > 0 \\ \dot{g}_a \cdot x_{a,int}, & g_a < 0 \end{cases} \qquad (4.5)$$

This simplified approach neglects the effect of the air velocity field on the interior surfaces. In this way a unique local moisture transfer coefficient is taken into account to characterize the whole surface of the building component and, consequently, its hygroscopic performance.

The risk is to overestimate the moisture absorption where the air velocity is lower, i.e. at junctions between components where the so-called *dead zones* are generated. This topic will be addressed in Chapter 7 where the results obtained with the lumped model will be compared to those calculated with the CFD model.

Chapter 5

Experimental activities

Although this topic has been widely dealt in a comprehensive way by many authors, the moisture buffering effect is well-known in this specific research field but still not commonly considered in the early stages of building design.

The building envelope has had a rapid evolution with regard to its efficiency on thermal performance. This is due to the current European and national regulations that aim to achieve maximum energy efficiency but also maximum comfort for the user. In this scenario numerical models for HAM transfer should be adopted for determining the hygroscopic performance of buildings and the optimal humidity conditions.

A general need for more experimental data that quantify HAM transport in porous building material remains. Recent benchmark data for validating 1-D HAM simulation models produced in a large international project (Hagentoft et al., 2004) rely solely on numerical and analytical data because well-documented and accurate data are scarce.

In IEA-ECBCS Annex 41 (Woloszyn and Rode, 2008a) numerical models have been used to simulate heat and moisture transfer between indoor air and hygroscopic materials during transient changes in indoor humidity. To validate models that simulate moisture buffering, new experimental data are needed that accurately quantify the humidity exchange between environment and hygroscopic material in transient conditions. Experimental data are

available in the literature, but most data are not well suited to benchmark detailed numerical models because carefully planned laboratory experiments are best suited for model validation.

Within Subtask 2 of IEA-ECBCS Annex 41 (Roels, 2008) experimental and numerical data for 1-D heat and moisture transfer in a bed of gypsum board were compared. Comparing the numerical and experimental data serves a dual purpose of validating the numerical models as well as confirming the experimental data. However, as previous researches showed (Roels et al., 2004) that apart from the lack of good benchmark cases, also attaining uniformity in measuring material properties remains difficult, an inter-laboratory comparison of the measurement of the hygric properties by means od a round robin test was carried out. Not all material properties were measured, but they focussed on those relevant for indoor moisture buffering: water vapour transmission properties and the sorption isotherm. Both material properties were based on common measuring techniques, even described in international standards (UNI EN ISO 12571, 2013; UNI EN ISO 12572, 2006) but nevertheless an unacceptable spread in results was found.

In this Chapter the behaviour of gypsum plaster and wood fibre specimens when subjected to transient changes in the air humidity level is described. The dynamic response leads to the characterization of the hygroscopic performance of the material when applied in realistic conditions, such as interior finishing for rooms, where peaks of moisture due to occupancy or vapour production occur. The un-steady regime doesn't account for reaching the moisture equilibrium content in specimens, but for load/release cycles which, as will be described later, lead to the determination of hygric properties in a less time-consuming way.

5.1   Measuring device description

The experimental activity was carried out at the laboratories of Technische Universität Wien.

Figure 5.1 shows the measurement equipment used for the experiments that have been developed in the Research Centre for Building Physics and Building Acoustics Laboratory (Korjenic and Bednar, 2011). Experimental trials were conducted using a fibreboard panel and two gypsum plaster specimen in non-steady state conditions to determine the moisture absorption and desorption characteristics. The test results were used to establish the required material parameters for the HAM model.
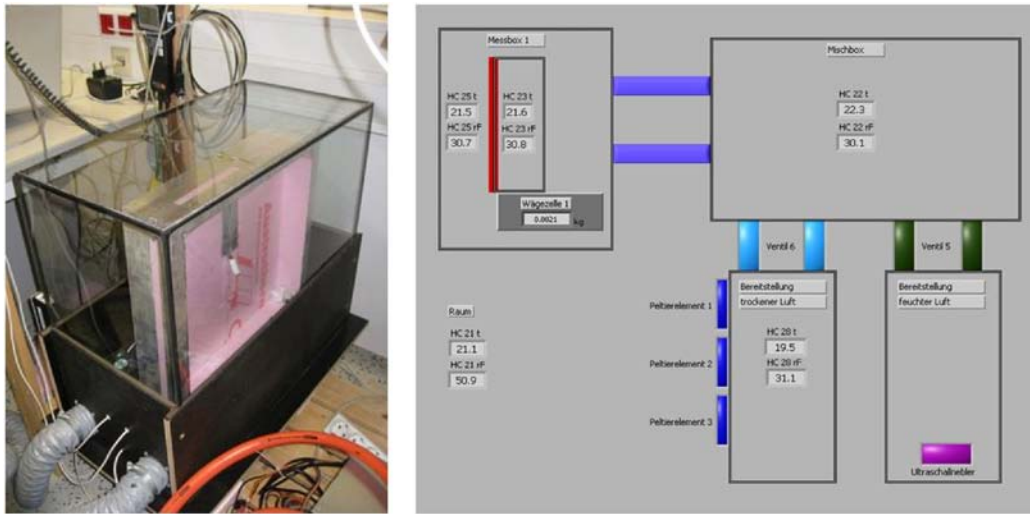
Figure 5.1: The measuring device. a) The climate chamber, b) The remote control system.

The test set-up consists in a plexiglass climate chamber where conditioned air is supplied trough a pre and return hose deriving from a mixing box, where moist air is set at specified levels of temperature and relative humidity through a remote control system. Fans are used to ensure the well-mixing of the air. Two Vaisala HUMICHIP 17204HM temperature and humidity sensors were placed in the mixing box and in the climate chamber. The samples were weighed using a Sartorius MP51 scale. Temperature, humidity and mass were recorded at 1 min intervals using a digital multimeter with an integrated scanner.

The sample frames are composed by a 0,03 m thick XPS insulation boards; 0,06 m thick XPS edge strips are applied to a base plate that measures 0,46 m × 0,43 m with a resulting specimen area of 0,17 m^2. The sample thickness

is 0,01 m and an air cavity at the back with the same thickness contains temperature and RH sensors too. The XPS sample frame joints and the sensor openings through the sample frames were hermetically sealed with aluminium tape. The temperature and humidity sensors were secured in the air space of the mixing box, and calibrated to five humidity levels using the reference apparatus: a Mitchell dew point monitor Optidew.

5.1.1 Gypsum plaster and wood fibre: measurement of hygroscopic properties

Aim of this section is to compare two building materials with different buffer capacities. For this purpose the wood fibre and the gypsum plaster were chosen to be measured in the climate chamber. As the wood fibre, due to its sorption properties, reacts in a more sensitive way to the transient change of air humidity, the effect of hysteresis is more visible.

The wood fibre specimen has been automatically weighed every 60 seconds for 45 days, setting its dry density as Tara; temperature and relative humidity were also continuously monitored through sensors positioned in front of and behind the XPS box. To minimize the external influences the measuring system has been built in a controlled climate room with a temperature of 22 °C and a relative humidity of 50%.

The air humidity was kept constant for three to four days at 21%, 45%, 70% and 90% using increasing step functions. The air humidity was decreased using the same steps in descending order. Relative humidity in front and behind the specimen and change in mass were monitored for the different steps during both increasing and descending trends (Figure 5.2).

The covered range of relative humidity has allowed the evaluation of the material behaviour in the hygroscopic range, excluding liquid transport ($\varphi > 0,98$). Temperature was maintained constant (23 °C) throughout the experiment.

Wood, along with many porous materials, exhibits a notable difference between the amount of moisture contained in the material (at specific air hu-
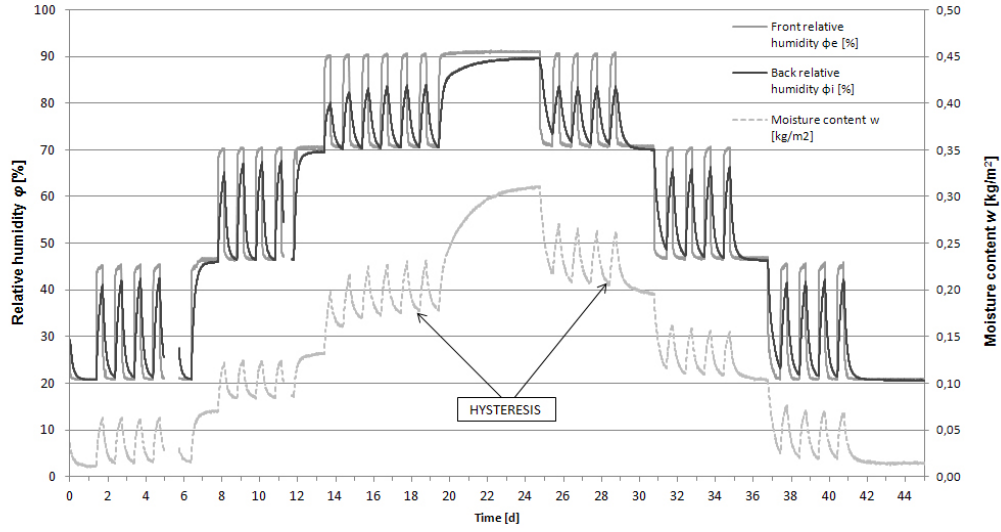
Figure 5.2: Measured sorption and desorption step cycles during the experiment for wood fibre.

midity) for humidification and drying. This effect is hysteretic. The research conducted by Enderby (1955) and Everett (1967) described the hysteretic effects in nature (independent domain theory). Based on their studies, Mualem postulated his phenomenological approach for modelling hysteretic processes in concrete floors using moisture absorption or desorption from porous materials (Mualem, 1973a,b). Mualem's independent domain theory hypothesizes that each pore volume forms an isolated system, and the medium is characterised by the pores distribution function. The function depends upon the radii of the pore openings and the radii of the individual pores based on the simplified theory of spherical pores.

The hysteretic behaviour is clearly visible in Figure 5.2 where the moisture content of the specimens, i.e. during the 70-90% RH step, is higher for the drying phase than for the wetting one. The high buffer capacity of the material produces an important difference in relative humidity levels between the air in front and behind the specimen, which increases with increasing RH step due to the inverse relationship between vapour permeability and moisture content inside the pores. Despite the reduced thickness (10 mm), this means a lower velocity in vapour transmission from the exposed surface

to the one on the air cavity for high RH levels because of the increasing number of saturated pores. The same effect occurs in the desorption phase, whereby the air present in the cavity reaches the hygroscopic equilibrium with the air in the climate chamber more slowly.

The step-function method in transient regime highlighted the dynamic response of the material when subjected to cyclic moisture loads, as indeed happens in real occupied environments with. In this case a 8 hours high-moisture level, followed by a 16 hours low-moisture level schedule was planned. The method therefore wants to study the buffer potential as well as the moisture sorption-desorption velocity. Before the descending phase the specimen was subjected for a longer period to the 90% RH level in order to reach the equilibrium moisture content and emphasize the hysteresis effect.
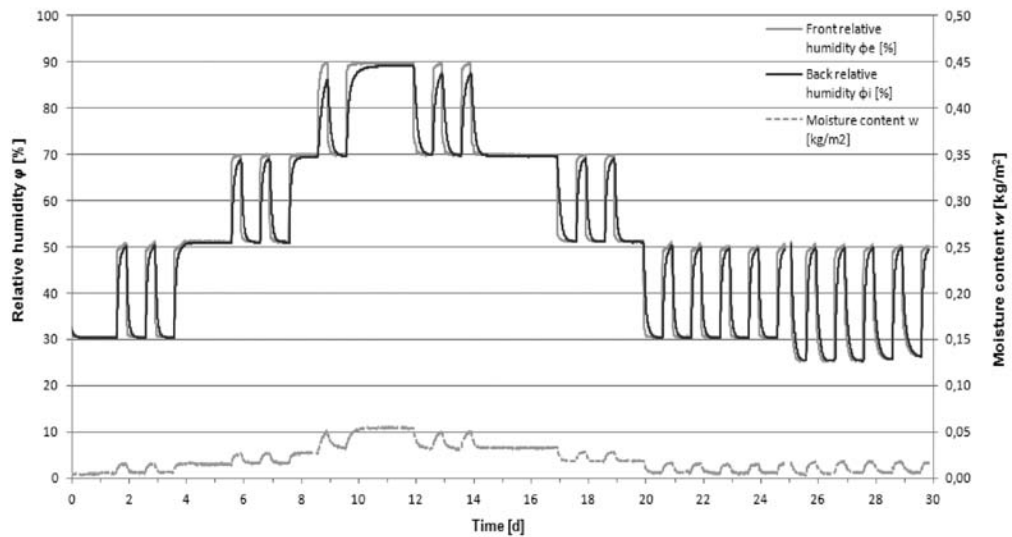
Figure 5.3: Measured sorption and desorption step cycles during the experiment for gypsum plaster.

The experimental test on the Gyproc gypsum plaster named "Pronto Grezzo" had the same purpose of the measurements made on the wood fibre. In this case the air humidity was kept constant for two days at 30%, 50%, 70% and 90% also using increasing step functions. In the gypsum plaster case the provided cycles were planned less in number than for the wood fibre. This was possible as a result of the rapid achievement of the stabilized periodic

regime by the specimen, of which a much smaller buffer capacity can be seen in favour of higher transmission properties (Fig.5.3). The desorption occurs faster and the RH difference between the two sides of the specimen at 70-90% step is much lower than in wood fibre; the anisotropic nature of the latter influences a lot its hygroscopic performance.

The mass change during the experiment is much lower than in the previous case, denoting a poorer hygroscopic performance with respect to wood fibre; moreover, for the same 8-16 h scheme, the higher the RH step the lower the desorption velocity. This is due to the smaller pore size of gypsum plaster and to the bond that form between water vapour and the dissolved salts (calcium sulfate dihydrate), which make slower the release process at high vapour concentration levels.

5.1.2 Calculation of sorption isotherm and vapour permeability

In this Chapter a comparison between applied methodology and standards UNI EN ISO 12571 (2013) and UNI EN ISO 12572 (2006) will be carried out.

The adopted methodology (Korjenic and Bednar, 2011) for the calculation of the vapour permeability and of the equilibrium moisture content at the different relative humidity steps is based on the control volumes method, where the 10 mm thick specimen was discretized in 5 internal nodes and 2 surface nodes (Figure 5.4).
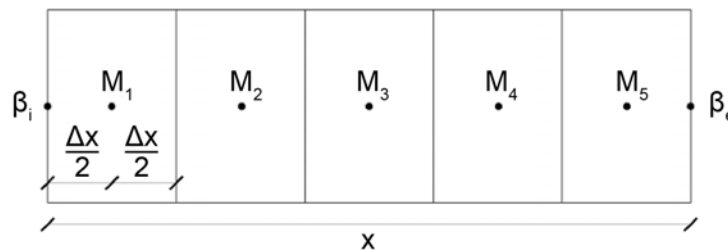
Figure 5.4: The control volumes discretization.

With reference to Equation 3.6 the change in mass, or moisture content Δw [kg/m³] in discretized form reads:

$$\Delta w = \frac{\dot{g}_{v,left \to cell} - \dot{g}_{v,cell \to right} \cdot \Delta t}{\Delta x_{cell}} \qquad (5.1)$$

where Δt [s] is the time step and Δx_{cell} [m] is the thickness of the cell. According to the vapour permeance M [kg/m²s Pa] equation:

$$M = \frac{1}{\frac{1}{\beta_i} + \sum \frac{x}{\delta} + \frac{1}{\beta_e}} \qquad (5.2)$$

and considering $M_{surf,i} = \beta_i$ and $M_{surf,e} = \beta_e$ at the boundaries, the density of water vapour flow $\dot{g}_v$ in discretized form reads:

$$\dot{g}_{v,left \to cell} = \frac{M_{left} \cdot M_{cell}}{M_{left} + M_{cell}} \cdot (p_{v,left} - p_{v,cell}) \qquad (5.3)$$

$$\dot{g}_{v,cell \to right} = \frac{M_{right} \cdot M_{cell}}{M_{right} + M_{cell}} \cdot (p_{v,cell} - p_{v,right}) \qquad (5.4)$$

where the permeance of the cell M_{cell} is:

$$M_{cell} = \frac{2 \cdot \delta_{cell}}{\Delta x_{cell}} \qquad (5.5)$$

The moisture content $w_{cell}(t_1)$ at time step t_1 is:

$$w_{cell}(t_1) = w_{cell}(t_0) + \frac{[\frac{M_{left} \cdot M_{cell}}{M_{left} + M_{cell}} \cdot (p_{v,left} - p_{v,cell}) + \frac{M_{right} \cdot M_{cell}}{M_{right} + M_{cell}} \cdot (p_{v,cell} - p_{v,right})]}{\Delta x_{cell}} \cdot \Delta t$$
$$(5.6)$$

where $w_{cell}(t_0)$ is the moisture content at the previous time step. This simulation approach neglects the effect of hysteresis in the sorption/desorption process - as hysteresis is not modelled - and does not assume a local equilibrium between air and material, but inside the material.

The latter aspect represents the most important difference with respect to the approach of the standard UNI EN ISO 12571 (2013), and more precisely over the climatic chamber method here described (Paragraphs 7.3.1, 7.3.2 and 8.1):

> **Sorption curve**. *Put the specimen, if necessary in the weighing cup, in the drying oven and dry it until constant mass at the temperature specified in UNI EN ISO 12570 (2013). Constant mass is reached if the change of mass between three consecutive weighings, each made at least 24 h apart, is less than 0,1 % of the total mass. Put the test specimen in the climatic chamber. At first the humidity in the climatic chamber is the lowest of the range of values chosen for the test. Periodically weigh the specimen in the climatic chamber until it is in equilibrium with the environment (constant mass). Repeat the procedure for increasing humidities. A minimum of four approximately evenly spaced humidities in increasing order shall be selected in the range of 30 % to 95 % relative humidity.*

> **Desorption curve**. *The starting point for desorption is at a relative humidity of at least 95 %. This must be the point of the sorption curve or might be reached by sorption from dried test specimen. Put the test specimen in the climatic chamber. Periodically weigh the specimen in the climatic chamber until it is in equilibrium with the environment (constant mass). Constant mass is reached if the change of mass between three consecutive weighings, each made at least 24 h apart, is less than 0,1 % of*

*the total mass. Repeat the procedure for decreasing humidities.
A minimum if four approximately evenly spaced humidites in de-
creasing order shall be selected in the range of 95 % to 30 %
relative humidity.*

Hygroscopic sorption*. The moisture content, u, is calcu-
lated as follows for each specimen: $u = \frac{m-m_0}{m_0}$. For the sorption
curve or for the desorption curve, take the mean of the calculated
moisture contents for a set of specimen at each relative humidity.
After calculation of the mean moisture content of the various test
specimens at each relative humidity the sorption and desorption
curves can be drawn by joining the data points with straight lines.
[...].*

It is clear that the assumption of a local equilibrium only inside the mate-
rial results in an optimization of the measurement times, as it is not necessary
to wait for the sample to reach an equilibrium with the air in contact with,
and to repeat the weighing every 24 hours until the difference between the
results can be neglected. The transient regime for measuring those material
properties usually determined in steady-state conditions enables to charac-
terize the dynamic response of the material as actually happens in environ-
ments occupied according to certain time schedules. The method also allows
to combine the gravimetric measurement of the moisture content described
in the UNI EN ISO 12571 (2013) with the methodology of measurement of
the vapour transmission properties reported in UNI EN ISO 12572 (2006),
optimizing the time-consuming experiments related to the hygroscopic prop-
erties of materials.

A water vapour transmission test is commonly referred to as cup-method,
because the general measuring principle is sealing a vapour tight cup con-
taining a desiccant or saturated salt solution, with the test material. The
desiccant or saturated salt solution will realise a constant relative humid-
ity below the sample and when the cup is then placed in a test chamber
at constant temperature but at different relative humidity than the one in

the cup, a vapour pressure gradient is realised across the specimen. Regular gravimetric measurements of the cup are used to determine the weight gain (or loss) of the cup and hence the moisture flux g_v through the specimen. Assuming that the whole process can be described by Fick's law for vapour diffusion the water vapour permeability δ of the material can be determined. In Europe the vapour permeability is usually replaced by the vapour resistance factor μ (-) or equivalent air layer thickness s_d (m) as typical vapour transfer property of the building material:

$$\dot{g}_v = \delta_p \frac{\Delta p_v}{x} = \delta_a \frac{\Delta p_v}{\mu \cdot x} = \delta_a \frac{\Delta p_v}{s_d} \tag{5.7}$$

where δ_a [kg/(m s Pa)] is the the water vapour permeability of stagnant air.

As in the standard procedure, before testing the test specimens have been stored at (23 ± 5) °C, (50 ± 5) % relative humidity for a period long enough for their weight to stabilise and to allow the calibration of the weighing device. While the test conditions specified in the standards refer to specific values of relative humidity on the dry/wet side of the specimen (see figure below), and a constant temperature ($\pm$ 0,5 K) and RH ($\pm$ 3 %) chamber, the adopted methodology can be applied to non-standard intervals depending on the range you wish to investigate by controlling the humid air properties in the climate chamber as for the sorption curves method.

Dry cup tests (condition A) give information about the performance of materials at low humidities when moisture transfer is dominated by vapour diffusion; *wet cup* tests (condition C) gives guidance about the performance of materials under high humidity conditions. As stated in Roels et al. (2010), to validate models that simulate moisture buffering of hygroscopic materials, new experimental data are needed that accurately quantify heat and moisture transfer between humid air and hygroscopic materials. Anyway, apart from the lack of good benchmark cases, also attaining uniformity in mea-

Set	Condition °C - % RH	Temperature °C	Tolerances			
			Relative humidity %			
			Dry state		Wet state	
			Set point	Tolerance	Set point	Tolerance
A	23 - 0/50	23 ± 0.5	0	+ 3	50	± 3
B	23 - 0/85	23 ± 0.5	0	+ 3	85	± 3
C	23 - 50/93	23 ± 0.5	50	± 3	93	± 3
D	38 - 0/93	38 ± 0.5	0	+ 3	93	± 3

Figure 5.5: Test conditions in UNI EN ISO 12572 (2006)

suring material properties remains difficult. For this reason it was decided to perform first an inter-laboratory comparison of the measurement of the hygric properties of porous materials by means of a round robin test (Roels et al., 2004). Not all material properties were measured, but the round robin focussed on those properties relevant for indoor moisture buffering: the water vapour transmission properties and the sorption isotherm, according to the described international standards. Nevertheless an unacceptable spread in results was found and some corrections due to the use of different test assemblies were necessary; especially the coated specimens showed a notable spread. A part of this research (Chapter 4.2) was dedicated to the demonstration of the coating influence on the hygroscopic performance of gypsum plasters.

By using the described numerical model, the simulation of the sorption and desorption cycles at different relative humidity levels was carried out considering the measured boundary conditions. The input values are:

- the partial water vapour pressures p_v [Pa] derived from the measured temperature and relative humidity on both sides of the specimens;

- the weighed mass of the specimen, corresponding to the water content w [kg/m^3]

In the described model the surface moisture transfer coefficient is $\beta_i =$
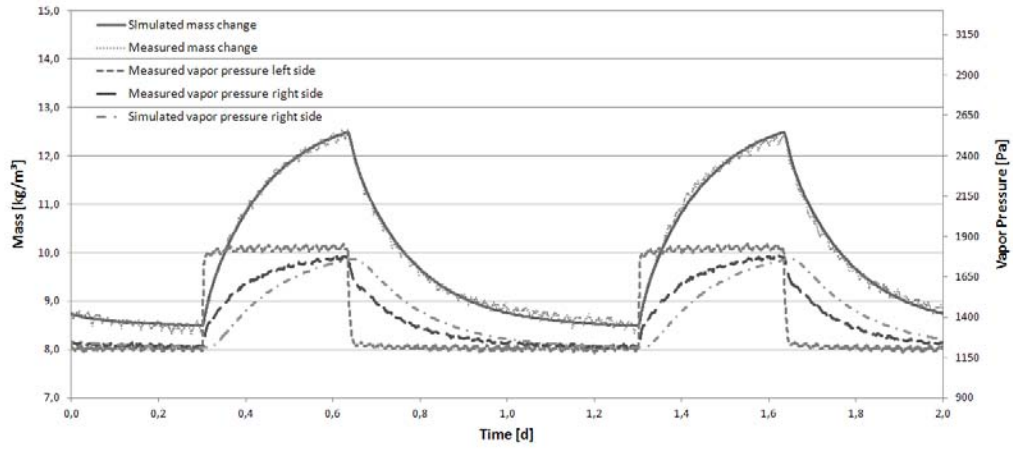
Figure 5.6: Fitting curves of sorption/desorption cycle for 21-45 % RH step change; wood fiber.
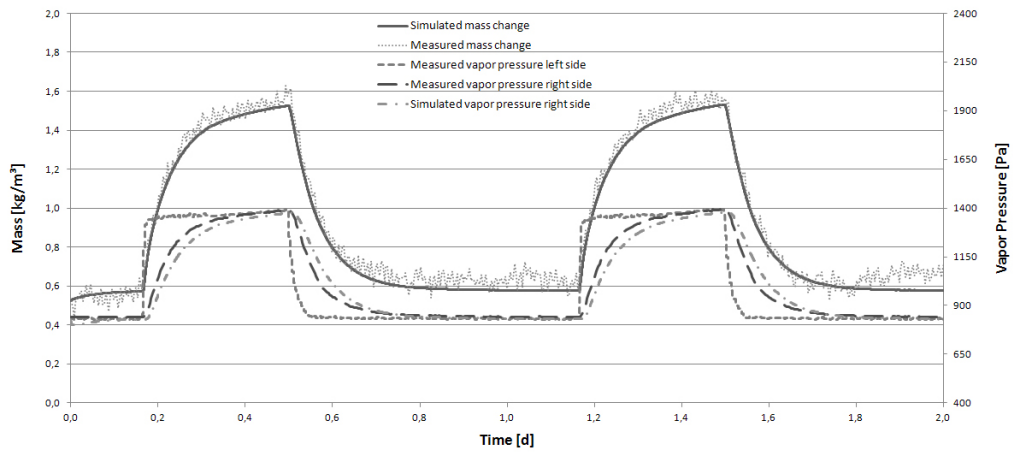
Figure 5.7: Fitting curves of sorption/desorption cycle for 30-50 % RH step change; gypsum plaster.

65

$2 \cdot 10^{-8}$ kg/(Pa m^{2}s) as in the NORDTEST Project (Rode et al., 2003). The same value will be used in the next simulation models.

As the hysteresis effect is not modelled, the moisture uptake and release has been fitted by two different curves for each RH transient step; both curves range between the upper and lower edge of the measured cloud of data as shown in Figure 5.8.
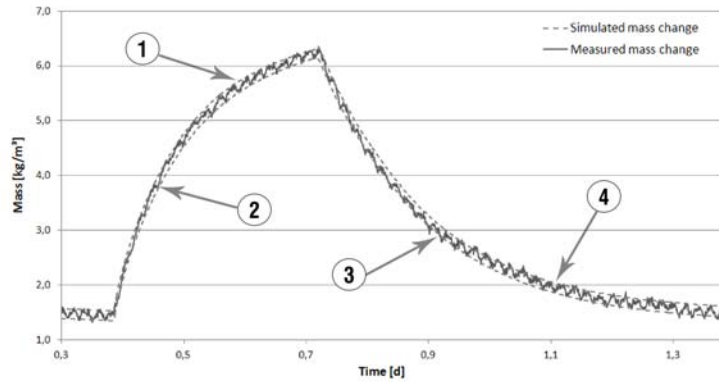
Figure 5.8: The upper and lower fitting curves of sorption/desorption cycle for 21-45 % RH step change; wood fibre.

Therefore the fitting process for each RH step resulted in the determination of 4 different values of vapour permeability - 2 for the sorption phase and 2 for the desorption phase, according to the derivative of the fitting curve - and 4 different values each for the minimum and maximum water contents. Of the latter, the average value between the maximum and minimum values for the same curve has been calculated in order to characterize the RH range (also represented with a mean value, see Tables 5.1 - 5.2) by means of a permeability value associated with an equilibrium moisture content $\bar{w}$.

The fitting has been carried out for the 6 RH steps (from a to f) generating a cloud of values of vapour permeabilities (Fig. 5.9-5.10).

The same procedure was attended to obtain the water content represented by the sorption and desorption curves. In this case the spread on results was less pronounced (Figure 5.11) and both the sorption and the desorption

66

Table 5.1: Increasing and decreasing RH steps with corresponding mean values for wood fibre.

Increasing RH steps [%]	Decreasing RH steps [%]	Mean RH value [%]
a) 21-45	d) 45-21	33
b) 46-70	e) 70-46	58
c) 71-90	f) 90-71	80,5

Table 5.2: Increasing and decreasing RH steps with corresponding mean values for gypsum plaster.

Increasing RH steps [%]	Decreasing RH steps [%]	Mean RH value [%]
a) 30-50	d) 50-30	40
b) 50-70	e) 70-50	60
c) 70-90	f) 90-70	80
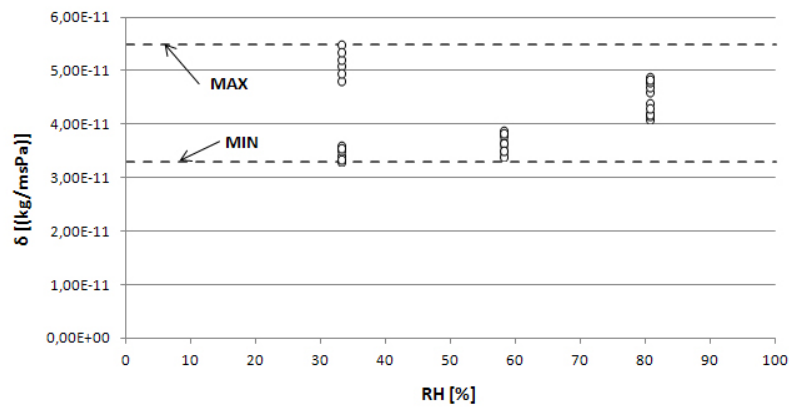
Figure 5.9: The generated cloud of vapour permeabilities for wood fibre derived from the numerical fitting.

67
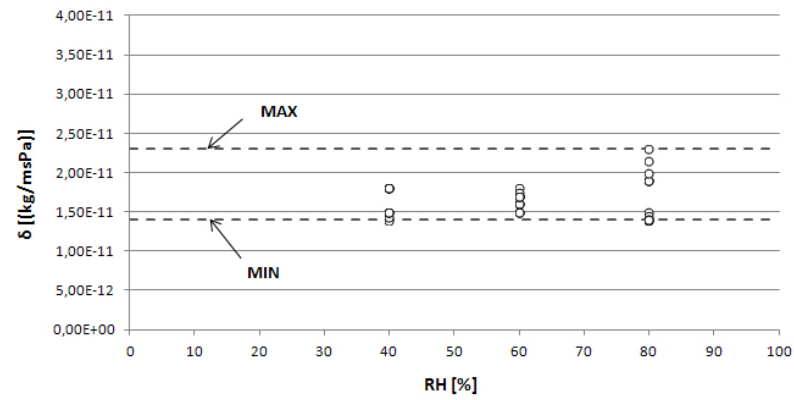
Figure 5.10: The generated cloud of vapour permeabilities for gypsum plaster derived from the numerical fitting.
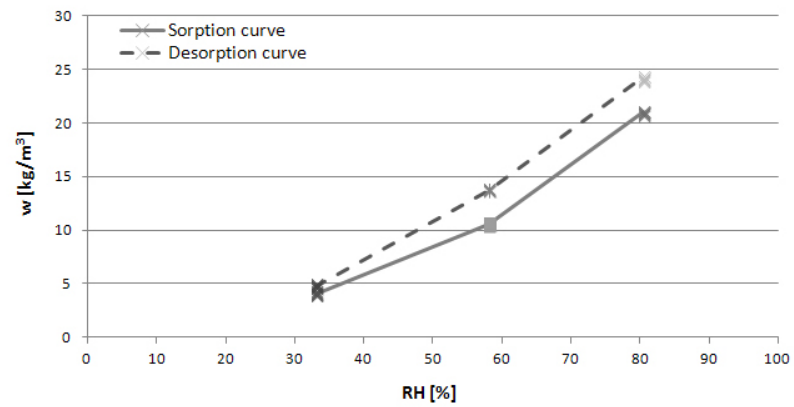
Figure 5.11: The generated sorption and desorption curves for wood fibre derived from the numerical fitting.

curves were denoted by a compact range of values. Anyway, even in this case an average value of w was calculated for each RH step.

68
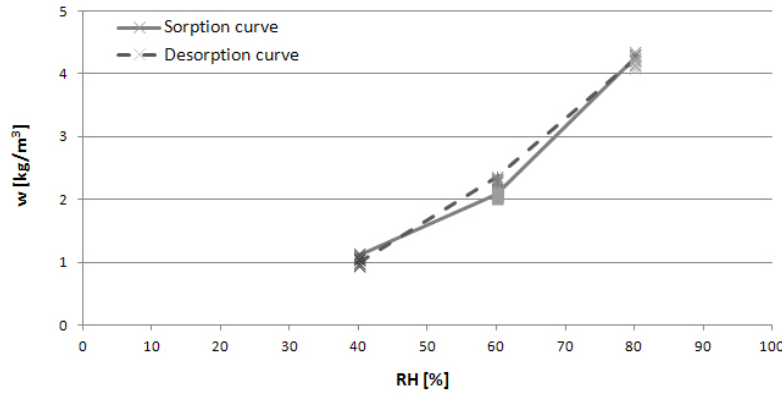
Figure 5.12: The generated sorption and desorption curves for gypsum plaster derived from the numerical fitting.

5.1.3 Measurement of *Moisture Buffer Value*

Apart from the will to use an international parameter - the MBV - to characterize the tested materials and give the manufacturers as Saint-Gobain PPC Italy the opportunity to compare their products with those from other industries, the choice of using a transient humidity range as [0,33-0,75] aimed at investigating the hygric performance of components in that interval of values which is usually advisable to comply in order to maintain optimum conditions of hygrothermal comfort for the user.

For this reason an MBV test was performed with a dual purpose of collecting new data on commercial products and of validating HAM-models able to simulate this very behaviour. The adopted numerical model was then validated by fitting the measured Moisture Buffer Value (MBV) test which was carried out according to the NORDTEST Protocol scheme (Rode et al., 2005) and by comparing the simulation results to those obtained from MB-Vsim, a specific arrangement of HAM-Tools modules (Ramos et al., 2012). The simulation tool is analysed in Chapter 4.

As in the previous test, the specimen were preconditioned and then put in the climatic chamber. Eleven MBV cycles were performed in order to reach the stabilized regime; the last 2 cycles were then used for the fitting process as shown in Figure 5.13.

69
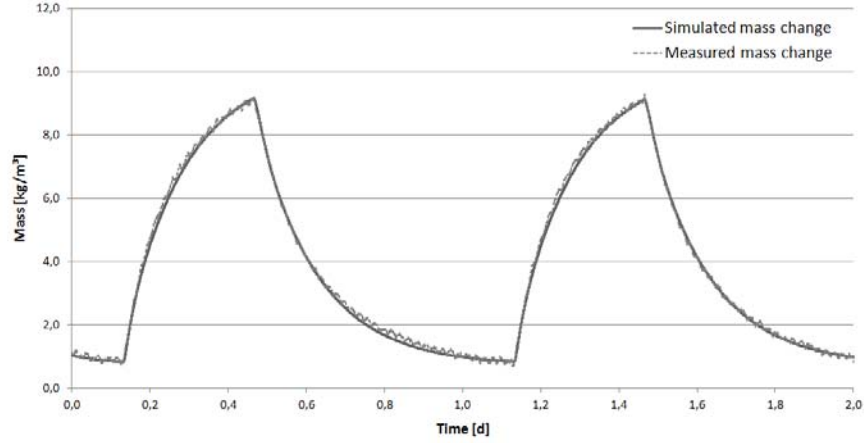
Figure 5.13: Fitting curves of MBV cycle (33-75 % RH); wood fibre.

The accuracy of the experimental results and the great care with which the measurements were conducted led to very satisfying matchings between the real behaviour of the specimens and the simulated one. As mentioned earlier, a simulation of the MBV test was also carried out with the MBVsim model in order to compare the two numerical solutions and validate the latter. The vapour permeability and sorption isotherm values calculated through the adopted model were used as input to characterize the material in the MBVsim model, while the indoor surface moisture transfer coefficient was set $\beta_i = 2 \cdot 10^{-8}$ kg/(Pa m^{2}s) as in the numerical solution, while no moisture exchange was allowed towards the back side of the specimen and $\beta_e = 1 \cdot 10^{-50}$ kg/(Pa m^{2}s).

The results showed that the numerical solutions of both simplified models fit the real behaviour with very good agreement (Fig. 5.14),

The results obtained for these materials are interesting since they showed that it was possible to simulate the hygric behavior of a material in a transient regime, using adequate numerical modelling and standard properties such as vapour permeability and sorption isotherm.

The simulations are, however, highly sensitive to the sorption curve used as data. For materials of low sorption capacity, such as the gypsum plaster
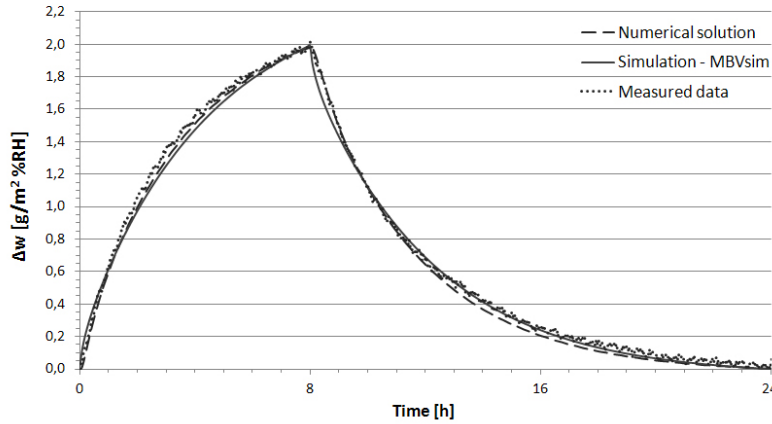
Figure 5.14: The MBV test simulation according to the adopted numerical model and to HAM-Tools; wood fibre.

samples, numerical results easily fit real behavior, while for the wood fibre samples, where the sorption capacity is a bit more relevant, the fitting between simulations and experiments is usually achieved only for a carefully selected scanning curve. In this case, both the materials real behaviours have been reproduced successfully.

The next steps aim at determining how much the hygroscopic performance of gypsum plaster, typically adopted as interior finishing in the traditional Italian building stock, is affected by the spreading of a coating layer.

5.2 Influence and characterization of coatings: the waterborne paint

In Italian buildings, especially dwellings, walls are very often plastered with gypsum plaster for levelling purposes. The gypsum plaster is generally covered with waterborne wall paint for decoration which represents a barrier for the water absorption or desorption. To know the hygric performance of a room in such real conditions, the water transfer properties of the painted gypsum must be known.

Wall paints can be roughly divided into waterborne and solvent borne paints. Waterborne wall paints are increasingly being used for their low odour and fast environmental friendly drying.

The newer waterborne paints are based on aqueous dispersions of synthetic vinyl-type binders, such as polyvinylacetate or polyvinylpropionate (co-)polymers, and acrylic polymers (Goossens, 2002). Moreover, paints containing volatile organic components have recently been prohibited by the European Commission for professional indoor use. The pressure to reduce volatile organic components and the industrial trend towards friendlier products with low toxicity of the product formulation led to the current expansion of waterborne types of coating.

The formulation of paint is determined by the type, size and/or concentration of its constituents in the wet state. Binders, surfactants, pigments, fillers, and additives control the characteristics of the final paint. The influence of surfactants, or more specific their hydrophilic part, on the moisture balance depends on their final location in the dry film.

Weathering has a significant influence on moisture transport properties. Because of their (slight) solubility in water, additives will evaporate and leach out of the coating. Consequently, the actual coating performance may vary in time, because the hygroscopicity decreases and the empty volume in the film increases. Coating free space may also result from degradation of binder and additives.

Fungal growth in indoor environments is always related to factors involving moisture. Many fungal problems occur in averagely dry places where dampness is only produced over short periods of time, like bathrooms. Porous finishing materials such as gypsum plaster may retain moisture over long periods of time, resulting in increased risks of fungal growth. In the case of transient moisture loads, fungal growth risks are therefore related to material properties. Considering this everyday reality, Adan et al. (2004) studied fungal growth of a single fungal species on gypsum-based materials both under steady state and transient indoor conditions to improve the understanding of the process inducing the fungal defacement of interior finishes.

Such improved insight should be a first step towards eco-friendlier, healthier and lasting control strategies of indoor fungal growth. Specially formulated organic coatings, preferably waterborne, may regulate moisture transport in gypsum based materials and consequently decrease risks of fungal growth. Experimental determination and description of moisture transport in the combined system of coating and base material are required for subsequent development of such coating systems.

Besides polymer, coatings consist of pigments and fillers and various additives, each of them affecting moisture transport. Pigments may lower moisture permeation, but non-ideality of pigmentation reduces this effect. Coating additives increase moisture solubility, but only little is known in detail.

In building science, knowledge is lacking about the moisture transfer properties of waterborne wall paints. Also the behaviour of painted substrates has not been examined sufficiently. The role of the paint constituents in the moisture transfer properties is unclear. This lack of knowledge is partly caused by the lack of simple measuring techniques. Anyway, aim of the present study is not the modelling or measuring of waterborne paints, but their influence once applied to the gypsum substrate, of which we calculated the hygroscopic properties when naked. This phase was carried out to obtain better insight into the moisture transfer properties of naked gypsum and painted gypsum.

Almost all dwellings in Italy have walls and ceilings plastered with gypsum. In controlling the relative humidity in these dwellings, the moisture behaviour of the gypsum plays an important role. The gypsum can absorb moisture from the indoor climate during periods of high humidity. It can also desorb moisture to the indoor climate in times of low humidity. It is well known that wood, for instance, is protected against high humidity by a coating. Wood can deteriorate due to the presence of water. However, gypsum does not deteriorate so strongly as wood does. Therefore, painting gypsum is not done to prevent deterioration of the gypsum. Gypsum is mainly painted for decorative reasons. However, it can also be a means to control the moisture transfer properties of the gypsum.

In this research, a specific product by Saint-Gobain PPC has been used, called Pronto Grezzo, composed by premixed gypsum plaster, anidrene, vermiculite, perlite, and specific additives. The measured hygroscopic properties of Pronto Grezzo are visible earlier in this chapter.

Below, it is shortly described how gypsum is produced. Three types of gypsum can be distinguished:

Gypsum $CaSO_4 \cdot 2\,H_2O$
Burned gypsum $CaSO_4 \cdot \frac{1}{2}\,H_2O$ (*Plaster of Paris*)
Dead burned gypsum $CaSO_4$

The gypsum found in nature is partly dehydrated to burned gypsum by heating it between 90 °C and 150 °C. Hardening the burned gypsum, $CaSO_4 \cdot \frac{1}{2}\,H_2O$ readily reabsorbs water under solidification and reconverts under swelling to the old condition ($CaSO_4 \cdot 2\,H_2O$). When gypsum is heated above 500 °C, dead burned gypsum is obtained, which only very slowly reacts with water. The hardening process is fast, therefore retarders are added to be able to apply the wet gypsum. The hardened gypsum consists of needle shaped entangled crystals. This creates a connected pore system. From this structure, the water transfer properties of gypsum can be explained.

After a drying period of one week, pieces of gypsum may still be present that have not reacted with the water. Gypsum continues to hydrate and may therefore disturb the water adsorption experiments. To obtain inert gypsum as much as possible, a second hydratation is carried out for one week. Afterwards, the gypsum is air dried at 50 % relative humidity as the other specimens.

In this phase two specimens of Pronto Grezzo gypsum plaster were actually prepared to be tested, and a twin climate chamber was set up to measure their hygroscopic properties simultaneously. Aim of this phase is a better understanding of the hygric performance of the same material when coated with different paints.

A first step consisted in making the 2 specimens in laboratory as accurate as possible in mixing the water/powder ratio, in order to achieve the same physical and chemical behaviour during the test. Probably due to the

74

uncertainty of the measurement instruments and to manual preparation of the specimens, the results show some deviation especially with regard to the sorption isotherm, which is shown in Figure 5.15.
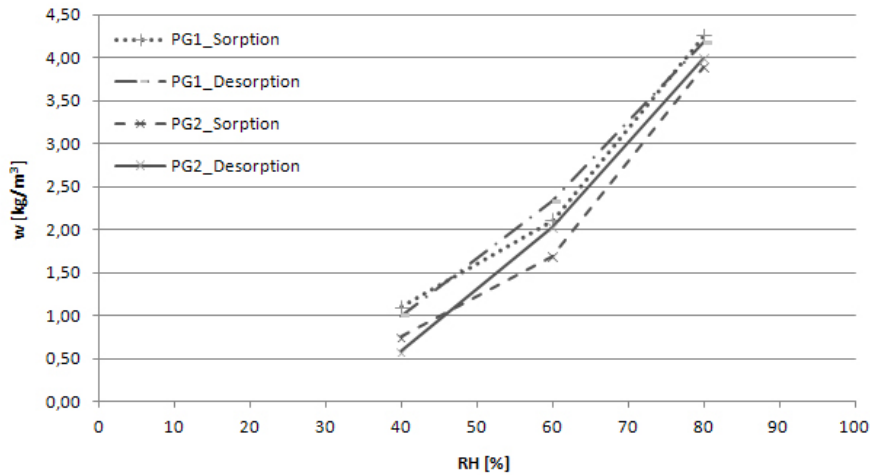
Figure 5.15: Sorption isotherms for the two Pronto Grezzo specimens (PG1 and PG2).

The deviation, obtained despite the two products were produced by mixing the ingredients in the same manner and under the same environmental conditions, and using the same measuring device, it is significant as with the utmost attention is possible to run into systematic and accidental errors.

First, a validation of the adopted numerical model and of MBVsim was carried out by fitting the measured data of naked gypsum plaster as shown in Figure 5.16 and 5.17. As the measured data for the 33-75 % RH step were not available, the fitting was carried out on the 30-50 % RH step. This process only aimed at confirming the validation the simulation tool already done with the wood fibre, as a different RH step cannot be compared to the MBV step.

Uncertainty of measured data is visible as well as the deviation between the 2 simulation models. However, the results show a good agreement between measured and simulated data.

In order to test two different waterborne paints commercially available in Austria which differ in the μ-value were used to coat the samples. The two
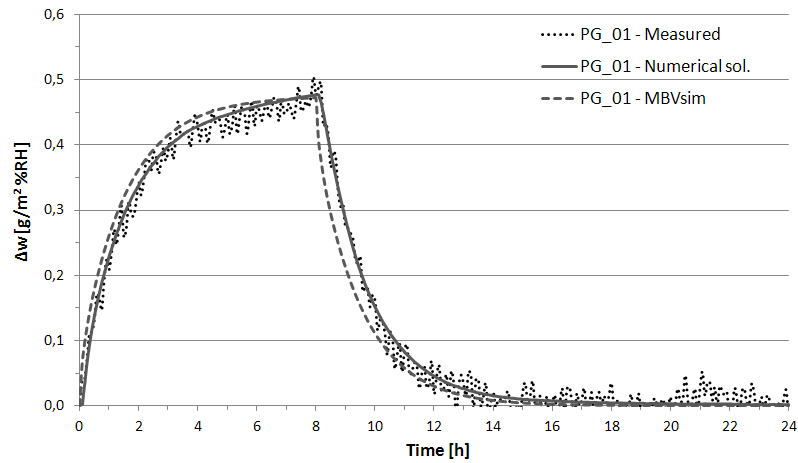
Figure 5.16: Fitting of Pronto Grezzo specimen PG1 using the adopted numerical model and the simulation tool MBVsim (30-50 % RH step).
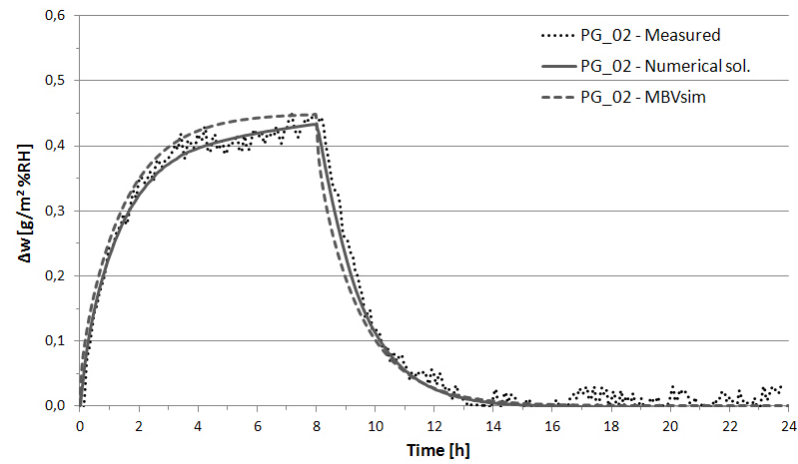
Figure 5.17: Fitting of Pronto Grezzo specimen PG2 using the adopted numerical model and the simulation tool MBVsim (30-50 % RH step).

paints are *Silkat-Innenfarbe* and *Objekt Meister-Weiß* by Farben Gnatz.

Once the MBVsim model has been validated (the matching was successful for both the wood fibre and the gypsum plaster), it was used to reproduce the MBV test in the climate chamber for every RH step. In this way the missing data can be simulated with a very good approximation, avoiding time-consuming experiments for additional measurement cycles. In Figure 5.18 and 5.19 the fitting of the coated specimens are shown and compared to the hygroscopic performance of the naked gypsum plaster simulated with MBVsim.

With respect to the previous matchings, two aspects differ during the fitting process:

- a minor spread on the measured data is visible for the coated specimens with respect to the uncoated ones, probably due to the paint contribution to uniform the material surface;

- an higher deviation is visible during the desorption phase for the data simulated with MBVsim.

In our case, the input data for the material properties ($\delta(w)$ and $w(\varphi)$) in MBVsim are those fitted through the numerical solution.

Unlike the numerical model, where each RH step results in a single value of vapour permeability, MBVsim uses the whole set of hygroscopic properties to characterise the material behaviour in transient regime, interpolating the values between the determined intervals in the range $0 < \varphi < 1$. This difference between the two models leads to the generation of a curve with an increased slope during the desorption process, which turns out to be faster.

Comparing the measurements for the uncoated and the coated specimens, the results show a decrease in the buffer potential equal to 15 % for the specimen coated with the *Silkat-Innenfarbe*, while the *Objekt Meister-Weiß* paint - which was characterized by an higher μ value - caused a decrease in the MBV equal to 23 % (see Figure 5.20).

In Ramos et al. (2012) different approaches were adopted to model the paint layer. In the first approach , the coating was simulated as a layer with
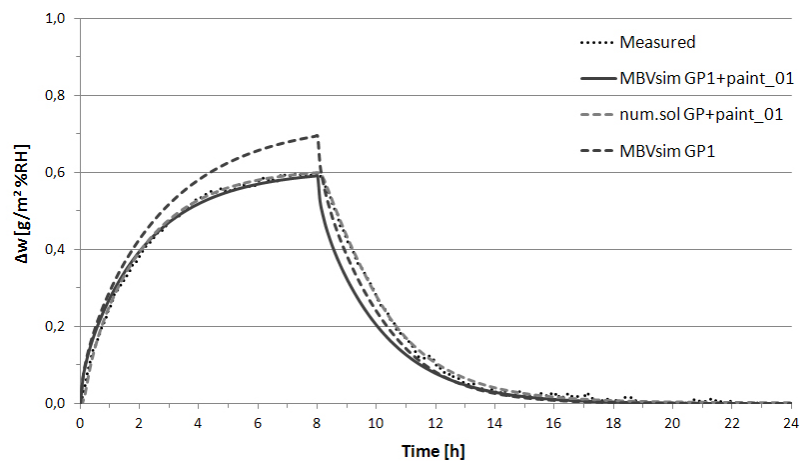
Figure 5.18: Fitting of Pronto Grezzo specimen PG1 coated with paint *Silkat-Innenfarbe*.
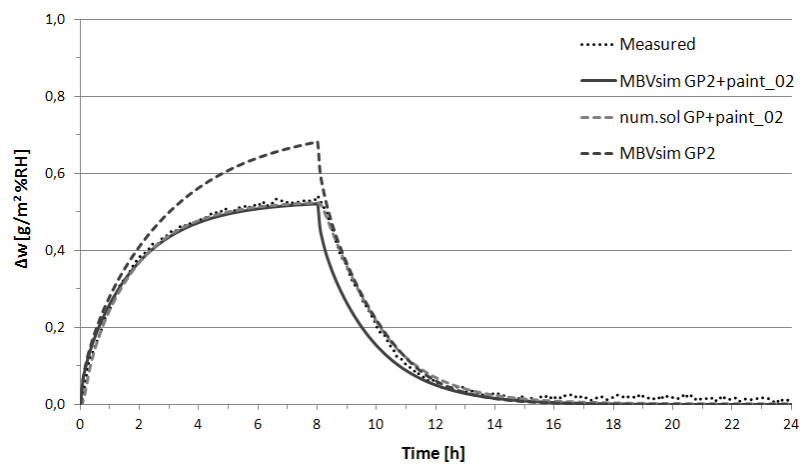
Figure 5.19: Fitting of Pronto Grezzo specimen PG2 coated with paint *Objekt Meister-Weiß*.

constant vapour resistance s_d (RH = 54 %), corresponding to the mean value in the given variation range. In the second approach, the s_d value of the coating was defined as a function of RH, where the latter was found as the average value between the material surface and the air in each calculation step. In the third approach the coating was modelled as a layer with moisture storage capacity. As there were no measurements of the coatings' sorption curve, specific data for simulation were taken from the literature (Goossens, 2002). Finally, an interpretation of the standard vapour transmission measurement procedure was performed, assuming a possible effect of hysteresis through a correction coefficient. The idea that supports this interpretation is that the coating's s_d value depends on moisture content and not on equilibrium RH, and so it is possible to find the correct value from the same basic data.

Since the modelling of the paint is not one of the objectives of this thesis, the influence of the coating was evaluated at the experimental level and then validated through the adopted simplified model in order to use it later to simulate the environmental performance of a room, where the different investigated materials are used as a finish.
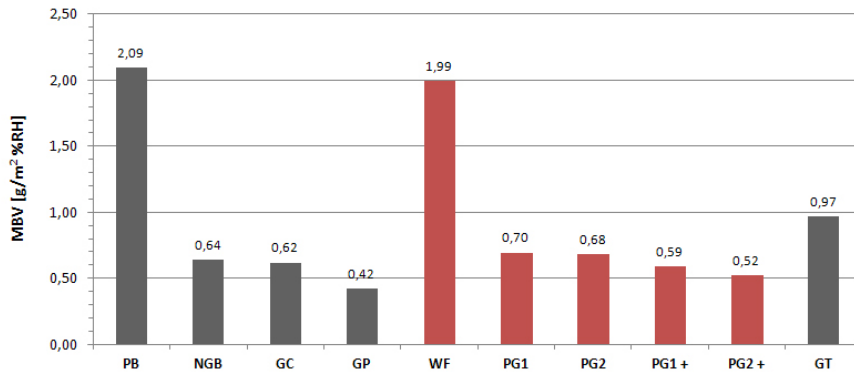
Figure 5.20: MBVs for different materials from literature (grey) and for the measured ones (red). PB: plasterboard, NGB/GC: gypsum board, GP: gypsum plaster, WF: wood fibre, PG1/PG2: naked Gyproc gypsum plaster, PG1+/PG2+: coated Gyproc gypsum plaster, GT: gypsum + lime plaster.

5.3 Uncertainty in analytical and numerical fitting of experimental data: influence on numerical simulation

Since for building materials a single value of permeability is usually given by the manufacturers, while in the numerical model which has been described $\delta = f(w, \varphi)$, the maximum and minimum value of the cloud of data generated during the experimental phase for each material were considered for a sensitivity analysis in order to evaluate how much the spread on results affects the hygroscopic performance of a material characterized by 2 different values of δ (for wood fibre $\Delta\delta_{min-max} = 2, 20 \cdot 10^{-11}$ kg/(m s Pa), for gypsum plaster $\Delta\delta_{min-max} = 0, 90 \cdot 10^{-11}$ kg/(m s Pa)).

The numerical fitting process resulted in a very good matching between the calculated and the measured data. As the aim of this study is also to consider the optimization of measurements by reducing the time of testing and the identification of the most relevant parameters for the proposed target, a sensitivity analysis was carried out by creating a correlation between the vapour permeability values and the water content values. This means combining the sorption curve first with the maximum and then with the minimum value of vapour permeability (kept constant); the same procedure was carried out for the desorption curve. In this way 4 scenarios were built and the same material was characterized by a normalized set of hygroscopic properties (Table 5.3).

The whole room simulation was performed by using HAM-Tools. A simple room with 3 layers exterior walls was chosen as case study: 10 cm foam insulation, 25 cm aerated concrete, 3 cm wood fibre. Apart from the measured properties of wood fibre, the material data were taken from Annex 24 (*Material Properties - Final Report, Volume 3*). A 1-D HAM (Heat Air and Moisture) transfer simulation has been carried out for the first week of January with Turin weather data.

In the 55 m^3 volume room the air temperature was maintained constant

Table 5.3: Scenarios for sensitivity analysis using wood fibre calculated properties.

N°	Curve	Vapor permeability [kg/(m s Pa)]
CASE 1	Sorption	$3,30^{-11}$
CASE 2	Sorption	$5,50^{-11}$
CASE 3	Desorption	$3,30^{-11}$
CASE 4	Desorption	$5,50^{-11}$

(20 °C), while the relative humidity was left floating and monitored; no solar radiation through openings was taken into account. An office moisture gain schedule of 80 g/h per person was set for a 10 people occupation from 9 to 17 h. The outdoor and indoor moisture transfer coefficient are $\beta_e = 2 \cdot 10^{-7}$ kg/(m s Pa) and $\beta_i = 2 \cdot 10^{-8}$ kg/(m s Pa) respectively; air change rates of 0,3 - 0,5 - 0,75 h^{-1} through a mechanical ventilation system with outdoor air conditions are simulated.

In order to determine how uncertainty on measured vapour permeability influences the hygroscopic behaviour of indoor finishing, the introduced sensitivity analysis with the different couplings was carried out. The results for the 3 scenarios using wood fibre as a finish are shown in figures 5.21, 5.22 and 5.23.

After the weekly RH trend using wood fibre was simulated, the same procedure was carried out by using the calculated properties of Gyproc Pronto Grezzo gypsum plaster.

Since at first sight the results for wood fibre - for which the difference between the maximum and minimum value of water vapour permeability were higher then for gypsum plaster - didn't produce a large spread in the RH trend, the simulation for Pronto Grezzo, less hygroscopic and sensible to variations, was performed only by using one of the two specimen's properties, which were actually very close (see Fig. 5.15). The results are shown in figures 5.24, 5.25 and 5.26.

Figure 5.21: φ trend for the 4 scenarios with a 0,3 h^{-1} air change rate. Wood fibre finishing.
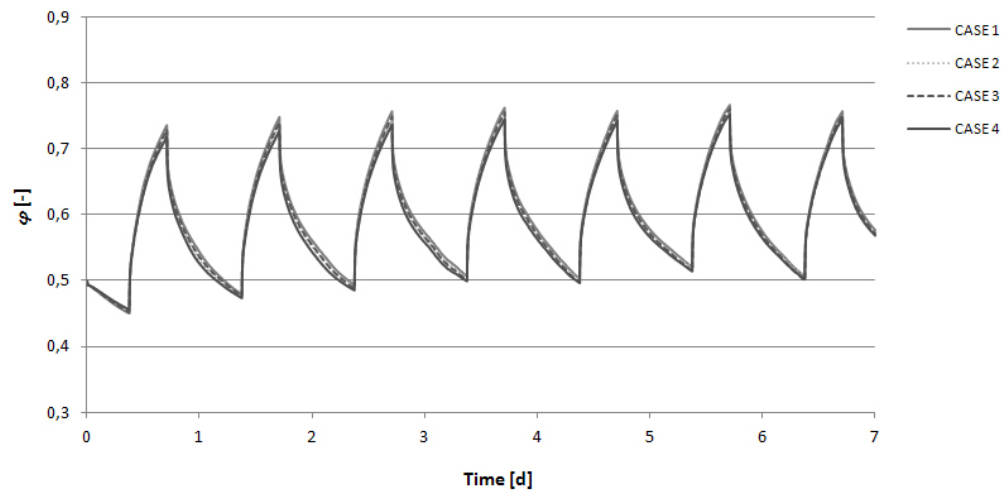
Figure 5.22: φ trend for the 4 scenarios with a 0,5 h^{-1} air change rate. Wood fibre finishing.
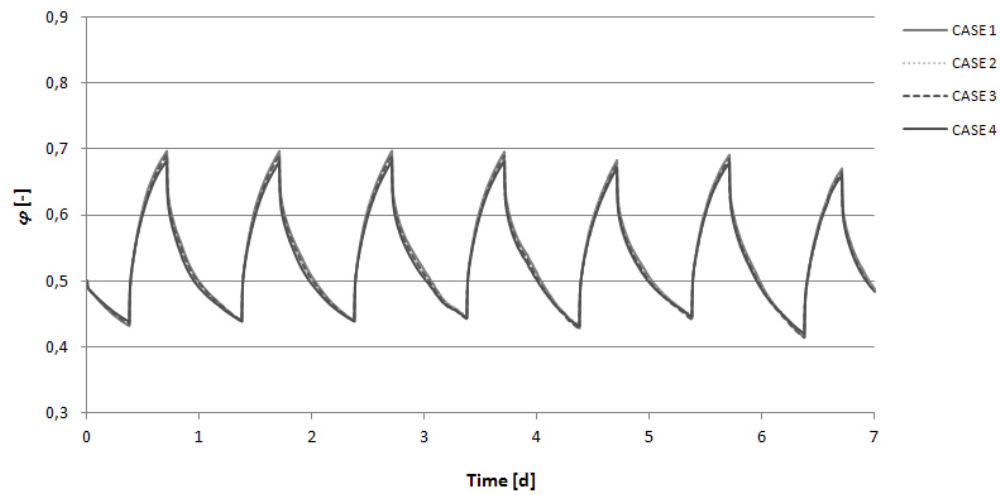
Figure 5.23: φ trend for the 4 scenarios with a 0,75 h^{-1} air change rate. Wood fibre finishing.
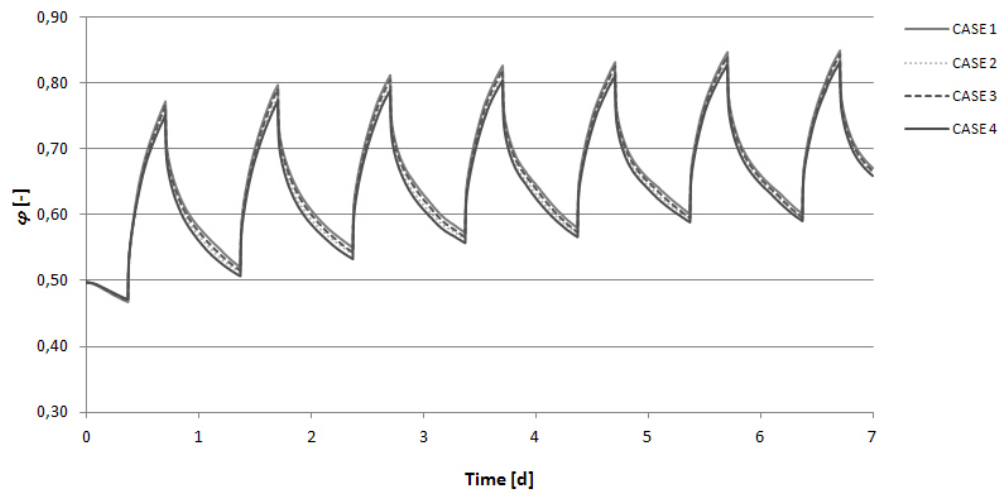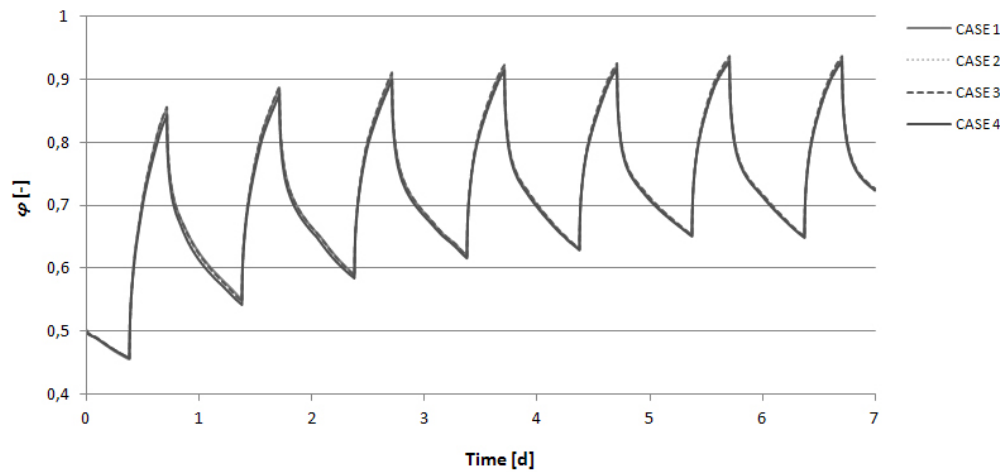

Figure 5.24: φ trend for the 4 scenarios with a 0,3 h^{-1} air change rate. Gypsum plaster finishing.
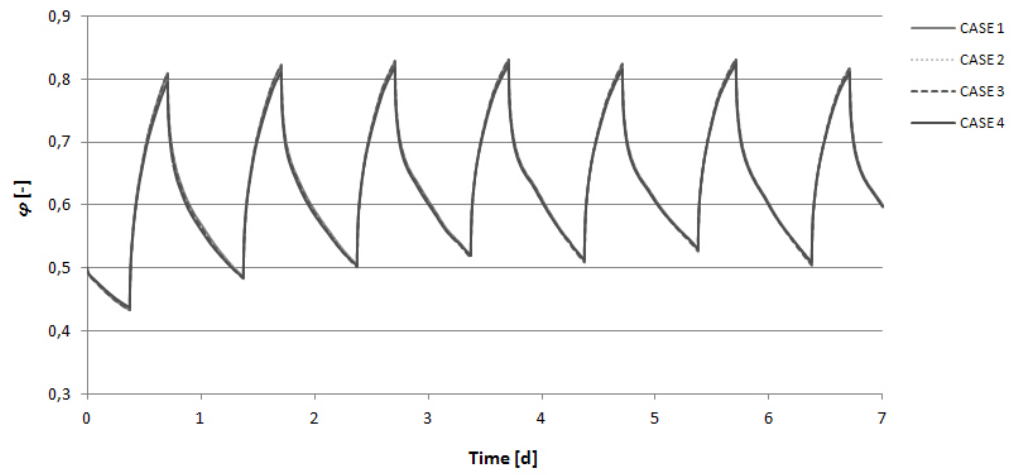
Figure 5.25: φ trend for the 4 scenarios with a 0,5 h^{-1} air change rate. Gypsum plaster finishing.
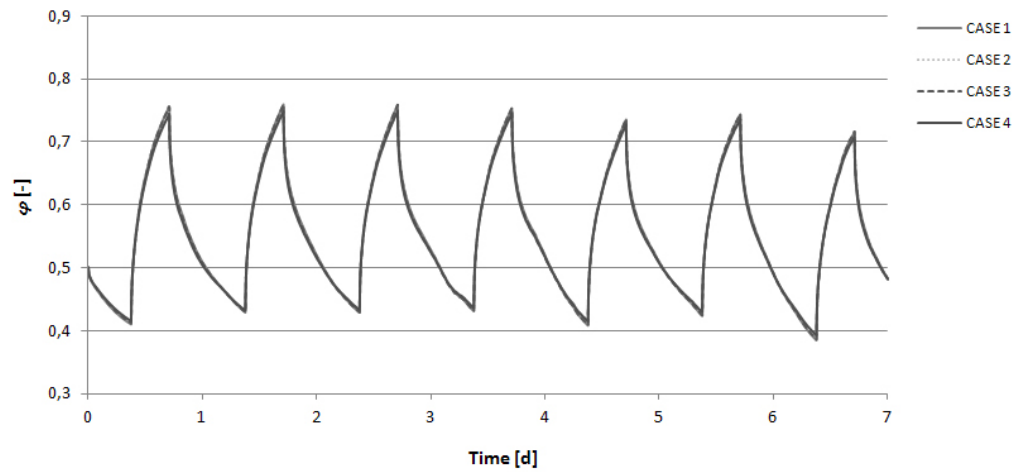
Figure 5.26: φ trend for the 4 scenarios with a 0,75 h^{-1} air change rate. Gypsum plaster finishing.

Apart from the higher buffer capacity of wood fibre in dampening the peaks of moisture production in the environment, which results in a reduced fluctuation of the air humidity during the loading cycles with respect to the application of the plaster, it is clearly visible that the deviations on results is not appreciable, especially when the plaster is applied. Although a considerable range of values has been generated by means of the best-fit process, the spread on results concerns the vapour permeability, while the sorption isotherm for both the wood fibre and the gypsum plaster didn't deviate significantly during the matching phase. The dynamic behaviour of the buffer materials is most likely influenced by the estimated equilibrium moisture content (the model assumes only the equilibrium between the air and the surface of the material) with respect to a variation of the diffusion properties which are, moreover, characterized by a different order of magnitude.

The only case where the variation of the hygroscopic properties leads to a minimum deviation is for the simulation scenarios where a 0,3 h^{-1} air change rate using the wood fibre is applied. The deviation is caused by the low ventilation rate which favours the diffusion mechanism through the finishing material and its buffering effect and by the uncertainty on the measured data. A deeper understanding of how much the variation of the ventilation rate and of the moisture production rate affect the RH trend inside the room will be analysed in Chapter 6.

In Fig. 5.27 the average value of relative humidity at the end of the week as function of the ventilation rate is shown for the two materials. When the wood fibre is analysed, a maximum $\Delta RH_{max} = 2\%$ between the simulations with a 0,3 h^{-1} is reached (66-68% RH), while for gypsum plaster the difference between the set of simulation with the same ventilation rate reaches $\Delta RH_{max} = 1\%$ (73-74%). In Fig. 5.28 the standard deviation of relative humidity for the considered scenarios represents the dynamic response of the finishing materials during the moisture loading signals.

After analysing the results, it is clear that a single RH step function is enough to characterize the hygroscopic properties (vapour permeability and sorption isotherm) of a porous material if the aim is simulating the room
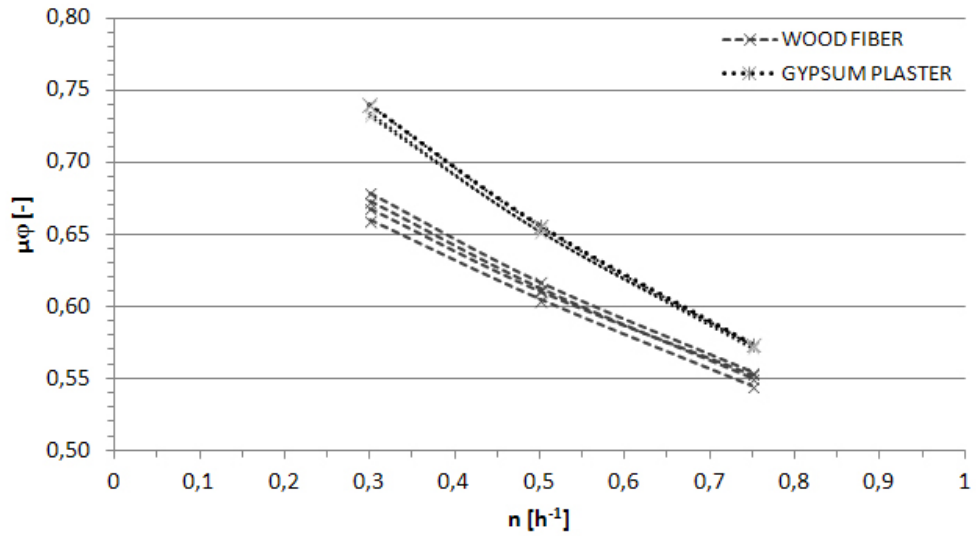
Figure 5.27: Average values of relative humidity for the four scenarios, with 0,3 - 0,5 - 0,75 h^{-1} air change rate. Wood fiber (WF) and gypsum plaster (PG) application.
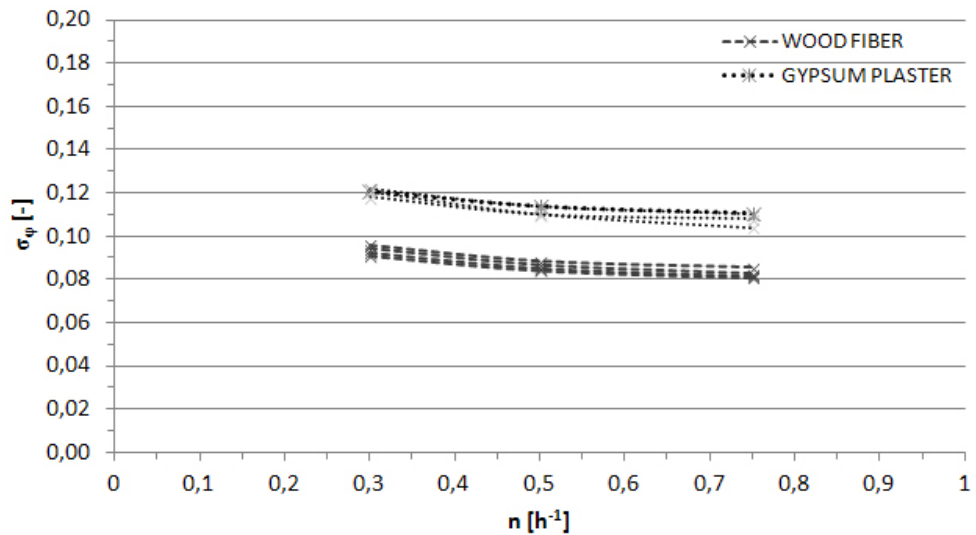
Figure 5.28: Standard deviation of relative humidity for the four scenarios, with 0,3 - 0,5 - 0,75 h^{-1} air change rate. Wood fiber (WF) and gypsum plaster (PG) application.

hygric performance in transient conditions with an HAM model. It would be recommendable to use the MBV step (33-75 %) in order to collect new experimental data to be compared with other results from literature by means of a unique index. HAM models such as HAM-Tools and the MBVsim arrangement have been validated for the MBV test simulation and the reliability of measured data was analysed. The study demonstrated as time-consuming experiment like those related to the measurement of the hygroscopic properties of materials, which can take more than 1 month in transient regime (45 days for the wood fibre and 30 days for the gypsum plaster) and even more in stationary conditions - according to the reference standards - can be reduced to a couple of weeks: the first for pre-conditioning the specimens (33 % RH, 23 °C) and the second for the measurement phase. Usually 4 days are enough to reach a stabilised regime for the specimen.

In Chapter 6 also the coated gypsum will be considered within the simulation of the room hygroscopic performance, underlining more how the action of painting the finishes in our environments modifies the ability of materials to moderate the humidity of the air, according to different ventilation rates and moisture production rates.

5.4   Discussion

An experimental determination of the hygroscopic properties of porous materials is needed to quantify the HAM-transfer between moist air and building envelope during transient changes in relative humidity. The main aim is to validate models able to simulate the moisture buffer of materials.

Although experimental data are available from literature, only carefully planned measurements are best suited for this model validation. This case study showed how vapour permeability and sorption isotherm can be determined by sorption and desorption cycles in transient regime. As uncertainty on measurements is given by neglecting the assumption of a local equilibrium, an analysis on reliability of data was carried out by simulating the sorption cycles for the different steps of RH and fitting the material properties. Afterwards a sensitivity analysis was carried out by taking into account the generated cloud of data to find out how much the spread on measurements influences the HAM simulation.

The simulation of an office room during a typical winter week in Turin, with an 9-17 h occupation schedule for moisture production, showed that no significant deviation of results was affected by using the different fitted sorption properties of wood fibre. As we can observe, the application of wood fibre causes a lower average value of relative humidity within the room, due to a higher MBV value. The more performing sorption properties of wood fibre lead to a higher spread in the results for the low air change rate (0,3 h^{-1}) with respect to the gypsum plaster, when considering the variation of the four scenarios. Anyway the value of the spread itself (2% ΔRH) can be neglected. Therefore, in the opinion of the author the investigation on the moisture buffer effect of hygroscopic materials should focus more on the position of such materials in the room and on the influence of ventilation.

Even the RH levels used for the measurements can be reduced and an average value of permeability can be used as representative of the measured product, avoiding time-consuming experiments and using every branch of the measurement to simulate the relative humidity using a model without hysteresis.

Chapter 6

The room factors in the HAM-transfer

The main objective of this section is to calculate by means of the numerical simulation the buffer capacity of gypsum plaster for different environmental conditions, in order to analyse the relationship between the buffer effect dependent on the material level and the hygroscopic performance influenced by the environmental factors applied to the internal environment.

The author underlines that the main aim of this research is the understanding of the material's hygroscopic performance by means of different testing conditions. For this reason the study does not focus on the accomplishment of optimal environmental condition for satisfying the user hygrothermal comfort according to the related standards with a proper environmental design, but wants to deepen the understanding of the dynamic response of porous materials. The research subject is therefore the building component and not the user.

6.1   Definition of the case study

The study involved the modelling of a single environment (simple room), in agreement with the dimensional standards determined by the UNI EN ISO

13791. The floor area is 19,8 m^2, for a total volume of 55,4 m^3. The geometry of the room is represented in Figure 6.1, while its dimensions are shown in Table 6.1.
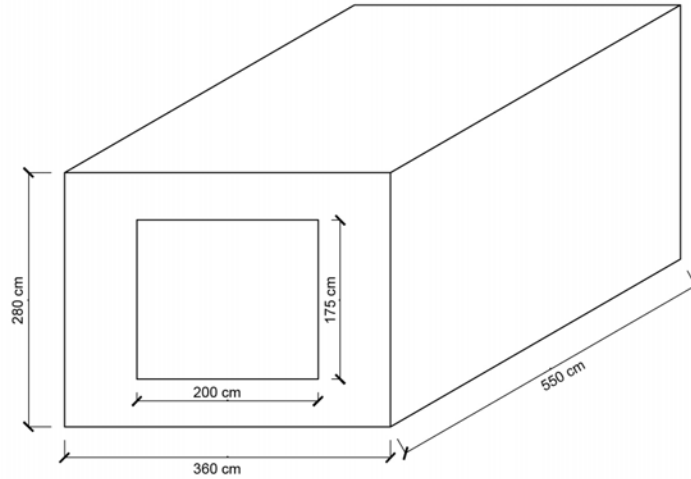
Figure 6.1: The simple room model according to standard UNI EN ISO 13791.

Table 6.1: Size and dimensions of the simple room building component.

Component	Size [m]	Area [m^2]
South window	1,75 × 2,00	3,00
South wall	3,60 × 2,80	6,58
East wall	5,50 × 2,80	15,40
North wall	3,60 × 2,80	6,58
West wall	5,50 × 2,80	15,40
Roof	5,50 × 3,60	19,80
Ceiling	5,50 × 3,60	19,80

The stratigraphy of the envelope has been defined for the modelling phase, with an internal finish based on gypsum plaster as regards the building components. In order to evaluate only the contribution of the internal layer in

90
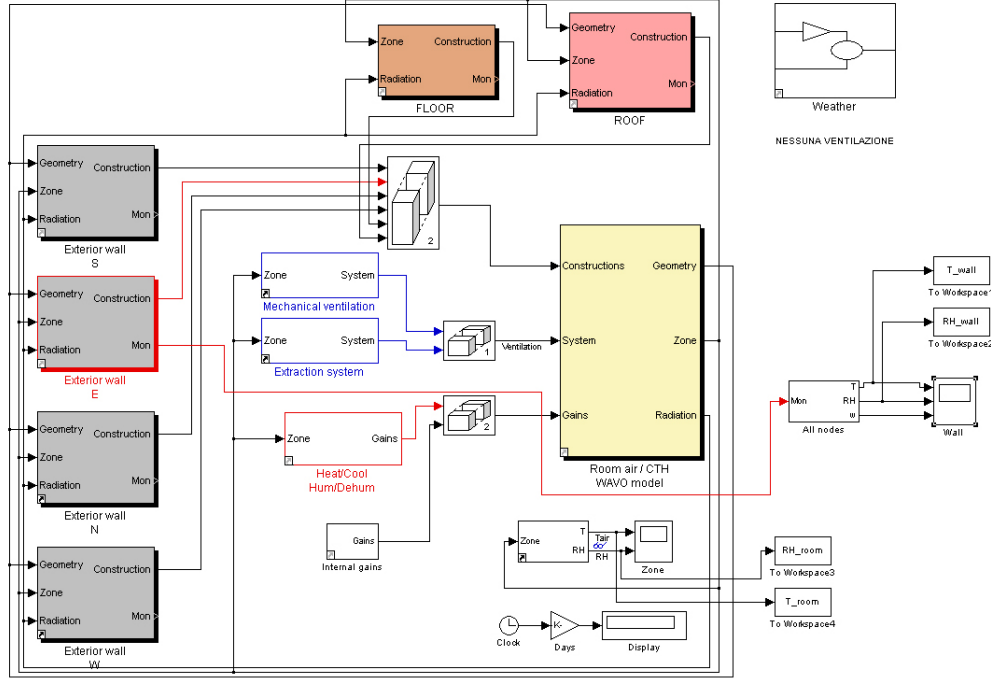
Figure 6.2: The test room model in HAM-Tools.

the hygrometric control, an additional resistance to steam and water was placed between the insulation and the plaster, for the walls (Fig. 6.4) and the roof, while the floor was considered against the ground.

Figure 6.3 shows the *Exterior Wall* block in HAM-Tools.

The case has been modelled according to the values reported in Table 6.2. Aside from the experimental data of the Gyproc gypsum plaster hygroscopic properties calculated previously (δ and $w(\varphi)$), those listed in Fig. 4.2 (Chapter 4) are the experimental material data calculated using a round robin test and reported in IEA Annex 24, subsequently used in IEA Annex 41 and inserted into the material database HAM-Tools software. As the focus is on the moisture buffer performance of the plaster, no measurements for its thermal properties were carried out but those from IEA Annex 24 were used.

The simulations were carried out for a period of 7 days (January 1$^{\text{st}}$ -
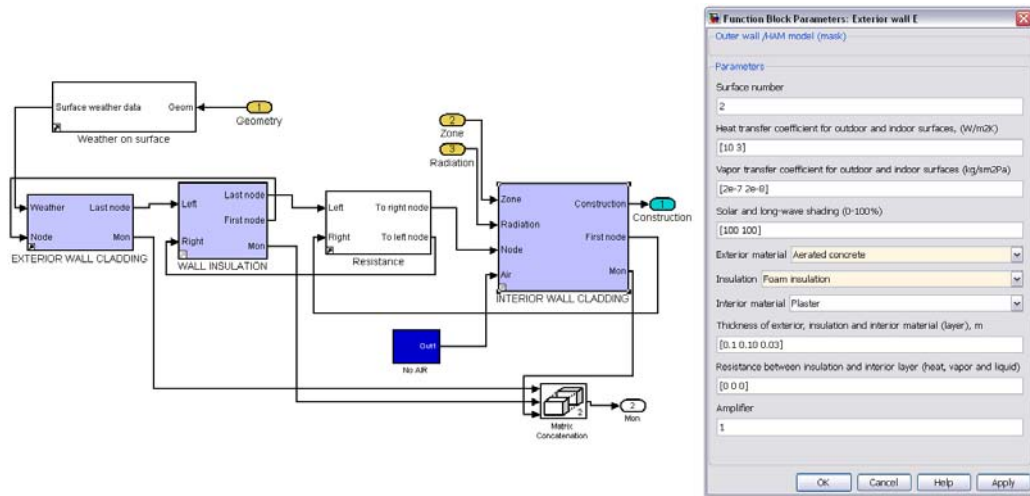
Figure 6.3: The *Exterior Wall* block in HAM-Tools.
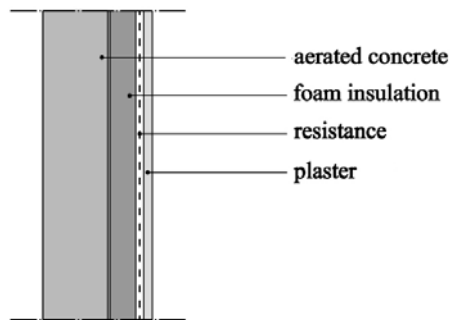
Figure 6.4: The exterior wall stratigraphy with the thermal, vapour and liquid resistance layer.

7th) using the weather data file for Turin. In Fig. 6.5 the trends of relative humidity and absolute humidity for the considered simulation period are shown and the average outdoor absolute humidity for each day is represented in order to be used during the moisture balance of the room air.

The climate file used derives from the IGDG - Italian Climatic data collection "Gianni De Giorgio" and has been adapted according to the HAM-Tools input format reported below.

Table 6.2: Structure of the simple room envelope for the selected case study.

Component	Composition (ext-int)	Thickness (m)
Double glazing window	4 (6) 4	0,014
External wall	Aerated concrete	0,25
	Polystyrene	0,10
	Gypsum plaster	0,03
Floor	Polystyrene	0,30
	Concrete slab	0,25
Roof	Wooden panel	0,25
	Polystyrene	0,15
	Gypsum plaster	0,03

Table 6.3: The HAM-Tools format in Simulink for the weather data file input.

Parameter	Unit
Time	s
Air temperature	$\times 10$ °C
Dew point temperature	$\times 10$ °C
Global irradiation on horizontal surface	W/m^2
Diffuse irradiation on horizontal surface	W/m^2
Normal direct irradiation	W/m^2
Incident long wave irradiation	W/m^2
Illuminance, global	lx
Illuminance, diffuse	lx
Illuminance, direct	lx
Wind direction	deg
Wind speed	m/s
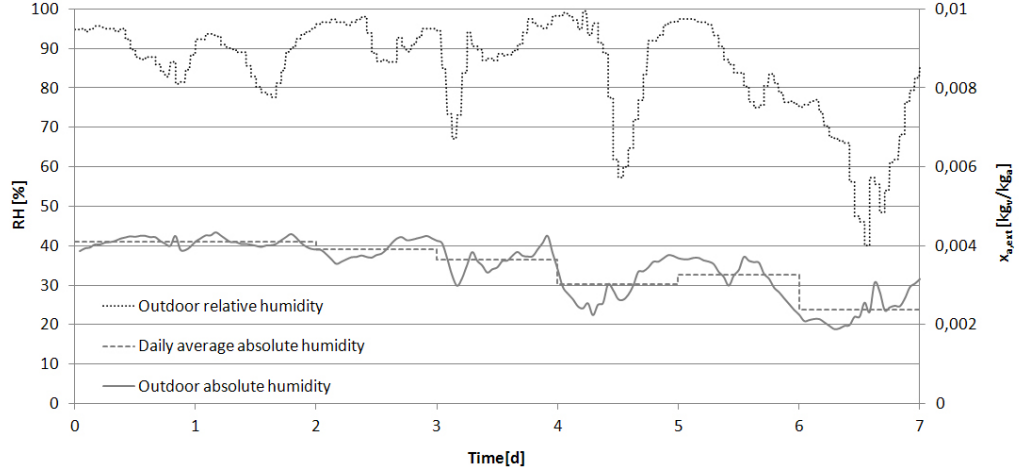
Figure 6.5: Relative humidity and humidity ratio trends according to the used weather data file for Turin. First week of January.

6.2 The room factors: influence on hygro-scopic performance

At the moment most of the simulation tools only consider the influence of ventilation rate and indoor moisture gains on the hygroscopic performance of environments. In order to highlight how considering an indoor hygroscopic interaction between the building components and moist air can affect the relative humidity level inside a room, a numerical simulation has been carried out. The 2 cases in Figure represent the same environment without hygroscopic interaction between indoor air and building components ($\beta_{int} = 0$) and with interaction ($\beta_{int} = 2 \cdot 10^{-8}$) by using a gypsum plaster finishing (Gyproc Pronto Grezzo data) under ventilated conditions (0,3 h^{-1} air change rate) and moisture generation schedule (80 g/h, 8 hours gain followed by 16 hours without gain). A clear influence of the buffer effect of gypsum plaster is visible in the dampened RH level for the hygroscopic case. Without the presence of the hygroscopic material the average indoor relative humidity value is increased by 11 %.

The main objective of this section is to calculate, by means of numerical
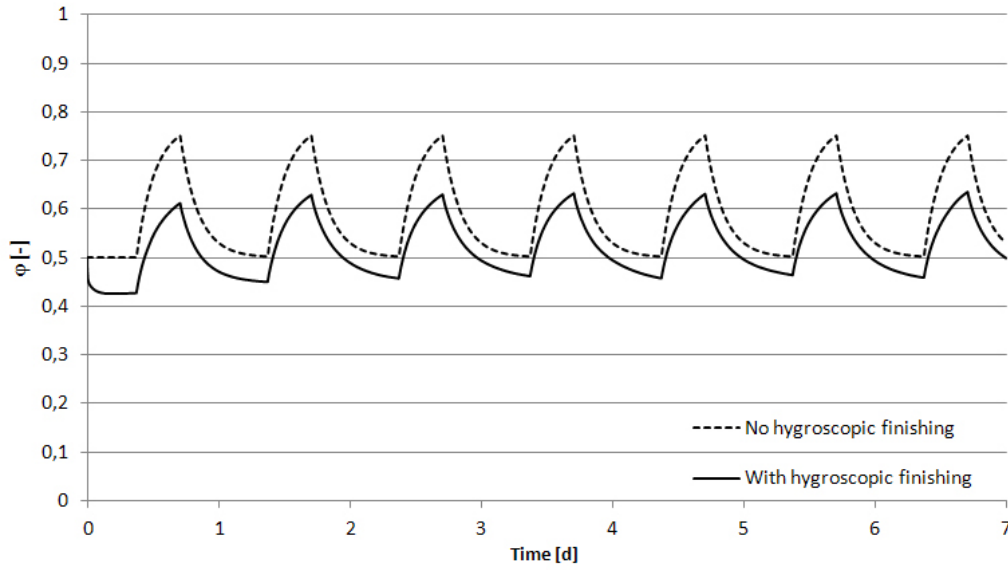
Figure 6.6: The relative humidity trend inside a room when considering or not the hygroscopic interaction between building components and indoor moist air, under the same boundary conditions.

simulation, the hygroscopic performance of the simple room when gypsum plaster is applied for different environmental conditions, in order to analyse the relationship that exists between the buffer effect dependent on the material level and the indoor environmental performance when influenced by the room factors. The two room factors considered for the mass balance of the room were ventilation and moisture production rate.

6.2.1 Ventilation

Since the primary application of the investigated material is for residential - domestic environments - numerical simulation assumes a certain air change rate with outdoor air through a mechanical ventilation system which provides the air flow through two openings (supply and exhaust air vents) located in the walls. With reference to recent studies (Li, 2011), the same three different levels of ventilation rate used in Chapter 5 were chosen for the simulation $(0{,}35 - 0{,}50 - 0{,}75 \text{ h}^{-1})$, plus a fourth high ventilation rate ($\rightarrow \infty$). A

further scenario in absence of ventilation has the purpose of considering the hygroscopic absorption as the only mechanism of attenuation of the moisture load, in order to quantitatively evaluate the effect that the activation of the ventilation has on the moisture buffering capacity of the material.

Figure 6.7: The ventilation block in HAM-Tools.

6.2.2 Moisture gain

The second factor is related to the humidity load, another key parameter in studies on the moisture buffering. In the simulation a zero moisture production rate first and an intermittent moisture load profile after were considered. The average value of moisture gain was calculated by the mass balance for each respective ventilation rate in order to maintain a constant value of RH = 50 % (constant temperature) according to the following equation:

$$\dot{G}_a(x_{a,ext} - x_{a,int}) - \dot{G}_{gen} = 0 \tag{6.1}$$

where $\dot{G}_a$ [kg/s] is the air flow rate, $x_{a,ext}$ and $x_{a,int}$ the moisture content in outdoor and indoor air respectively. The indoor humidity ratio has been considered constant and calculated according to Eq. 4.4 and to the designed

boundary conditions, while $x_{a,ext}$ is the average daily outdoor moisture content in air deriving from the hourly data contained in the weather data file. In Table 6.4 the designed boundary conditions for indoor air are listed.

Table 6.4: The considered boundary conditions for the indoor environment.

θ_{int} [°C]	20
UR [%]	50
$p_{v,s}$ [Pa]	2340
p_v [Pa]	1170
$x_{a,int}$ [kg$_v$/kg$_a$]	0,0076
V [m^3]	55

In order to balance the indoor air humidity of the ventilated and conditioned room with a proper moisture load, a simplified calculation was carried out by considering an average value for outdoor absolute humidity during the day for each of the 3 designed air ventilation rates and finding the respective moisture generation rate $\dot{G}_{gen}$ day by day. A mean value for the moisture production rate was then calculated above the daily results (see Table 6.5), obtaining $\dot{G}_{gen,av}$ [g/h].

Table 6.5: Average daily moisture generation rates for the respective ventilation rates.

Ventilation rate n [h^{-1}]	Average daily moisture generation rate $\dot{G}_{gen,av}$ [g/h]
0,35	94
0,50	134
0,75	201

The values for the moisture generation rate $\dot{G}_{gen}$ [g/h] in Table 6.7 were calculated taking into account the duration and intensity of the vapour production (see Table 6.6). As in the Annex 41 workshops, the schedule was

Table 6.6: Daily schedule for the moisture generation rate.

Moisture generation rate $\dot{G}_{gen}$ [g/h]	Moisture generation period [h]	Moisture generation interval [h]
$2 \times \dot{G}_{gen}$	7:00-9:00	2
$0 \times \dot{G}_{gen}$	9:00-17:00	8
$1 \times \dot{G}_{gen}$	17:00-22:00	5
$0,5 \times \dot{G}_{gen}$	22:00-7:00	9

proposed considering standard residential users, with a two-hour morning peak due to the use of the bathroom (double load) followed by lack of production during the hours when the room is not occupied (i.e. due to working time 9.00-17.00 h). The unit load $\dot{G}_{gen}$ obtained from the hourly average is produced during the evening hours for a longer period than in the morning (17.00-22.00 h), while during the night a constant halved generation until the next morning is considered, representing the latent load in the bedroom due to the occupant breathing.

Figure 6.8 shows the daily schedule for moisture production related to a ventilation rate of 0,35 h^{-1}, with the higher morning peak and the lower gain during the evening hours and during night, while in Figure 6.9 the Gain block for the moisture generation signal in HAM-Tools is shown.
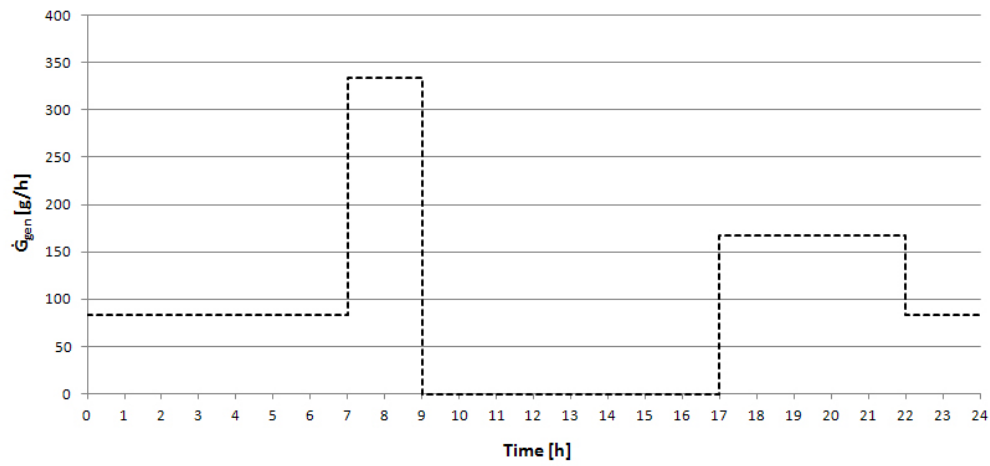
Figure 6.8: Daily schedule for moisture production related to a ventilation rate of 0,35 h^{-1}.
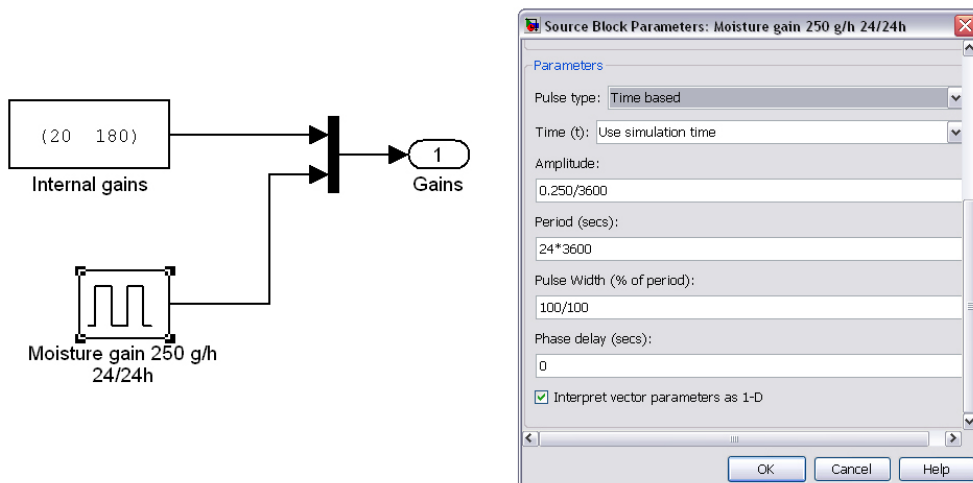
Figure 6.9: The gain block in HAM-Tools.

99

The value of $\dot{G}_{gen,av}$ was therefore weighed on an hourly average taking into account the production program according to Equations 6.2 and 6.3:

$$\dot{G}_{gen,av} = [2 \cdot \dot{G}_{gen} \cdot (2h) + 0 \cdot \dot{G}_{gen} \cdot (8h) + 1 \cdot \dot{G}_{gen} \cdot (5h) + 0, 5 \cdot \dot{G}_{gen} \cdot (9h)]/24 \quad (6.2)$$

thus

$$\dot{G}_{gen} = (\dot{G}_{gen,av} \cdot 24)/13, 5 \quad (6.3)$$

The values for $\dot{G}_{gen}$ reported in Table 6.7 were then obtained.

Table 6.7: Moisture generation rates for the respective ventilation rates.

Ventilation rate n [h^{-1}]	Moisture generation rate $\dot{G}_{gen}$ [g/h]
0,35	167
0,50	238
0,75	357

6.3   Simulation scenarios and environmental parameters

Once the amount of vapour to be produced and the respective ventilation rate have been defined, and considering a preconditioned thermal zone, the initial humidity of the material was set at 50 % (equilibrium conditions with indoor air). As described in Chapter 4 the lumped model considers a single node in the middle of the room according to the well-mixed air method. During the simulation, the temperature was kept constant (20 °C), while the relative humidity was left in free floating.

Table 6.8: The generated simulation scenarios.

Ventilation rate n [h^{-1}]	0 [g/h]	167 [g/h]	238 [g/h]	357 [g/h]
0,35	CASE 1_0	CASE 1	CASE 2	CASE 3
0,50	CASE 4_0	CASE 4	CASE 5	CASE 6
0,75	CASE 7_0	CASE 7	CASE 8	CASE 9
No vent.	CASE 10_0	CASE 10	CASE 11	CASE 12
$\to \infty$	CASE 13_0	CASE 13	CASE 14	CASE 15

To study the influence of the room factors on the buffer capacity of the hygroscopic material, each of the average rates of moisture production shown in Table 6.7 was coupled to the different ventilation rates, giving origin to a matrix with 9 test cases. In order to evaluate the behaviour of materials under "border line" boundary conditions, some additional test cases were introduced, considering scenarios with:

- no water vapour production;

- 3 cases with no ventilation;

- 3 cases with a very high ventilation rate

for a total of 20 test cases (Table 6.8).

The indoor temperature is controlled through a heating/cooling system with infinite capacity, and maintained in the range of 20-21 °C. In HAM-Tools the heating system contribution is entirely convective, as shown in Fig. 6.10.

A constant internal load of 200 W and the convective portion of the incoming solar radiation in the environment through the glazing envelope were also considered, in order to simulate realistic boundary conditions of environment occupation. Any de/humidification system was taken into account.

The structure was considered impermeable to air (no air flow for infiltration/exfiltration); the removal of moisture therefore occurs only through the mechanical ventilation and the vapour diffusion (and buffering) through the interior finishing layer.
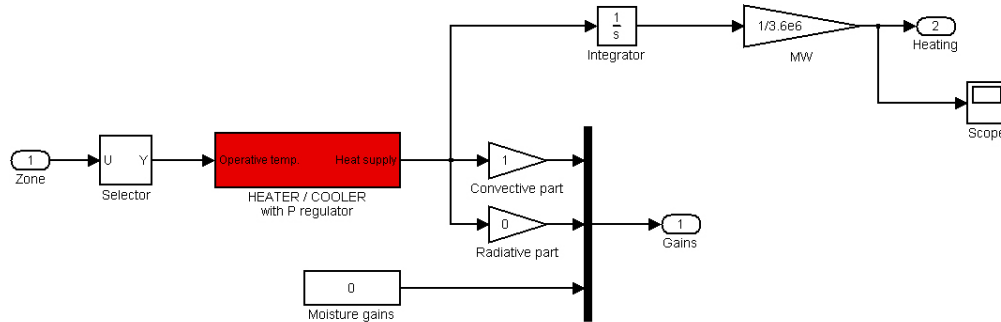
Figure 6.10: The heating/cooling system block in HAM-Tools.

6.3.1 Results

The main environmental parameter for evaluating the macroscopic effects caused by the variation of the room factors is the relative humidity. The outdoor air which for the winter conditions of the reference location (Turin) is characterized by a low moisture content (see Fig. 6.5) is constantly introduced through a controlled mechanical ventilation system. The main visible effect is the lowering of the indoor relative humidity level, with a trend directly proportional to the air flow.

This is the typical winter condition occurring in the north Italian residential building stock when no de/humidification system is provided; the temperature is kept constant at design value (20 °C) and indoor air is usually "dry" in terms of vapour concentration.

As can be seen from Figures 6.11 to 6.14 each graph aims at evaluating the contribution of the internal moisture production by increasing the amount of gain gradually, while the ventilation rate is kept constant. This allows a better understanding of how much a sudden change in the number of occupants influences the internal moisture load if the ventilation rate is not adapted to the new conditions.

For every graph the no-moisture generation scenario has been represented, showing what happens if no water vapour is produced when ventilating with outdoor air and conditioning at 20 °C.

102
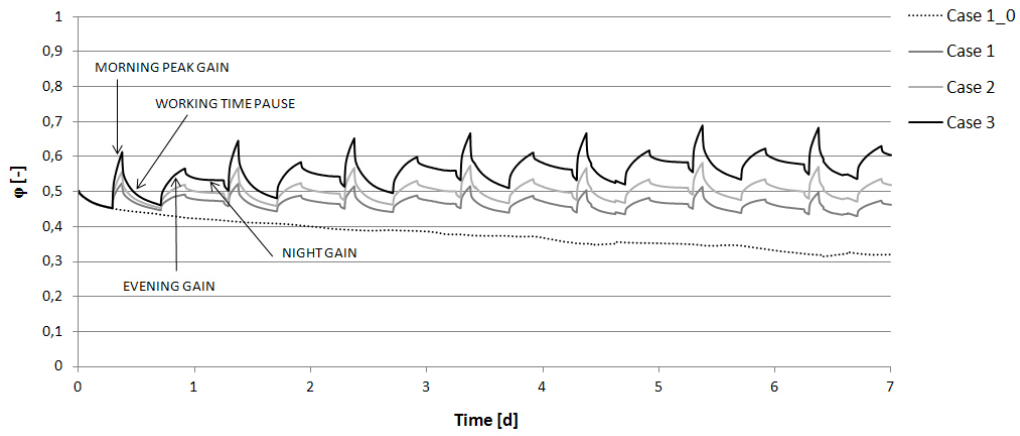
Figure 6.11: RH trend for the scenarios related to a ventilation rate of 0,35 h^{-1}.
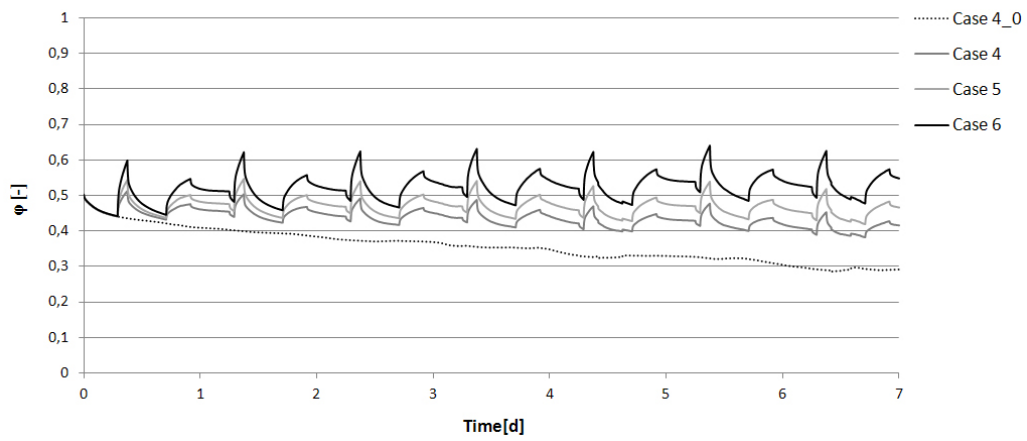
Figure 6.12: RH trend for the scenarios related to a ventilation rate of 0,50 h^{-1}.

103
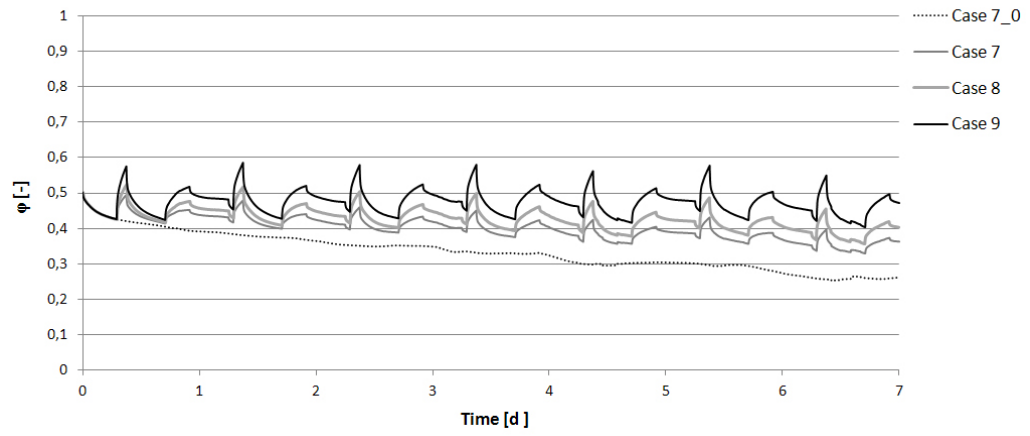
Figure 6.13: RH trend for the scenarios related to a ventilation rate of 0,75 h^{-1}.
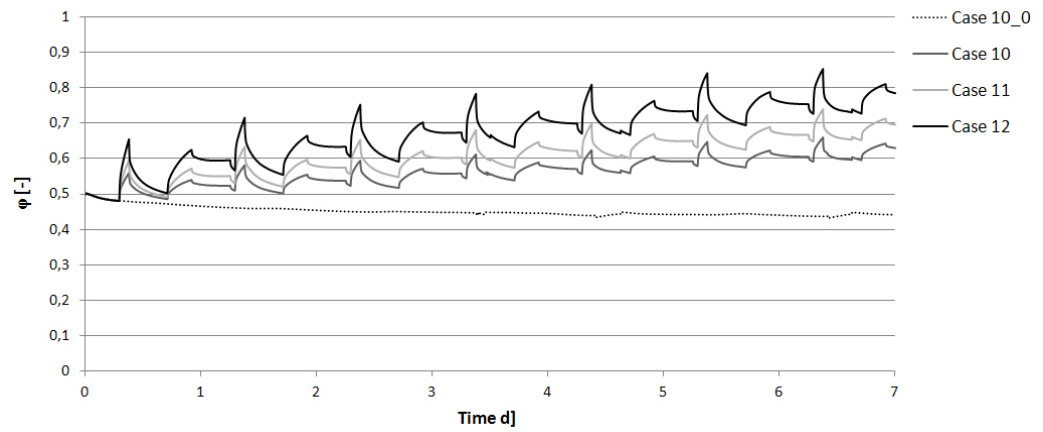
Figure 6.14: RH trend for the scenarios related to a no-ventilated room.

The first group of results for the 0,35 and 0,50 h^{-1} air change rate highlights a certain accomplishment of the imposed RH condition during the moisture balance calculation. Excluding the no-moisture generation scenario, the relative humidity range starts at 50 % and goes from a minimum peak of 44 % (for the 167 g/h gain) to a maximum of 69% (for the 357 g/h gain). The influence of the moisture generation schedule is clearly visible: the morning peak which produces a $\Delta RH_{max} \approx 15\%$, the desorption during the 8 hours stop due to the working time pause with no occupancy in the room, the evening gain followed by a reduced load during the night with a slower decay of the humidity level.

The increase of the ventilation rate (Fig. 6.13) leads to an higher level of humidity removal through the vents: the moisture gain affects less the indoor RH level if compared to the ventilation mechanism. The outdoor air flow rate characterised by a low vapour concentration level reaches a higher temperature due to the indoor heating system and moves therefore to a lower RH value as the moisture gain is not balanced properly.

The fourth group of results in Fig. 6.14 shows the RH trend for the "border line" boundary condition represented by absence of ventilation. In this case the moisture gain is not balanced and the gypsum plaster buffer effect is not sufficient to dampen the peaks the RH level reaches 86 % during the last day of simulation for a moisture gain of 357 g/h. Moreover the different generation rates have clearly visible affection on the RH level.

In the no-moisture generation scenario a stabilized humidity level is reached after a first phase of absorption carried out by the finishing, which results: the level goes from 50 % to approximately 45 % and is not further lowered because of the equilibrium moisture content condition established between the gypsum plaster and indoor air.

By evaluating the ratio between the standard deviations of indoor absolute humidity and of moisture gain $[\sigma_{x_{int}}(\sigma_{\dot{G}_{gen}})]$ for the 20 test cases (Fig. 6.15) it is clear how, when no ventilation is considered, the deviation of absolute humidity with respect to the average value is directly proportional to

the standard deviation of indoor gains. The ventilation activation and the
introduction of outdoor air leads to a "flattening" effect for the curve: the
increased ventilation rate reduces gradually the effect of the internal loading
signal as stated previously.
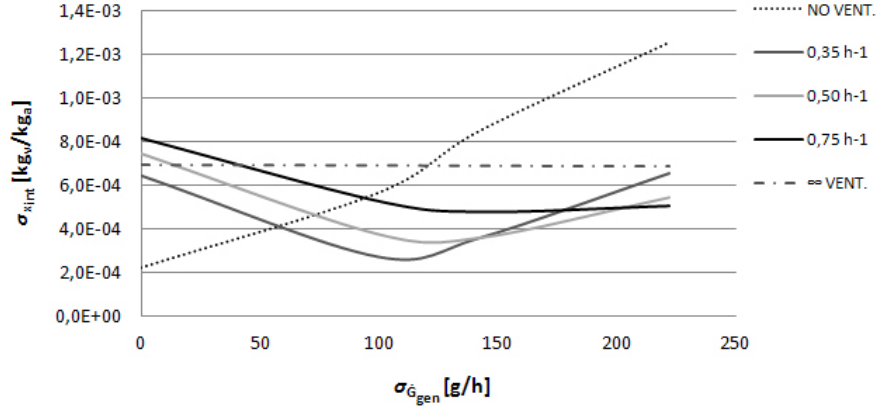
Figure 6.15: Ratio between the standard deviations of indoor absolute humidity and of moisture gain $[\sigma_{x_{int}}(\sigma_{\dot{G}_{gen}})]$ for the 20 test cases.

The hourly profiles of the moisture flows through the zone allow to distinguish between the positive moisture fluxes [kg/s] entering by the inlet vent and the negative (exhaust) fluxes for both the diffusion and ventilation mechanisms. From the results the vapour diffusion to building elements $\dot{G}_{diff}$, calculated according to Eq. 3.25, appears to be mainly negative and therefore buffered by the gypsum plaster layer. The results are normalized on the whole considered internal surface (walls and ceiling) for a totale area A=64 m^2.

The vapour infiltration through the constantly activated ventilation system $\dot{G}_{vent}$ (see Eq. 3.26) is always negative and continuously removing the produced humidity. Because of the mass balance between the diffusion and the ventilation the two mechanisms share the humidity removal. Figures 6.16 and 6.17 show the trends for $\dot{G}_{diff}$ and $\dot{G}_{vent}$ for the first set of simulations (0,35 h^{-1} air change rate), while in Figure 6.18 the unventilated scenario is considered (high RH level in indoor air) and the diffusion represents the unique way for moisture transport ($\dot{G}_{vent} = 0$), except for CASE 10_0 in

which any moisture is generated ($\dot{G}_{diff} = 0$).
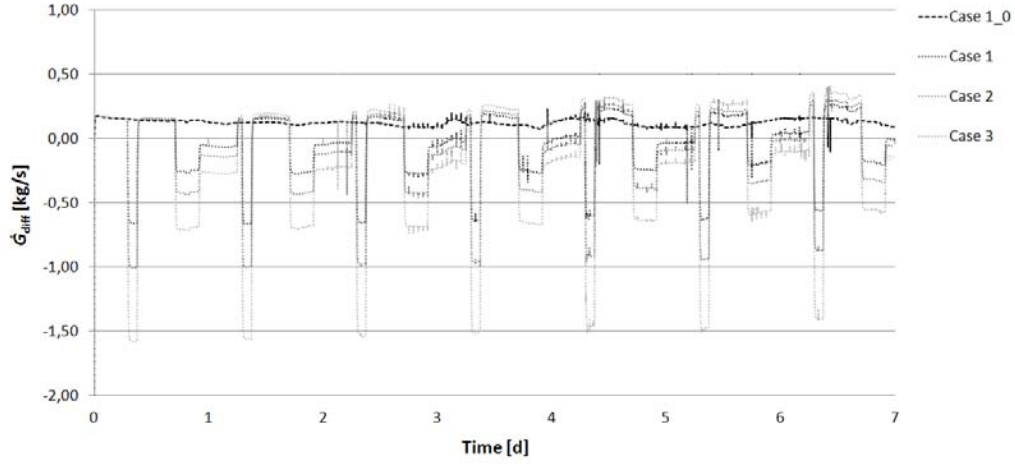
Figure 6.16: $\dot{G}_{diff}$ trend for the 0,35 h^{-1} air change rate.
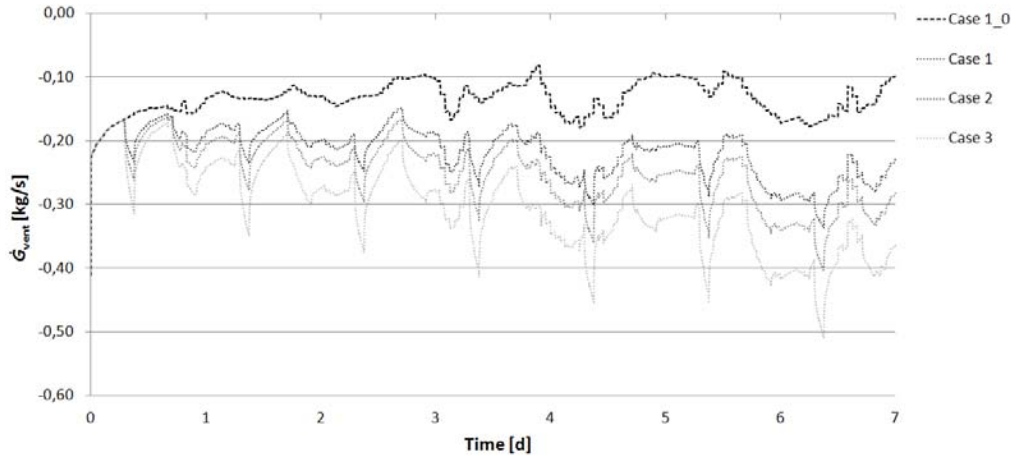
Figure 6.17: $\dot{G}_{vent}$ trend for the 0,35 h^{-1} air change rate.

Considering the moisture content variation in time dw/dt [kg/(m^{3}s)] inside the gypsum plaster layer it is clear that, for the same ventilation rate, the change in mass is proportional to the moisture gain generated in the simple room. Figure 6.19 shows the trend for the gypsum moisture content variation during the simulation period for the test cases related to the 0,35 h^{-1} ventilation rate.

107
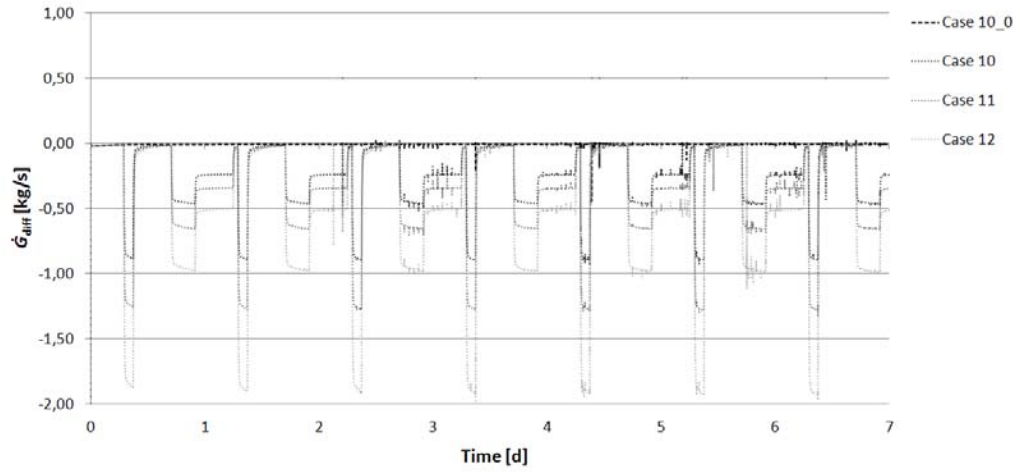
Figure 6.18: $\dot{G}_{diff}$ trend for the unventilated scenario.

The vapour generation schedule is clearly visible where the moisture content variation within the gypsum plaster leads to a higher absorption for a short time period (morning) or to a reduced load due to the evening and night gain schedule.

The dw/dt graph has been realized taking into account the moisture balance for the nodes in the 3 cm thick gypsum plaster layer (see Fig. 6.3). The latter has been modelled with a surface node and 3 internal nodes by using the pre-defined block in the HAM-Tools library as shown in Fig. 6.20.

Although the starting moisture content for the materials which compose the exterior wall was set at 50 % as for the indoor air RH, the ventilation with low absolute humidity causes a sudden desorption by the plaster of a part of the initial moisture to get into equilibrium with air. This response takes place for each of the simulated scenarios but it is most noticeable for CASE 1_0 where the absence of vapour production results in a non-interference with the process of balance achievement.

With a detailed analysis of the hygroscopic content variation per unit volume [g/m³h] as a function of the thickness of the gypsum plaster (3 cm thick), it can be noticed as the hourly oscillation of the moisture content involves mainly the first few centimetres of the material, that results in participating
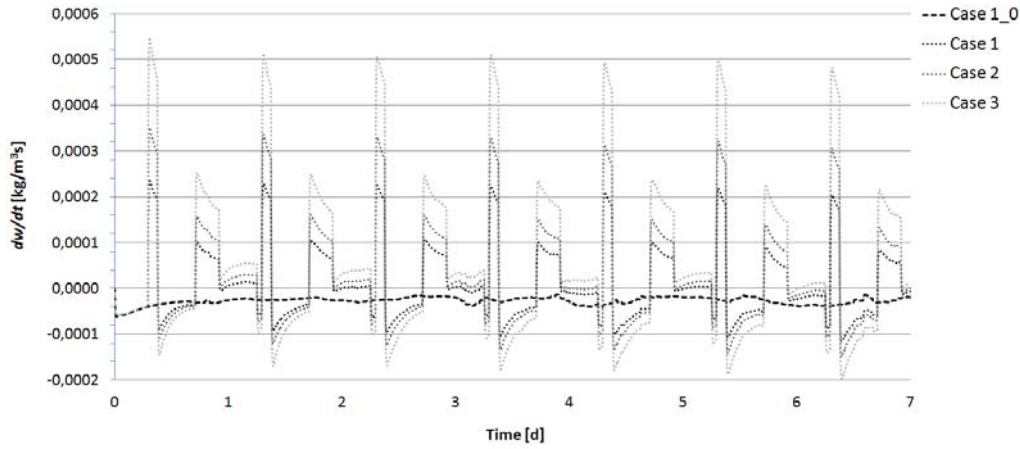
Figure 6.19: dw/dt trend for the 0,35 h^{-1} ventilation rate.

actively in the damping of the solicitation, attenuating the cyclic loading without involving the deeper layers of the wall, giving it a dynamic response characterized by the hygroscopic properties of the material, which describe its storage capacity (sorption isotherm) and transmission (permeability) of moisture.

This behaviour is also determined analytically through the moisture penetration depth d_m (see Eq. 3.12-3.13) when the material is subjected to cyclic moisture concentration load according to an angular frequency ω.

Figure 6.21 is an example of the dw/dt spatial variation trend according to the described numerical model for CASE 3 (high moisture generation gain, low ventilation rate). The curves represent the hourly trends for the moisture content during the 7$^{\text{th}}$ day.

Since the regulatory field still seems to be lacking with regard to the characterization of the hygroscopic performance of the environment under dynamic conditions, it would be interesting to explore the theme from the point of view of the analytical calculation method. the dynamic behavior of the wall that follows a transient change in indoor humidity is not unlike what occurs in the thermal field when the component is stimulated by a cyclic heat wave. in this case, the reference standard is EN 13786:2008 (*Thermal performance of building components: Dynamic thermal characteristics - Cal-*

109
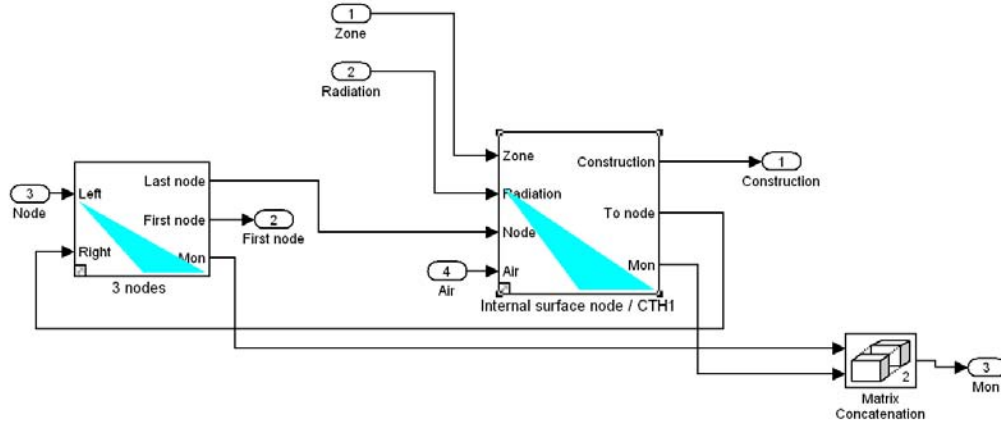
Figure 6.20: The gypsum plaster discretization in the *Simple Room* model. The 3 cm thick layer is composed by a surface node in contact with air and 3 internal nodes.

culation methods) and the dynamic parameter that describes the response (towards the internal environment) of the component to a stress (from the internal environment) is the thermal admittance. in the field of characterization in dynamic regime of a hygroscopic material the only reference standard appears to be the ISO 24353:2008 (*Hygrothermal performance of building materials and products: Determination of moisture adsorption/desorption properties in response to humidity variation*) and concerns only the determination of the transient response in the experimental field, while the method of calculation has not yet been standardized.

As can be seen from Figure 6.22, the amount of water absorbed and released per unit volume of the material $w_{abs/rel}$ has a course directly proportional to the size of the latent load in the environment. This quantity decreases instead with the increase of the rate of change of air, since the increase of the vapour flux $\dot{G}_v$ removed through ventilation. For example, for an average rate of production of water vapour of 238 g/h and in absence of ventilation, the amount of water accumulated in the material is equal to 46,2 kg_v/m^3; for the same latent load and with a ventilation rate of 0,5 h^{-1} the accumulation is reduced to 4,9 kg_v/m^3. For a ventilation rate tending to
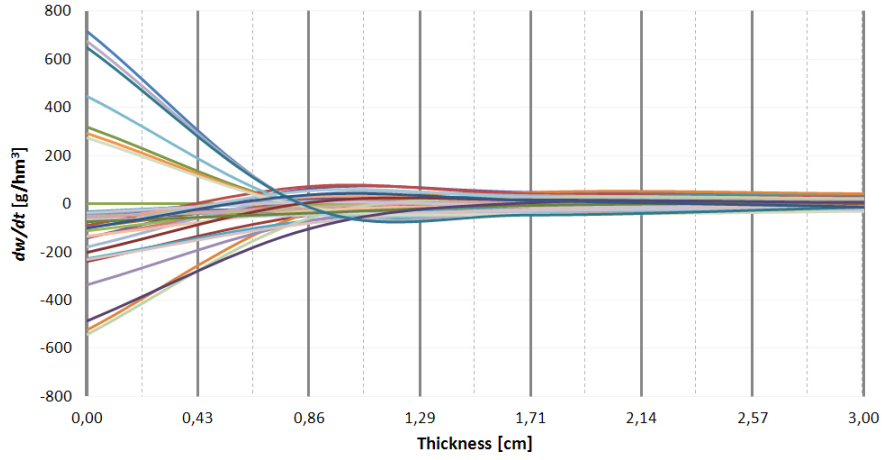
Figure 6.21: dw/dt trend for the 0,35 h^{-1} ventilation rate. Each curve represent the moisture content (every 6 hours) within the layer during the simulation period. 3 cm thick gypsum plaster layer.

infinity the internal moisture load has no more influence on the hygroscopic material buffer, which at the end of the simulation period carried out for all test cases a quantity of water equal to about 32 kg_v/m^3. It can therefore be said that the buffer capacity of the material is strongly influenced by the ventilation rate.

Similarly to what was found from Fig. 6.15, the analysis of the dynamic response of the material to the solicitation in the environment (Fig. 6.23) shows a gradual reduction of the fluctuation of the hygroscopic content absorbed and released with the increase of the ventilation rate: the derivative of the curve tends to zero.

Similarly to what represented by the isotherm adsorption, the total moisture content buffered at the end of the simulation period in relation to the average RH was evaluated for all the test cases. From the data reported in Figure 6.24 it can be seen as the gypsum plaster, when ventilation is activated and an internal moisture gain is running, starts the absorption process in correspondence with a $\mu_{RH} \approx 45$ %; below this value the desorption takes place because of the equilibrium moisture content. The minimum value corresponds to the hygroscopic content related to the test cases with a ventilation rate $\to \infty$, ($\mu_{RH} \approx 27$ %); the maximum hygroscopic content is reached in

111
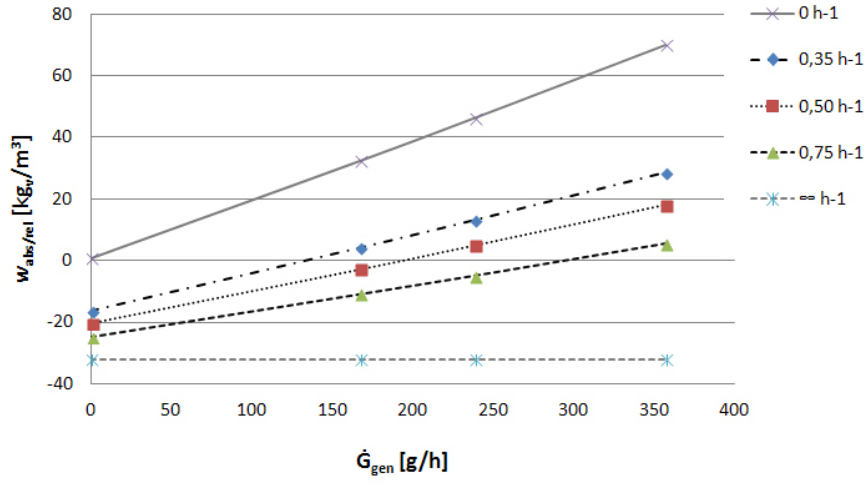
Figure 6.22: Ratio between the amount of water absorbed and released per unit volume of the material $w_{abs/rel}$ and the moisture gain $\dot{G}_{gen}$.
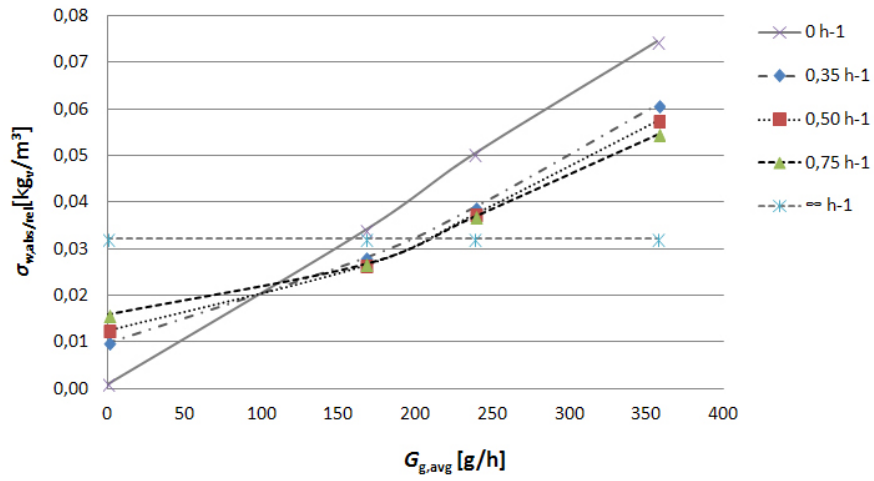
Figure 6.23: Ratio between the standard deviation of the amount of water absorbed and released per unit volume of the material $w_{abs/rel}$ and the moisture gain $\dot{G}_{gen}$.

the unventilated scenarios with a water vapour production of 357 g/h ($\mu_{RH} \approx$ 70 %).
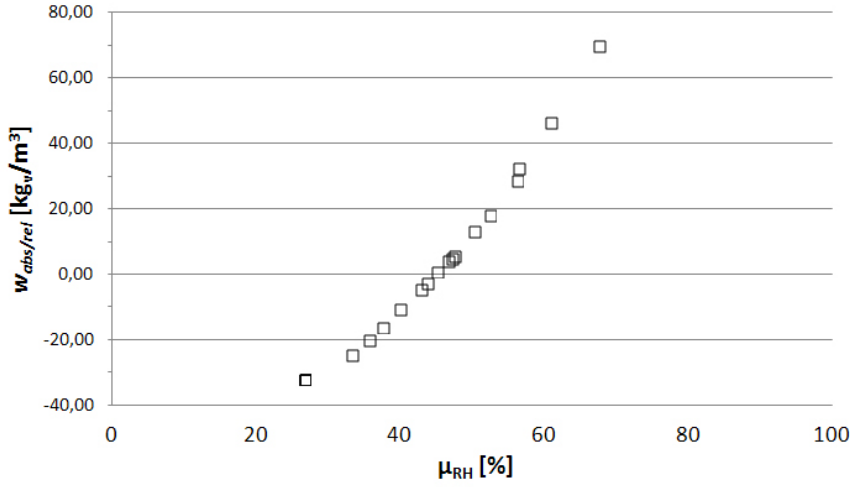
Figure 6.24: Ratio between the amount of water absorbed and released per unit volume of the material $w_{abs/rel}$ and the average value of relative humidity μ_{RH} for all the simulated scenarios.

6.4 Discussion

The buffering properties cannot directly represent the hygroscopic performance of a finishing material when put in environmental conditions, as it is influenced by the so-called room factors, such as the ventilation rate and the internal moisture gains. By means of numerical simulation the moisture content trend of gypsum plaster layer, when subjected to changes in the internal latent load and ventilation rate, has been studied together with the internal fluctuations of relative humidity.

Through a controlled mechanical ventilation system the outside air, which in the winter conditions of the reference location (Turin) is characterized by a low absolute humidity, enters into the room. The main effect is the lowering of the indoor relative humidity level, with a trend directly proportional to the air change rate. Furthermore, considering the relationship between the standard deviations of the absolute humidity of indoor air and the moisture production for the 20 cases it was shown that, in the absence of ventilation, the deviation of the specific humidity compared to the average value is directly proportional to the standard deviation of internal gains. The activa-

tion of the ventilation, with the consequent release into the environment of outside air causes a "flattening" of the curve: the increase of the ventilation rate gradually reduces the effect of the internal solicitation on the indoor vapour concentration.

Relatively to the incoming/outgoing water vapour flux from the thermal zone, it has been shown how when any ventilation rate is running, the only mechanism for removing the environmental moisture load is the diffusion through the structure. By increasing the ventilation rate, the vapour flux for diffusion decreases, while with a inversely proportional trend the vapour flux removed by the ventilation increases.

Analysing the variation of moisture content per unit volume dw/dt of the gypsum plaster it is evident how this is, with a constant ventilation rate, directly proportional to the moisture gain solicitation in the environment. The same variation, when related to the thickness of the plaster layer allows to understand how the hourly oscillation of the hygroscopic content interests mainly the first few centimetres of the material. The amount of water absorbed and released per unit volume of the material $w_{abs/rel}$ has a trend directly proportional to the amount of latent gain in the environment. This quantity decreases instead with the increase of the air change rate, since the vapour flux $\dot{G}_v$ removed through ventilation increases. For example, for moisture production of 238 g/h and with any ventilation, the amount of water accumulated in the material is equal to 46,2 kg$_{\text{v}}$/m^3; for the same moisture gain and with a ventilation rate of 0,5 h^{-1} the accumulation is reduced to 4,9 kg$_{\text{v}}$/m^3.

The ratio between the total absorbed moisture content at the end of the simulation period and RH (weekly average) allows to highlight as the gypsum plaster, according to the considered room factors, starts the absorption process in correspondence with a $\mu_{RH} \approx 45$ %; below this value the desorption takes place. The minimum value corresponds to the moisture content related to the test cases with a ventilation rate $\rightarrow \infty$, ($\mu_{RH} \approx 27$ %) while the maximum moisture content is reached in the absence of ventilation and with a production of water vapor average of 357 g/h ($\mu_{RH} \approx 70$ %).

Chapter 7

CFD vs. lumped model applied to HAM: a comparison between HAM-Tools and Comsol

The CFD model has the advantage that overcomes the limitation of the zonal-model, but encounters another limitation. In currently available CFD software, there is no CFD model that the simulation of mass transfer can be extended from fluid region to solid region directly. In the whole-building moisture transport studies, the mass coupling between the indoor environment and the wall system is usually achieved by third party programming. Basically, the moisture flux on the surface of the wall calculated by CFD is used as the input for the wall model to determine the distribution of the moisture inside the wall material at each time step (i.e. using MatLab), and the mass fraction on the wall surface is calculated and sent back to the CFD model as the boundary condition for the next time step.

In the Annex 41 research project (2004-2008) of the International Energy Agency (IEA), which was carried out to explore the complex physics governing the whole building heat, air and moisture transfer, there were several models developed throughout this initiative to couple 3-D CFD simulations with hygrothermal models of walls. For instance, Neale (2007) solved the heat and moisture transport in air and porous materials by developing a

simplified hygrothermal model in MATLAB that was coupled to FLUENT software. By using this model, the moisture surface coefficient is calculated and compared with the Chilton-Colburn analogy results. But the finite difference model is difficult to extend or modify to fit new simulation conditions.

Steeman et al. (2009) used the effective penetration depth (EPD) approach to couple CFD and moisture transport inside the wall. By using this EPD model, the profile of indoor temperature and relative humidity can be obtained in the whole building simulation, and the local moisture behaviour of the wall can be evaluated. While the EPD models do allow the simplified quantification, it has been argued that the reliance on the moisture penetration depth concept necessitates comprehensive material properties (Janssen et al., 2007). In the EPD model, the penetration depth, which is an estimation value based on the calculation of the sudden moisture level change on the surface of the material, has to be known in the model. This may limit the application and accuracy of the model.

Besides the Annex 41 project, other recent studies were carried out to couple CFD simulations with hygrothermal models of walls. Amissah (2005) coupled a 1D HAM model to a low-Reynolds number κ-ε turbulence model, with independent execution and information exchanged at every time step. The HAM model supplied realistic boundary conditions for the CFD simulation, while CFD results supported direct modeling of convective mass transfer. Erriguible et al. (2006) coupled indirectly a 2-D CFD model with a 2-D hygrothermal material model. In these models, similar limitations can be found, and the main reason is that all these models are not simulated in one single simulation environment.

The objective of this phase is to establish a coupled CFD model in a single simulation environment to study the HAM transport in the simple room influenced by the room factors. A numerical method is utilized to investigate the indoor environment and moisture transport process in the simple room and inside the wall system influenced by the moisture loads and ventilation conditions.

The comparison between the CFD and the lumped model aims to demon-

strate how a simplified model can be reliable in predicting the RH variation inside a room, taking into account the indoor material buffering effect. Results from literature demonstrated how the simulations made with the lumped model (HAM-Tools) over-estimate the moisture dampening effect than what was actually measured experimentally (Ramos et al., 2012), concluding that:

> "The more canonical approach represented by using different surface moisture transfer coefficients for different parts of the specimens didn't provide an acceptable agreement, since the simulated RH curve would be distorted compared to the measurements. The best way to match both the simulations and the measurements was reducing the sample area by half of what was actually used in laboratory tests".

The authors then focused on the air-flow pattern, comparing experimental measurements results to theoretical ones. An appreciable difference between the measured hygroscopic inertia and the calculated $I_{h,d}$ was found due to the air velocity field which caused the development of several dead zones inside the test chamber. This meant that the perfect mixing of the room air, a simplification commonly assumed in HAM simulations, had a clear impact on the results of this kind of problem. If perfect mixing is assumed, all the hygroscopic surfaces would be fully active; but since this is not true, the flux chamber simulations overestimated the moisture buffering effect.

The confirmation of the chamber's air imperfect mixing was found in some positions of the sensors, between which the pressure difference reached 400 Pa in certain periods. The coefficient for imperfect mixing of air C_r was introduced as correction factor in the Hygric Inertia Index (we report Eq. 2.13):

$$I_{h,d} = \frac{\sum_{i=1}^{n} A_i \cdot C_{r,i} \cdot MBV_i + \sum_{j=1}^{m} C_{r,j} \cdot MBV'_j}{n \cdot V \cdot \tau}$$

Figure 7.1 shows the development of the so-called "dead zones" for a given ventilation rate, especially in the room corners. The results calculating the velocity field [m/s].
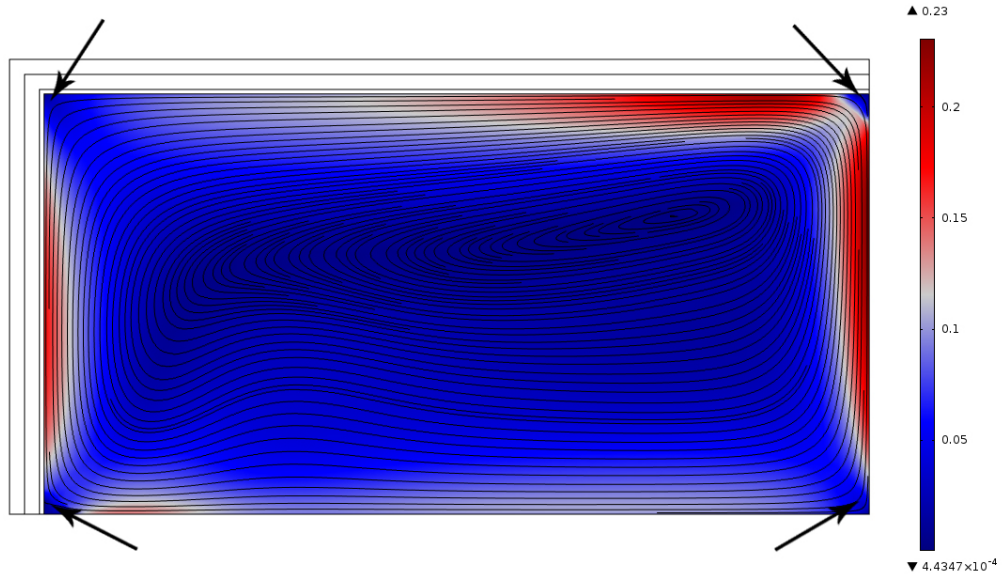
Figure 7.1: Velocity field of air inside the simple room with the indication of the dead zones.

In this Chapter the fitting between the time variation of the vapour concentration in the CFD model and in the lumped one as first step towards the matching between the two simulation tools is presented. The CFD output - in this case the relative humidity variation ? is an average value over the room air volume, depending on the air velocity field. The HAM-Tools lumped model doesn't consider the air mixing and its distribution over the room volume, and for this reason the outputs will correspond to the entire and homogeneous volume.

In order to analyse the vapour concentration variation inside a room, a full-scale test room has been designed, considering an hygrothermal scenario (isothermal conditions, constant air change rate and a moisture production schedule). Running the simulation with the 2 different tools two main target are proposed:

- the understanding of the real air volume influencing the average output value due to the vapour concentration distribution over the room;

- the fitting with the results obtained with the lumped model through a correction factor (*Room reduction*), which will rectify the surface moisture transfer coefficient.

An example scheme of the proposed targets is shown in Figure 7.2.

7.1 COMSOL Multiphysics

COMSOL Multiphysics is an interactive environment for modelling and solving all kinds of scientific and engineering problems (COMSOL Multiphysics User's Guide, 2012). The software provides an integrated desktop environment with a *Model Builder* where you get an overview of the model and access to all functionality. Conventional models for one type of physics can be extended into multiphysics models that solve coupled physics phenomena.

Using the built-in physics interfaces and the advanced support for material properties, it is possible to build models by defining the relevant physical quantities - such as material properties, loads, constraints, sources, and fluxes - always applying these variables, expressions, or numbers directly to solid and fluid domains, boundaries, edges, and points independently of the computational mesh. The software can perform various types of studies including stationary and time-dependent (transient) studies.

When solving the models, the simulation tool uses the proven finite element method (FEM). The software runs the finite element analysis together with adaptive meshing (if selected) and error control using a variety of numerical solvers.

There are many application modes available in the COMSOL environment that are built based on the PDEs. These modes, such as acoustics, diffusion, and heat transfer, provide predefined templates and interfaces that are easy for users to set up the simulation environment for that area of physics. For some particular fields of physics, the specialized modules are provided with
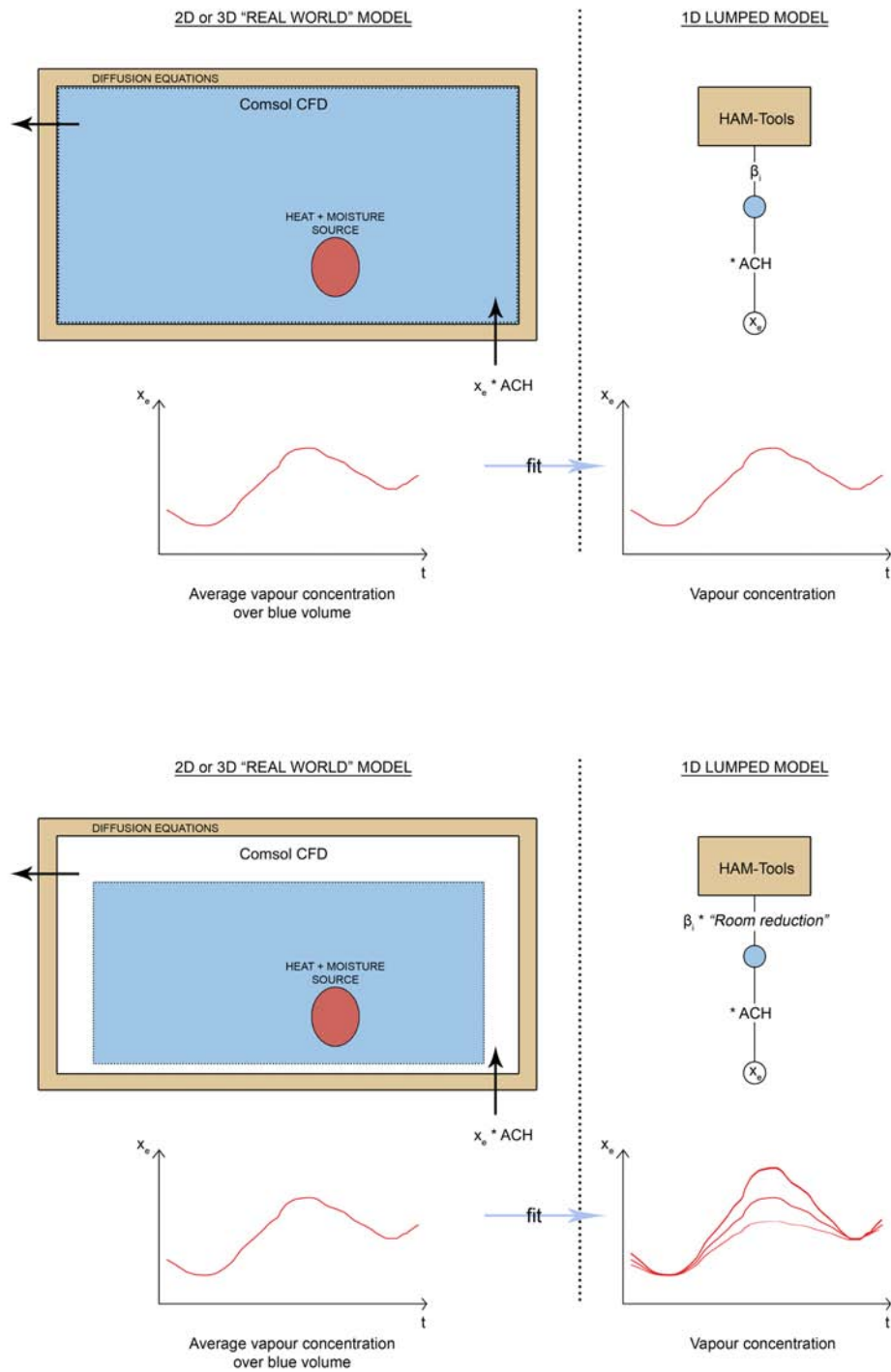
Figure 7.2: Scheme of the fitting process between the HAM-Tools lumped model and the CFD "real world" model.

the standardized terminology, material libraries, and the equations adapted to the specific area. For example, in the *Chemical Module*, the porous media flow can be described by the Darcy's law application mode or by the Brinkman equations application mode. The former is a common approach for the mass and momentum transport in a homogenous porous media, while the latter is for the case where the transport of momentum by shear stresses in the fluid is of importance. COMSOL has especially provided the ways for building multi-physics models for the coupled field analysis. This coupling can happen in the sub-domains or on the boundaries. In the sub-domain the COMSOL multiphysics feature can combine two or several application modes or PDEs into a single model by adding them to the simulation environment. For the coupling on the boundaries where PDEs are needed to describe the boundary, the weak form can be used.

The software has been mainly used for two branches of the building physics simulation, which have been coupled in a unique procedure as will be explained later:

- Moisture transport in building components;

- Moisture balance of air with CFD.

This part of the research has been carried out, as for the experimental activities described in Chapter 5, in collaboration with the Vienna University of Technology.

7.2 Validation of diffusion equation in Comsol

Due to the simplified modelling of the air volume, HAM-Tools considers that each part of the wall absorbs the same amount of moisture, over-estimating the material buffer (Ramos et al., 2012). In real conditions, the influence of the ventilation system and of the air velocity pattern takes to the development of dead zones, where the moisture buffer is less due to a higher surface

vapour resistance. The calibration of the HAM-Tools simplified air ventilation lumped model will be then carried out by using the computational fluid dynamics from COMSOL.

This section is mainly based on the validation, by using HAM-Tools, of the equations of coupled heat and moisture transfer in building components implemented in Nusser and Teibinger (2012) using the physical approach modelled in WUFI, a well-known and worldwide used commercial software for calculating the HAM-transfer developed at the Fraunhofer Institute for Building Physics.

Regarding the transport process, the coupled heat and moisture transfer are calculated from WUFI according to the following equations:

$$\frac{dH}{dT}\frac{\partial T}{\partial t} = \nabla(\lambda\nabla T) + h_v\nabla[\delta_p\nabla(\varphi p_{v,s})] \tag{7.1}$$

$$\frac{dw}{d\varphi}\frac{\partial \varphi}{\partial t} = \nabla(D_\varphi\nabla\varphi) + \delta_p\nabla(\varphi p_{v,s}) \tag{7.2}$$

where $dw/d\varphi$ [kg/m³] is the moisture storage capacity, D_φ [kg/(ms)] the liquid conduction coefficient and h_v [J/kg] the latent heat of evaporation and dH/dT [J/(m³K)] is the volumetric heat capacity, calculated as:

$$\frac{dH}{dT} = (c_p + \frac{1}{\rho_0}c_{p,w}w)\rho_0 \tag{7.3}$$

where c_p and $c_{p,w}$ [J/(kg K)] are the specific heat capacities of the dry material and of water respectively.

In this approach the temperature and the relative humidity are the driving potentials. Both potentials are affecting both transport processes, so they have to be deviated with respect to space in both equations.

$$\delta_p\nabla(\varphi p_{v,s}) = \delta_p\varphi\frac{\partial p_{v,s}}{\partial T}\nabla T + \delta_p p_{v,s}\nabla\varphi \tag{7.4}$$

With Equation 7.4 the heat and moisture transport equation can be described in the following way:

$$\frac{dH}{dT}\frac{\partial T}{\partial t} = \nabla\left[\left(\lambda + h_v\delta_p\varphi\frac{dp_{v,s}}{dT}\right)\nabla T + h_v\delta_p p_{v,s}\nabla\varphi\right] \tag{7.5}$$

$$\frac{dw}{d\varphi}\frac{\partial\varphi}{\partial t} = \nabla\left[\left(\delta_p\varphi\frac{dp_{v,s}}{dT}\right)\nabla T + \left(D_\varphi + \delta_p p_{v,s}\right)\nabla\varphi\right] \tag{7.6}$$

and can be compared to Fick's second law equation model (Eq. 3.22) used in HAM-Tools, that is here reported again together with the heat transfer equation in order to have a direct comparison between the two models:

$$\rho_0 c_p\frac{\partial T}{\partial t} = -\frac{\partial}{\partial x}\left(\lambda\frac{\partial T}{\partial x} + \dot{g}_a c_{p,a}T + \dot{g}_v h_v\right)$$

$$\frac{\partial w}{\partial t} = -\frac{\partial}{\partial x}\left(\lambda_l\frac{\partial p_c}{\partial x} - \delta_p\frac{\partial p_v}{\partial x} + \dot{g}_a u\right)$$

Rearranging the transport equations 7.5 and 7.6 into matrix notation in order to input them in COMSOL, we finally get:

$$\begin{bmatrix} \lambda + h_v\delta_p\varphi\frac{dp_{v,s}}{dT} & h_v\delta_p p_{v,s} \\ \delta_p\varphi\frac{dp_{v,s}}{dT} & D_{\varphi+\delta_p p_{v,s}} \end{bmatrix}\begin{bmatrix} \nabla^2 T \\ \nabla^2\varphi \end{bmatrix} = \begin{bmatrix} \left(c_p + \frac{1}{\rho_0}c_{p,w}w\right)\rho_0 & 0 \\ 0 & \xi \end{bmatrix}\begin{bmatrix} \frac{\partial T}{\partial t} \\ \frac{\partial\varphi}{\partial t} \end{bmatrix} \tag{7.7}$$

After the implementation of the HAM transport equations in COMSOL, the validation with the HAM-Tool model has been carried out.

The study will match the two models by increasing gradually the level of complexity. As first approach to the matching between the results a simple 3-layers wall case study has been chosen, as shown in Figure 7.3: 10 cm foam insulation, 10 cm aerated concrete, 3 cm gypsum plaster (Gyproc Pronto Grezzo); apart from the plaster's properties, the other material data were taken from Annex 24 (*Material Properties - Final Report, Volume 3*).

Several simulation have been carried out in order to evaluate the influence of the layer discretization on the hygrothermal performance results in HAM-Tools an COMSOL. As the increase of the mesh detail leads to a longer
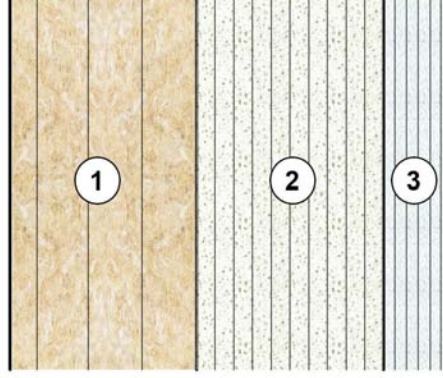
Figure 7.3: The *simple wall* model. From exterior to interior: 1) Foam insulation; 2) Aerated concrete; 3) Gypsum plaster.

simulation time, this process aimed at defining the best detail level for an acceptable simulation time, especially with regard to COMSOL. After the detail of the wall discretization was set for the three layers at 4, 10 and 6 nodes respectively (*fine mesh* settings), a 1-D HAM transfer simulation has been carried out focusing on the temperature and the relative humidity trends within the wall. Both the variables were monitored at nodes n. 3, 9 and 17 (central nodes of the layers) by using the two simulation tools.

In this phase any CFD was used to solve the indoor air in COMSOL, but only the indoor boundary conditions were set because the target was the moisture diffusion process within the building component first.

The simulations have been carried out using the climate data for Turin as outdoor boundary conditions, for the first two weeks of January. The indoor temperature and relative humidity were set respectively to 20 °C and 50 % and maintained constant throughout the simulation period; the same values were set for the materials' starting conditions, then left floating.

The heat and moisture transfer coefficient are:

- outdoor: $\alpha_{ext} = 10$ [W/(m²K)] and $\beta_{ext} = 2 \cdot 10^{-7}$ [kg/(m²s Pa)];

- indoor: $\alpha_{int} = 3$ [W/(m²K)] and $\beta_{ext} = 2 \cdot 10^{-8}$ [kg/(m²s Pa)].
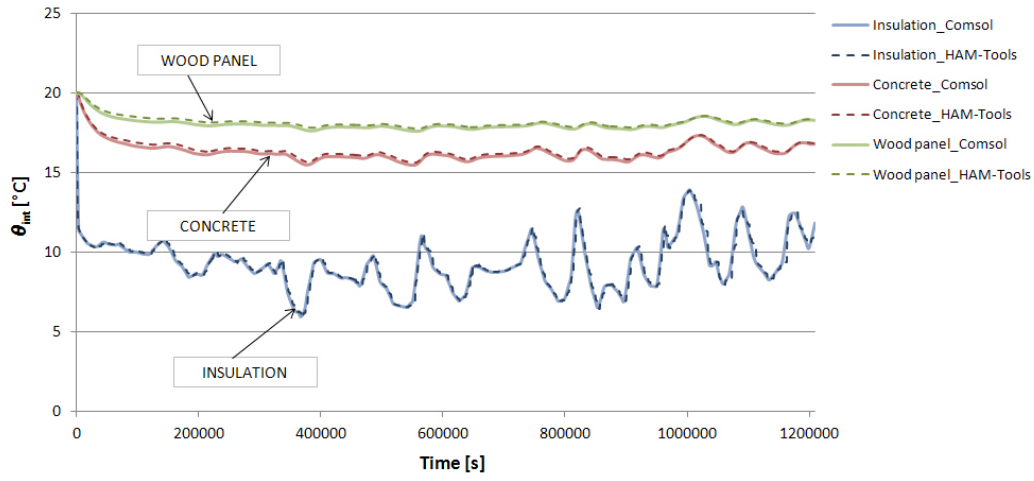
Figure 7.4: Temperature trend for nodes n. 3-9-17. First 2 weeks of January, Turin weather data.

Figure 7.5: Relative humidity trend for nodes n. 3-9-17. First 2 weeks of January, Turin weather data.

No solar radiation nor ventilation is taken into account for the air-tight structure.

The simulation results show the perfect matching between the two models for both the temperature and the RH trends (Fig. 7.4 and 7.5), validating the implemented equations from Nusser and Teibinger (2012).
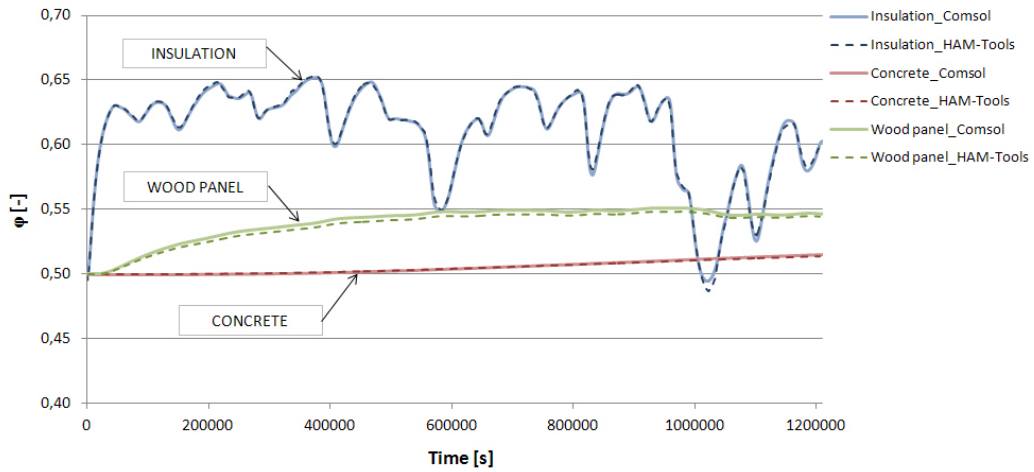
7.3 Influence of the ventilation configuration on the room hygroscopic performance

After ensuring that the HAM-transfer model for building components was implemented in the same way for both the simulation tools, the room level was considered and the two air models were compared.

As the solution time for CFD calculation is still a big issue, a 2-D model was set in a specific way to solve on the same platform both the air balance and the moisture transfer in porous media. Several attempts were performed on COMSOL to test the simulation time according to the calculation regime and the meshing size. Solving both the domains in a time dependent regime means a simulation time closer to real time, so it would take too long and no advantages derive from this approach. Since the influence of different flow patterns and velocity fields in the air volume on the moisture buffering was investigated, transient fluctuations of the velocity field on the component response to humidity variations can be neglected.

The air movement inside the simulated room is turbulent with mixed convection condition. In COMSOL, two turbulence models are available: the κ-ε model and the κ-ω model. Theoretically, the κ-ε model is based on the assumption that the Re number is moderate or high and the turbulence in boundary layers is in equilibrium. The κ-ω model provides a better prediction in the free flows close to the wall, but is less accurate in the free-stream flow simulation. In addition the κ-ω model is harder to reach convergence. Meanwhile, the accuracy of CFD simulation results is related not only to the turbulent model selection, but also it depends on the wall surface conditions. In this 2-D simulation of the momentum, heat and mass coupling in different regions, using κ-ε model is a fair trade-off of saved computational resources compared to the more complicated turbulence models.

The balance equations for the coupled heat and moisture transfer in air and within the building components were set to be solved in sequence in the COMSOL environment according to the following order:

- Air velocity field with CFD: steady state regime. For solution time

126
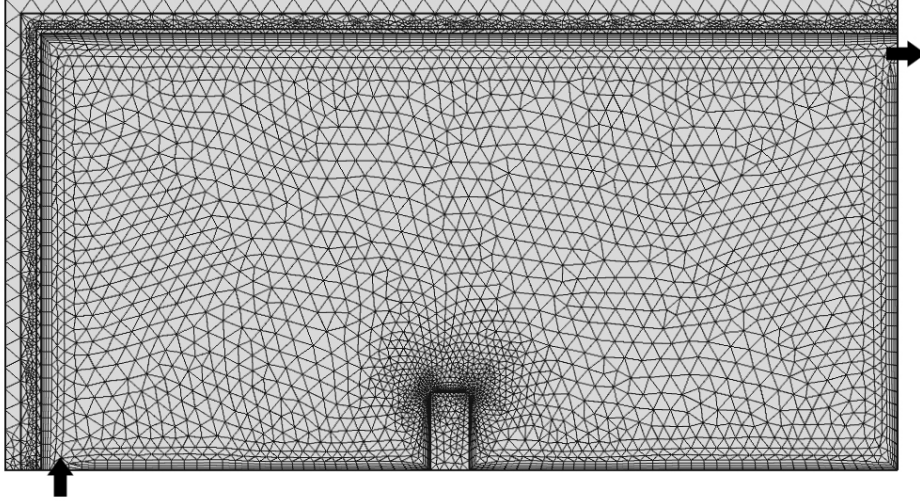
Figure 7.6: Mesh definition for the air velocity field calculation. The inlet and outlet position is indicated.

and computing memory capacity reason - the use a coarse mesh (less detailed) is possible - the κ-ε turbulence model has been adopted.

- HAM-transfer: transient regime. After the air velocity field has been calculated for each point of the considered volume, the coupled heat and moisture transfer is solved for the zone and for the building components considering the boundary conditions reported below. The moisture source has been placed in the middle of the room and the average RH level over the air volume is monitored.

The study has been applied to the simple room as for the room factor investigation in Chapter 6. The room volume in HAM-Tools was adapted to fit the 2-D model in COMSOL, which provides a 1 m deep third dimension for the building components for a total of 14,85 m^3.

For the air velocity field calculation a ventilation rate of 0,5 h^{-1} has been considered. Since the inlet and outlet vents comply with the described room dimensions a 0,1×1,0 m vent area was set, considering a 1 m long
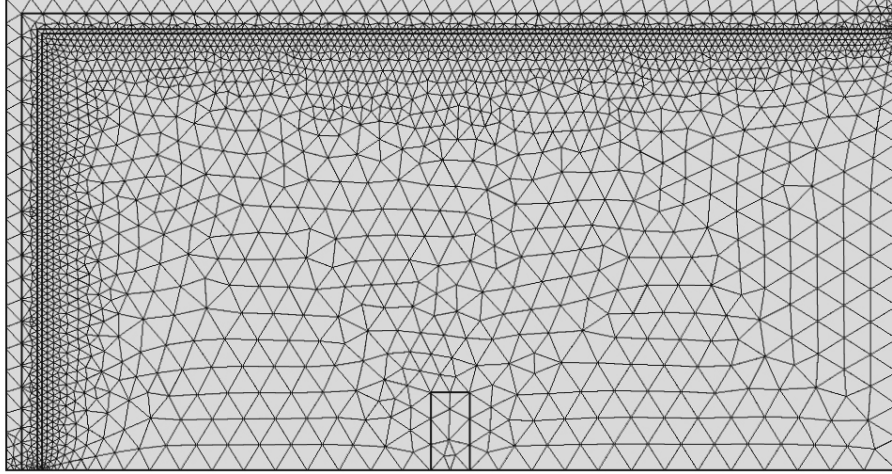
Figure 7.7: Mesh definition for the HAM-transfer calculation.

development along the wall. In this way the volumetric air flow to the zone in HAM-Tools was normalized on the vent section, allowing for input the air velocity parameter for the CFD calculation. Thus the corresponding air velocity at the inlet is 0,02 m/s.

The room is ventilated with outdoor air conditions (temperature and relative humidity) according to the same weather data file for Turin used in Chapter 6. The start RH level in the room and within the material was set at 30 % and the Gyproc Pronto Grezzo gypsum plaster is applied as interior finishing together with an aerated concrete + foam insulation envelope.

The study aims at demonstrating:

- the deviation between results obtained from HAM-Tools (lumped model) and COMSOL (CFD model) with regard to the indoor relative humidity trend when the environment for both the cases in which it is subjected to a cyclic moisture gain, constant for each scenario (200 g/h), or when there is no moisture load. According to recent studies from literature a higher relative humidity level is expected within the room, due

to the development of "dead zones" on the finishing material surface which do not fully interact in the moisture buffer process;

- the deviation on results between simulations carried out with different inlet and outlet vent position, in order to evaluate how the configuration can affect the RH trend and the moisture buffer.

7.3.1 Results

In Figure 7.8 the results for scenarios with and without moisture gain are shown (4 curves). The relative humidity trend is related to a 0,5 h^{-1} ventilation rate calculated with COMSOL and HAM-Tools.
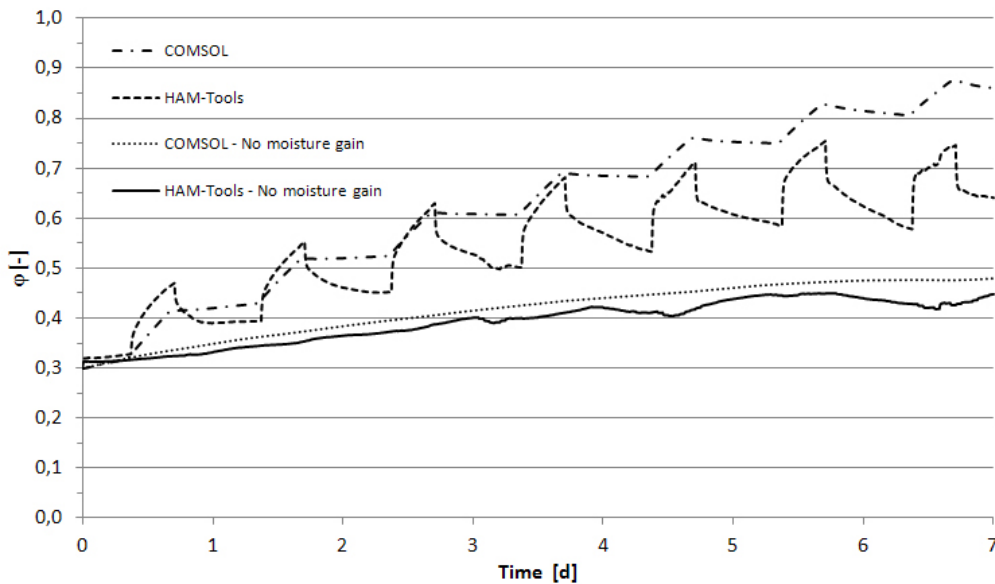
Figure 7.8: Relative humidity trend for a 0,5 h^{-1} ventilation rate. COMSOL and HAM-Tool results for scenarios with and without moisture gain.

While a certain fitting is reached between the curves with any vapour generation, the influence of the moisture gains on the RH trend denotes a clear separation between the simulation results obtained from COMSOL and HAM-Tools.

The cyclic load seems to have a lower impact for what concerns the RH peaks in the COMSOL environment, for which the curve looks flattened.

This behaviour is probably due to the RH averaging above the room volume, which involves the diversification between those zones directly affected by the moisture generation and those more distant not subjected to a sudden increase in the vapour concentration. This leads to a slower rise of the RH level during the loading period (8 hours) and to a likewise unloading phase that appears more like a "stabilisation" phase, where a real discharge of the RH level due to the ventilation mechanism does not occur.

The average value of relative humidity for the 4 cases is reported in Table 7.2. With respect to HAM-Tools results, the average relative humidity μ_φ [-] calculated in COMSOL denotes a $\Delta RH = +7\%$ for the case without moisture gain and a $\Delta RH = +10\%$ for the case with moisture gain.

Table 7.1: RH average value for the 4 simulated cases. 0,5 h^{-1} ventilation rate, 200 g/h moisture gain.

Moisture generation rate $\dot{G}_{gen}$ [g/h]	μ_φ [-] (HAM-Tools)	μ_φ [-] (COM-SOL)
0	0,39	0,42
200	0,57	0,63

In order to match the RH trends obtained from the two models, the following correction were applied to HAM-Tools:

- use of a correction factor $C_\beta = 0,4$ applied to the indoor surface moisture transfer coefficient β_{int}. This aims at reducing the buffer capacity of finishings by increasing their surface vapour resistance of 60 %;

- reduction of the building components area (-40 %). This aims at considering that not all the surfaces are involved in the moisture buffer.

Figure 7.9 shows the two approaches. In both the cases the calibration leads to an increase of the fluctuation amplitude of relative humidity - with an average RH value $\mu_{RH} = 58\%$ in either case - and not to a trend similar to the one obtained with COMSOL.
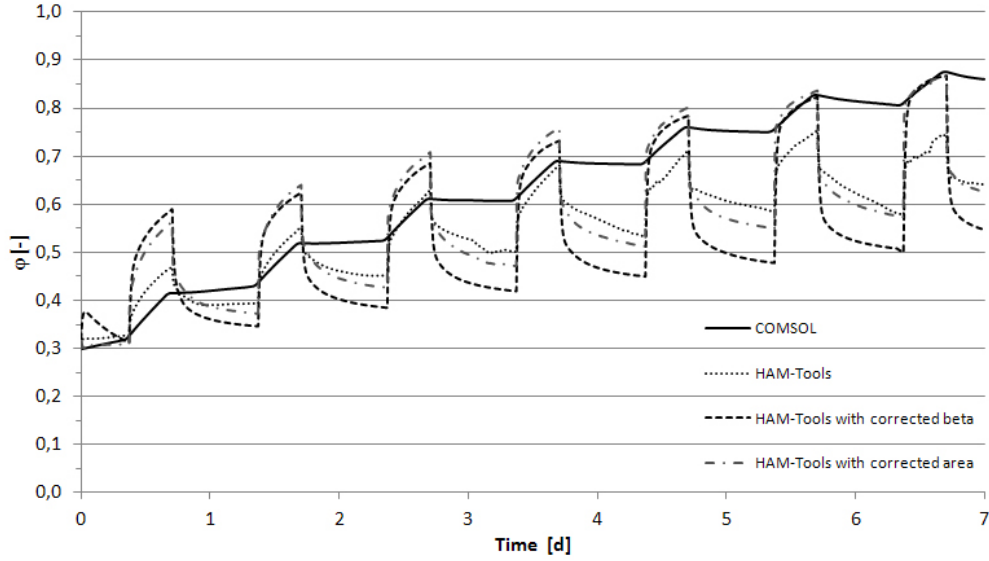
Figure 7.9: HAM-Tool calibration on the results previously obtained for the scenario with moisture gain. The graph show both the two cases: 1) application of a correction factor $C_\beta = 0,4$ to the indoor surface moisture transfer coefficient β_{int}; 2) and reduction of the building components area (-40 %).

The next step was the evaluation of the influence of the vents configuration on the RH trend inside the room. Five different vents position for the inlet and outlet have been considered, in order to make a sensitivity analysis by means of numerical simulation. A deviation between results is expected, due to the affection of the air velocity field on the indoor surface vapour resistance of building components which leads to different amounts of buffered moisture. The scenario that has been adopted for the sensitivity analysis is the 0,5 h^{-1} ventilation rate one, always considering a 200 g/h moisture gain for the whole week (Turin weather data).

In Fig. 7.10 a scheme of the 5 different vents configurations is shown, while in the next pages the air velocity field calculated in steady-state conditions and a snapshot of the respective relative humidity distribution over the air volume (transient conditions, 1 week simulation) according to vent configuration n.1-2-4 is reported (Figures 7.11 - 7.12 - 7.13).

131
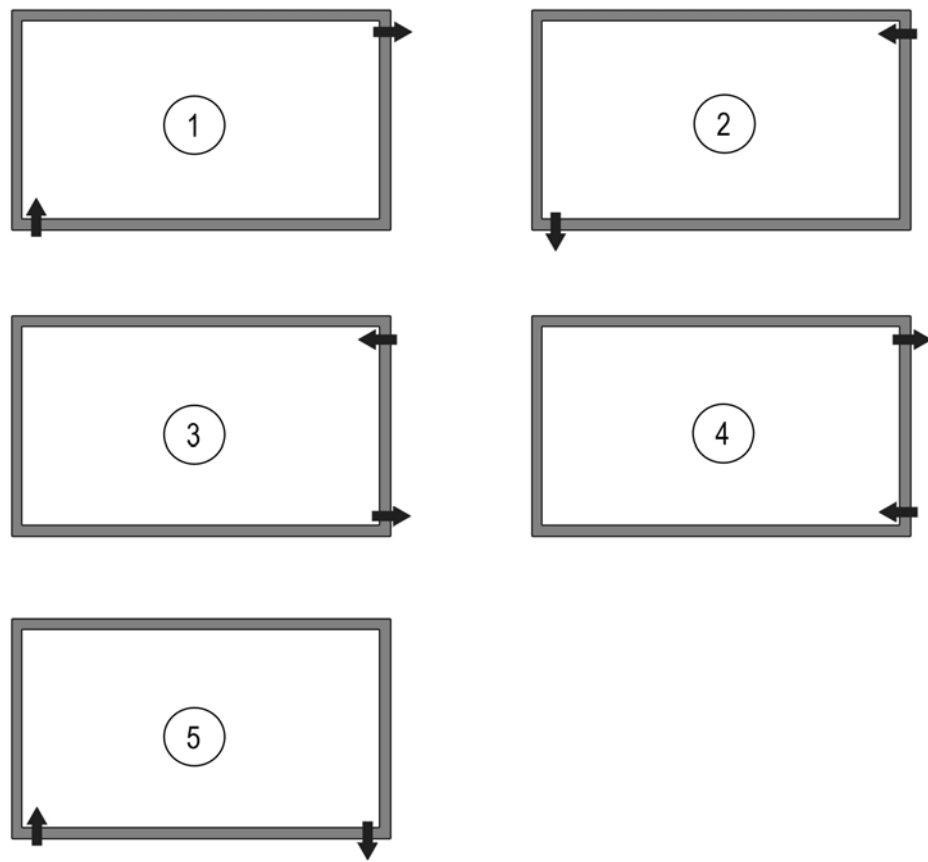
Figure 7.10: The 5 vents configurations considered for the air velocity field calculation in COMSOL.
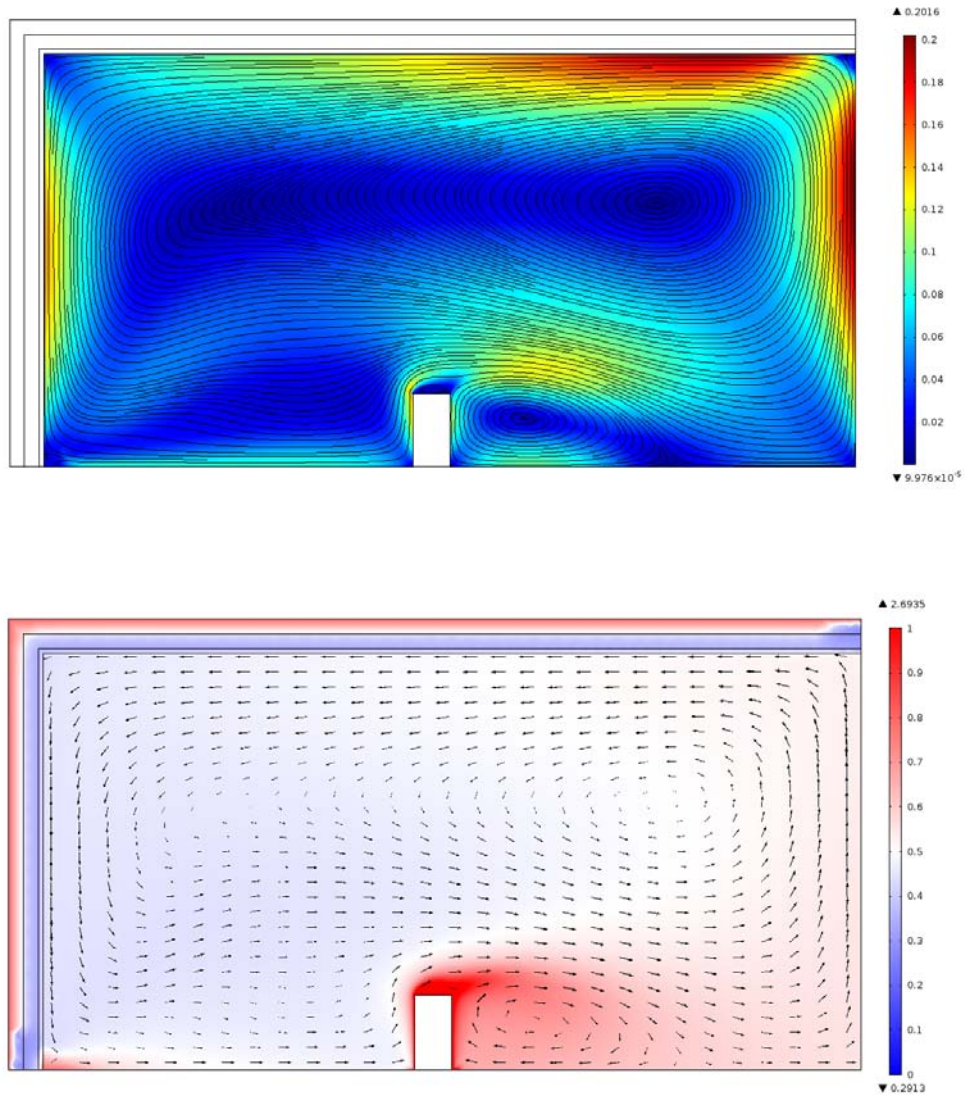
Figure 7.11: The air velocity field calculated in steady-state conditions and a snapshot of the relative humidity distribution in the air volume (transient conditions, 1 week simulation). Vents configuration n.1.
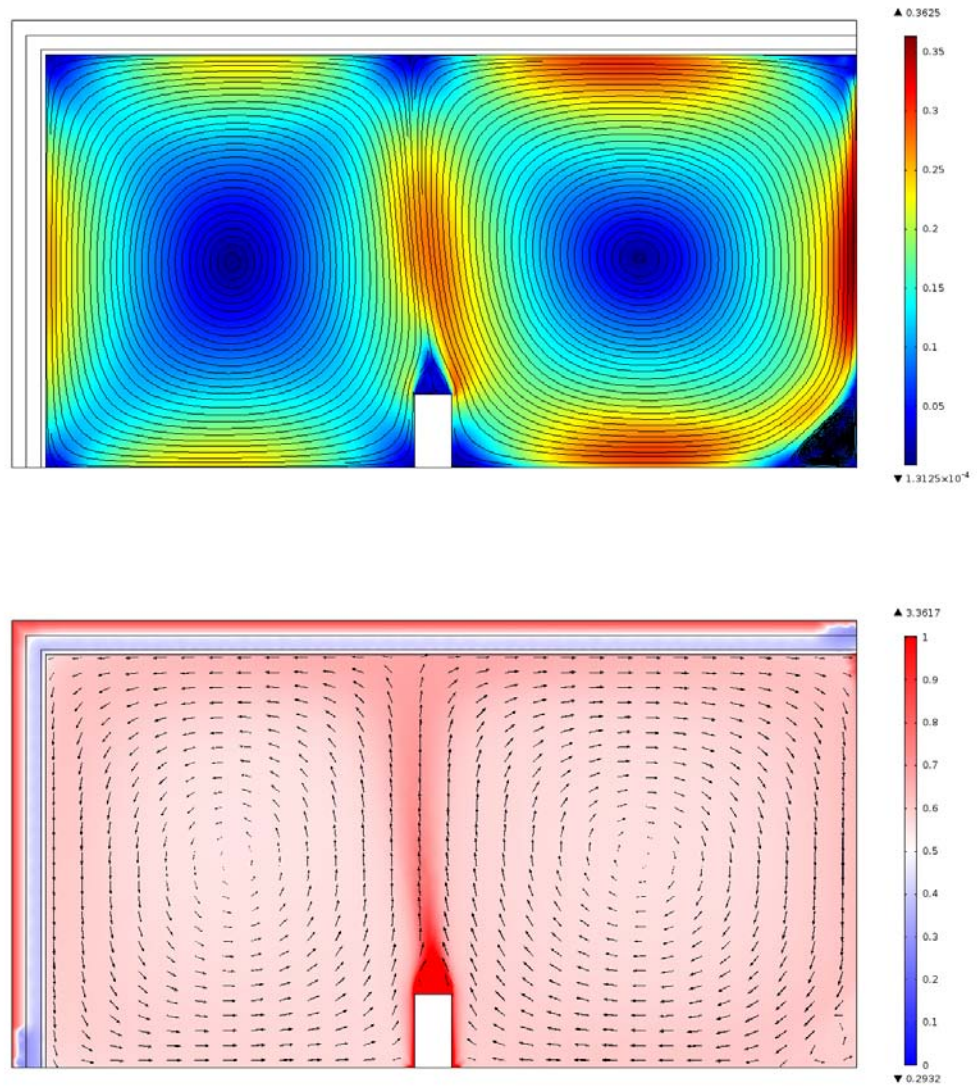
Figure 7.12: The air velocity field calculated in steady-state conditions and a snapshot of the relative humidity distribution in the air volume (transient conditions, 1 week simulation). Vents configuration n.2.
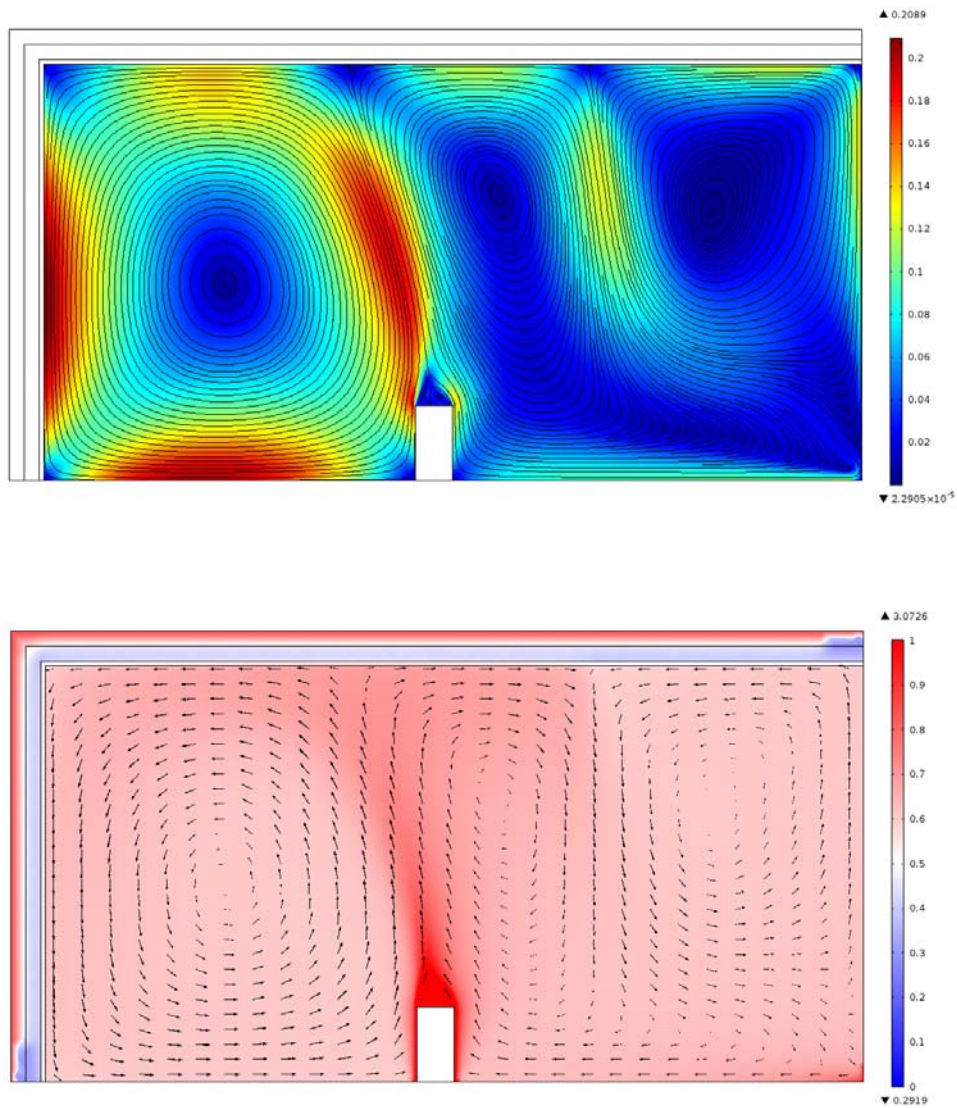
Figure 7.13: The air velocity field calculated in steady-state conditions and a snapshot of the relative humidity distribution in the air volume (transient conditions, 1 week simulation). Vents configuration n.4.

According to the different configurations, and therefore to the different air flow patterns, the zones with a reduced air velocity (i.e. $v < 0,02$ m/s) are clearly visible and not localized only in the corners of the room, but also in central areas of the walls. This leads to localized surface moisture transfer coefficient which are characterized by several vapour resistances; in this way the interior finishings do not interact in the same way with the moisture flux they come in contact with, defining a more detailed response to humidity variations by the building components.

The results highlight a deviation between the RH trends for the different vents configuration as expected. Figure 7.14 show the humidity trend for each case, while in Table the average value of RH is reported to compare which configuration is most inconvenient for the moisture dampening inside the environment.
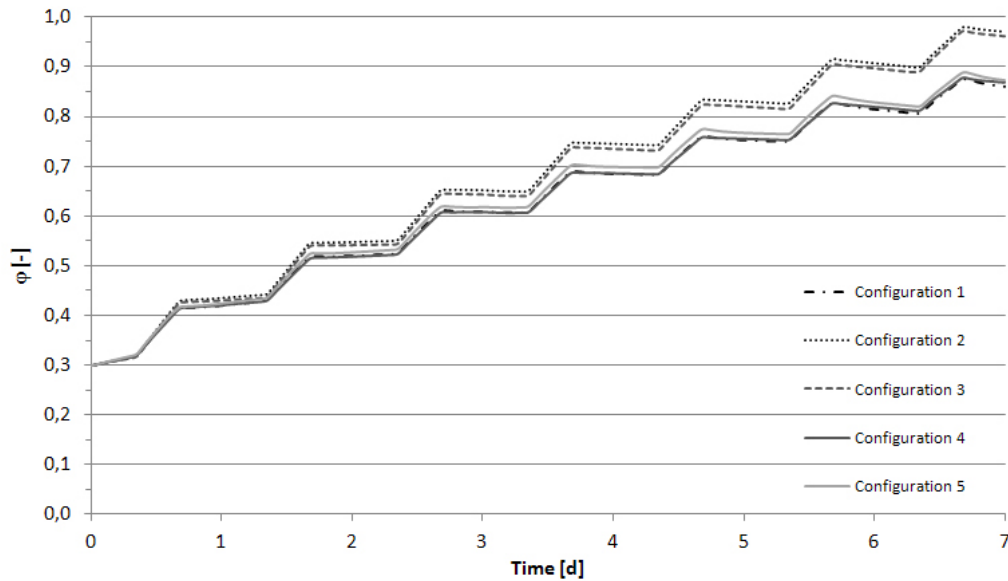
Figure 7.14: Relative humidity trend for a 0,5 h^{-1} ventilation rate. COMSOL results for scenarios with different vents configurations.

From the sensitivity analysis it is clear that configurations n.2 and n.3 are the most disadvantageous and lead to a higher RH level inside the room. This is probably due to the inlet vent position. Since the density of water vapour is lower than that of dry air, the generated moisture tends to go up,

Table 7.2: RH average value for the 5 simulated vent configurations cases. 0,5 h^{-1} ventilation rate, 200 g/h moisture gain.

$\mu_{\varphi,1}$ [-]	$\mu_{\varphi,2}$ [-]	$\mu_{\varphi,3}$ [-]	$\mu_{\varphi,4}$ [-]	$\mu_{\varphi,5}$ [-]
0,63	0,68	0,67	0,63	0,64

stratifying in the air volume in contact with the ceiling; the presence of the exhaust air vent in the upper part helps the moisture removal. A maximum $\Delta RH = 5\%$ is achieved between the lowest and the highest average RH value.

Anyway, configuration n.5 doesn't account for any vent in the upper part of the wall but still show an average RH level close to the fist solutions. The air velocity field is also responsible for the removed amount of moist air through the mechanical ventilation system, but how much this depends on one variable or another is still to be investigated.

7.4 Discussion

COMSOL Multi-physics provides simulation environment that by means of a coupling between HAM equations and of the heat and moisture transfer between indoor air and enclosure can be directly achieved without third party programming. In this thesis the fully coupled model was established in this single simulation environment. This model has several advantages: 1) it overcomes the main limitations of the currently available CFD coupling models in simulating the whole building HAM transport, and 2) it has great application potential such as for the aspects investigated in this thesis including influences of room factors on indoor environment, ventilation design, HAM-transport through wall system and prediction of the room hygric inertia.

The influence of the position of ventilation vents on the indoor RH trend, especially under low ventilation rates has been evaluated.

The comparison between the lumped model (HAM-Tools) and the CFD model (COMSOL), when the HAM-transfer is applied, generated uncertain-

ties. The first part of the investigation resulted in a good matching with regard to the diffusion equation implementation in COMSOL, validated by means of numerical simulation with HAM-Tools. The component behaviour with regard to the moisture transfer has been evaluated and both the simulation tools produce the same results.

The second phase, where the air zone has been solved with the CFD in COMSOL instead of using lumped conditions, was found critical with respect to the matching between the two software. The original intention to "rectify" the lumped model with another closer to reality generated difficulties in finding a correction coefficient able to match the results. The implementation of the Hygric Inertia Index through a deeper investigation of the air flow patterns (in Rode et al. (2002) only one ventilation scenario was considered) remains an open field. The CFD-HAM model on COMSOL should be validated by experimental data and needs to be improved and implemented. For this reason we can't assume it as the reference model and calibrate the lumped model with non-validated results.

Chapter 8

Conclusions

Indoor humidity level is important for building performance and occupants. The durability of building components is directly related to the humidity condition and materials inside buildings can get damaged if they are persistently under high levels of moisture concentration. The indoor humidity level is related to the room factors including moisture gains and ventilation conditions and to the moisture ab/desorption capacity of hygroscopic materials for interior finishing or furnishing of the building.

The phenomenon of the indoor humidity level being dampened by the dynamic moisture interactive process between hygroscopic materials and indoor air is recognized as moisture buffering effect. The buffering effect and the moisture ab/desorption performance of hygroscopic materials under different room factors were studied in this thesis by means of numerical simulation. The transient state indoor environment influenced by room factors, taking into account the moisture interactive process between indoor air and enclosure, was investigated numerically in this thesis. The CFD technique was employed in the numerical investigation.

A literature review on the experimental and numerical investigations on moisture buffering and whole building indoor environment was carried out. This review showed that the moisture buffering effect of hygroscopic materials had been extensively studied at the material level, i.e. the characterization of the buffering property of materials. However, the hygroscopic properties

of materials may not be representative of the buffering performance of the material at the room level because the indoor hygrothermal condition, room factors, and moisture buffering of hygroscopic materials influence each other.

The literature review also found that a CFD model in a single simulation environment to study the HAM transport including the moisture interaction between the indoor air and the envelope is needed, but yet to be developed. Using this kind of CFD model, detailed information of the moisture transport in a building and inside its envelope could be obtained, and the indoor humidity level influenced by the room factors could be predicted by the simulation of the involved HAM transport processes.

In this thesis the following issues have been presented:

- the fundamental theories of the hygroscopic material properties, the governing equations describing HAM transport in the convection and diffusion processes and the analogy between mass and heat transfer

- the experimental measurement of hygroscopic properties of porous building material under transient conditions;

- the study of the moisture buffering effect at the room level through the numerical simulation of the HAM transport in the whole room and its enclosure;

- the coupling between CFD-HAM models in a single simulation environment to study the HAM transport, including the moisture interaction between the indoor air and the envelope.

To further study the buffering effect under different room factors, the buffering effect was evaluated by the indoor humidity level change with respect to a room factor variation. The study found that without the presence of the hygroscopic material (non-hygroscopic test) the average indoor relative humidity value increased by 11 % at the ventilation rate of 0.3 h^{-1} when the room factor of moisture generation rate is set at 80 g/h, with respect to the scenario with hygroscopic finishing (gypsum plaster).

140

These cases studied the influence of moisture loads, ventilation rates, and ventilation vents design on the indoor environmental changes and on the HAM-transport through the building component.

The fully coupled CFD model to simulate HAM transports in the simulation domains of test room and wall was established. This model was built in COMSOL Multi-physics, a PDE basis simulation environment. The governing equations of the HAM-transport were coupled according to recent studies (Nusser and Teibinger, 2012). The coupling process of heat/moisture between the indoor air and gypsum plaster finishing were established by defining the CFD solution for indoor air.

8.1 Contributions

The moisture buffering performance of gypsum plaster and wood fibre under dynamic conditions has been evaluated experimentally and compared to the steady-state measurements usually carried out according to the standards UNI EN ISO 12571 (2013) and UNI EN ISO 12572 (2006). The influence of uncertainty of measured data on the whole room numerical simulation was studied.

The nature of buffering effect caused by hygroscopic material under different room conditions has been explained and its values at room level have been obtained. The relationship of indoor environment, buffering effect, room factors has been elaborated through simulated data.

A CFD coupling model has been developed in a single simulation environment to overcome the limitations in existing coupling models. This new model can have application potential such as prediction of indoor environment hygroscopic conditions and evaluation of ventilation design.

141

8.2   Recommended future work

The indoor environment influenced by moisture buffering effect and room factors has been numerically investigated in this thesis study. The buffering effect caused by hygroscopic materials - gypsum plaster - and the room factors including moisture generation and ventilation rates were studied. The relationship of indoor environment, buffering effect, and room factors has been elaborated through simulated data analysis, but need to be validated through experimental results.

Some additional parameters such as higher ventilation rates and other hygroscopic materials can be further investigated using an experimental method. Further studies regarding the influence of room factors and moisture buffering on the indoor environment considering the solar effect and ventilation strategy is recommended. Their combined influences on indoor environment and how moisture buffering effect works in these conditions have not been studied, but are expected to be significant for indoor environment control.

The fully coupled CFD-HAM model can be further developed and implemented to study transient processes; an experimental validation is needed. The simulation of the turbulent effects of mass transfer at the interface of hygroscopic finishing and indoor air is recommended for further development in the numerical model. This development will be helpful in investigating the moisture surface coefficient at the interior wall surfaces.

An implementation of the vapour diffusion through building components and their moisture buffer effect on indoor hygroscopic conditions should be carried out and considered within the national technical specification UNI/TS 11300-1:2008 (*Determinazione del fabbisogno di energia termica dell?edificio per la climatizzazione estiva ed invernale*) which, at the moment, only considers the influence of ventilation rate and indoor moisture gains for the de/humidification energy demand.

8.3 Related publications by author et al.

- Ronzino A., Corrado V. (2012). *Valutazione della capacità di accumulo igrico dei materiali superficiali interni attraverso la modellazione HAM.* In: - Energia: Nuove Opportunità di Innovazione per la Sostenibilità, ISBN: 9788890767609, Trieste, 11-14 Settembre, 2012

- Ronzino A., Corrado V., Neusser M., Wegerer P., Bednar T., (2013). *Impatto del moisture buffering sul clima interno di uffici ventilati meccanicamente.* 68° Congresso ATI - Energia, Ambiente, Macchine e Impianti, Bologna 11-14 Settembre, 2013

- Ronzino A., Neusser M., Wegerer P., Bednar T., Corrado V. (2013). *Impact of moisture buffering on indoor climate for mechanically ventilated offices.* In: Net Zero Energy Use in Buildings, p. 358-366, Ankara: Turkish Society of HVAC and Sanitary Engineers (TTMD), ISBN: 9789756907177, Istanbul, 3-4 October, 2013

Bibliography

M. Abadie and K.C. Mendonça. Moisture performance of building materials: From material characterization to building simulation using the moisture buffer value concept. *Building and Environment*, 44(2):388–401, 2009.

M.O. Abadie and N. Mendes. Comparative analysis of response-factor and finite-volumes based methods for predicting heat and moisture transfer through porous building materials. *Journal of Building Physics*, 30(1): 7–37, 2006.

O. Adan, H. Brocken, J. Carmeliet, H. Hens, S. Roels, and C.E. Hagentoft. Determination of liquid water transfer properties of porous building materials and development of numerical assessment methods: introduction to the ec hamstad project. *Journal of Thermal Envelope and Building Science*, 27(4):253–260, 2004.

A. Alturkistani, P. Fazio, J. Rao, and Q. Mao. A new test method to determine the relative drying capacity of building envelope panels of various configurations. *Building and Environment*, 43(12):22013–2215, 2008.

P. Amissah. *Indoor air quality - Combining air humidity with construction moisture*. PhD thesis, Univesrity of Strathclyde, Glasgow, U.K., 2005.

S. Atthajariyakul and T. Leephakpreeda. Real-time determination of optimal indoor-air condition for thermal comfort, air quality and efficient energy usage. *Energy and Buildings*, 36(7):720–733, 2004.

R. Barbosa and N. Mendes. Combined simulation of central hvac systems

with a whole-building hygrothermal model. *Energy and Buildings*, 40(3): 276–288, 2008.

C.G. Bornehag, J. Sundell, C.J. Weschler, T. Sigsgaard, B. Lundgren, M. Hasselgren, and L. Hägerhed-Engman. The association between asthma and allergic symptoms in children and phthalates in house dust: A nested case-control study. *Environmental Health Perspectives*, 112(14):1393–1397, 2004.

J. Carmeliet and S. Roels. Determination of the isothermal moisture transport properties of porous building materials. *Journal of Thermal Envelope and Building Science*, 24(3):183–210, 2001.

S. Cerolini, M. D'Orazio, C. Di Perna, and A. Stazi. Moisture buffering capacity of highly absorbing materials. *Energy and Buildings*, 41(2):164–168, 2009.

Z.Q. Chen and M.H. Shi. Study of heat and moisture migration properties in porous building materials. *Applied Thermal Engineering*, 25(1):61–71, 2005.

COMSOL Multiphysics User's Guide. *COMSOL Multiphysics User's Guide*, 2012.

M.J. Cunningham. Effective penetration depth and effective resistance in moisture transfer. *Building and Environment*, 27(3):329–337, 1992.

J.M.P.Q. Delgado, N. Ramos, E. Barreira, , and V.P. Freitas. A critical review of hygrothermal models used in porous building materials. *Journal of Porous Media*, 13:221–234, 2010.

J.A. Enderby. The domain model of hysteresis, part 1: independent domains. *Transaction of the Faraday Society*, 51:835–844, 1955.

A. Erriguible, P. Bernada, F. Couture, and M. Roques. Simulation of convective drying of a porous medium with boundary condtions provided by cfd. *Chemical Engineering Research and Design*, 84(A2):113–123, 2006.

146

D.H Everett. *Adsorption hysteresis*, volume 2, chapter 36, pages 1055–1113. Marcel Dekker, New York, 1967.

L. Fang, G. Clausen, and P.O. Fanger. Impact of temperature and humidity on the perception of indoor air quality. *Indoor Air*, 8:80–90, 1998.

P. Fazio, J. Rao, A. Alturkistani, and H. Ge. Large scale experiment investigation of the relative drying capacity of building envelope panels of various configurations. In *Proceedings of the 3rd International Building Physics Conference*, pages 361–168, 2006.

P. Fazio, A. Alturkistani, J. Rao, and Q. Mao. A new testing method to evaluate the relative drying performance of different building envelope systems using water trays. *Journal of ASTM International*, 6(9), 2009.

E. Goossens. *Moisture transfer properties of coated gypsum*. PhD thesis, Eindhoven University of Technology, 2002.

C. Hagentoft, A.S. Kalagasidis, B. Adl Zarrabi, S. Roels, J. Carmeliet, H. Hens, J. Grunewald, M. Funk, R. Becker, D. Shamir, O. Adan, H. Brocken, M. Kumaran, and R. Djebbar. Assessment method of numerical prediction models for combined heat, air and moisture transfer in building components: benchmarks for one-dimensional cases. *Journal of Thermal Envelope and Building Science*, 27(4):327–352, 2004.

A. Holm and K. Lengsfeld. Moisture buffering effect: Experimental investigations and validation. In *Proceedings of the 10th Conference on Thermal Performance of the Exterior Envelopes of Whole Buildings*, Clearwater Beach, Florida, 2007.

H. Janssen, B. Blocken, and J. Carmeliet. Conservative modeling of the moisture and heat transfer in building components under atmospheric excitation. *International Journal of Heat and Mass Transfer*, 50(5-6):1128–1140, 2007.

T. Kalamees, J. Vinha, and J. Kurnitski. Indoor humidity loads and moisture production in lightweight timber-frame detached houses. *Journal of Building Physics*, 29(3):219–246, 2006.

A. Karagiozis and M. Salonvaara. Hygrothermal system-performance of a whole building. *Building and Environment*, 36(6):779–787, 2001.

A. Korjenic and T. Bednar. Developing a model for fibrous building materials. *Energy and Buildings*, 43:3189–3199, 2011.

M.K. Kumaran, P. Mukhopadhyaya, S.M. Cornick, M.A. Lacasse, M. Rousseau, W. Maref, M. Nofal, J.D. Quirt, and W.A. Dalgliesh. An integrated methodology to develop moisture management strategies for exterior wall systems. In *Proceedings of the 9th Canadian Conference on Building Science and Technology*, pages 45–62, Vancouver, B.C., 2003.

Q. Li, J. Rao, and P. Fazio. Development of ham tool for building envelope analysis. *Building and Environment*, 44(5):1065–1073, 2009.

Y. Li. *An experimental and numerical study of the influence of room factors and hygroscopic materials of wood paneling on the indoor environment.* PhD thesis, Concordia University, Montreal, Canada, 2011.

H. Liu, J. Zhang, X. Tang, and Y. Lu. Fuzzy control of mixed-flow grain dryer. *Drying Technology*, 21:807–819, 2003.

J. Lstiburek. Moisture, building enclosures and mold. *HPAC Heating, Piping, Air Conditioning Engeneering*, 74(1):77–81, 2002.

Y. Mualem. Modified approach to capillary hysteresis based on a similarity hypothesis. *Water Resources Research*, 9:1324–1331, 1973a.

Y. Mualem. A conceptual model of hysteresis. *Water Resources Research*, 10:514–520, 1973b.

A. Neale. A study in computational fluid dynamics for the determination of convective heat and vapour transfer coefficients. Master's thesis, Concordia University, Montreal, 2007.

B Nusser and M. Teibinger. Coupled heat and moisture transfer in building components - implementing wufi approaches in comsol multiphysics. In *Proceedings of the COMSOL Conference, Milan*, 2012.

T. Ojanen and M. Salonvaara. Comparison of measured and simulated moisture buffering results. Technical report, 2004.

O.F. Osanyintola and C.J. Simonson. Moisture buffering capacity of hygroscopic building materials: Experimental facilities and energy impact. *Energy and Buildings*, 38(10):1270–1282, 2006.

T. Padfield. Humidity buffering of the indoor climate by absorbent walls. In *Proceedings of the 5th Symposium on Building Physics in the Nordic Countries, Chalmers University of Technology, Göteborg*, volume 2, pages 637–644, 1999.

C.R. Pedersen. *Combined Heat and Moisture Transfer in Building Constructions*. PhD thesis, Technical University of Denmark, 1990.

J. R. Philip and D. A. De Vries. Moisture movement in porous materials under temperature gradient. *Transaction American Geophysical Union*, 39, 1957.

M. Qin, R. Belarbi, A. Aït-Mokhtar, and A. Seigneurin. An analytical method to calculate the coupled heat and moisture transfer in building materials. *International Communication in Heat and Mass Transfer*, 33 (1):39–48, 2006.

N.M.M. Ramos, V.P. de Freitas, and J.P.Q. Delgado. Hygroscopic inertia of a room. evaluation of finishing materials contribution. Technical report, IEA Annex 41, 2005.

N.M.M. Ramos, Kalagasidis A.S., de Freitas V.P., and Delgado J.M.P.Q. Numerical simulation of transient moisture transport for hygroscopic inertia assessment. *Journal of Porous Media*, 15(8):793–804, 2012.

C. Rode and K. Grau. Moisture buffering and its consequences in whole building hygrothermal modeling. *Journal of Building Physics*, 31(3):333–360, 2008.

C. Rode, T. Mitamura, J. Schultz, and T. Padfield. Test cell measurements of moisture buffer effects. In *Proceedings of the 6th Symposium on Building Physics in the Nordic Countries, Trondheim, Norway*, ISBN: 82-91412-02-2, pages 619–626, 2002.

C. Rode, K.K. Hansen, T. Padfield, B. Time, T. Ojanen, and Arfvidsson J. Nordtest workshop on moisture buffer capacity summary report. Technical Report ISSN 1601-2917, ISBN 87-7877-129-3, Technical University of Denmark, 2003.

C. Rode, Holm A., and T. Padfield. A review of humidity buffering in the interior spaces. *Journal of Thermal Envelope and Building Science*, 27(3): 221–226, 2004.

C. Rode, R. Peuhkuri, L.H. Mortensen, K. Hansens, B. Time, A. Gustavsen, T. Ojanen, J. Ahonen, K. Svennberg, L.E. Harderup, and J. Arfvidsson. Moisture buffering of building materials. Technical Report ISSN 1601-2917, ISBN 87-7877-195-1, Technical University of Denmark, 2005.

S. Roels. Experimental analysis of moisture buffering. Technical report, IEA Annex 41, 2008.

S. Roels and H. Janssen. A comparison of the nordtest and japanese test methods for the moisture buffering performance of building materials. *Journal of Building Physics*, 30(2):137–161, 2006.

S. Roels, J. Carmeliet, H. Hens, O. Adan, H. Brocken, R. Cerny, Z. Pavlik, C. Hall, M. Kumaran, L. Pel, and R. Plagge. Interlaboratory comparison of hygric properties of porous building materials. *Journal of Thermal Envelope and Building Science*, 27:307–325, 2004.

S. Roels, P. Talukdar, C. James, and C. Simonson. Reliability of material data measurements for hygroscopic buffering. *International Journal of Heat and Mass Transfer*, 53:5355–5363, 2010.

M. Salonvaara, A. Holm, H. Kunzel, and A. Karagiozis. Moisture buffering effects on indoor air quality experimental and simulation results. In *Proceedings of the 9th Conference on Thermal Performance of the Exterior Envelopes of Whole Buildings*, 2004.

A. Sasic Kalagasidis. *User's guide to the International Building Physics Toolbox*, 2002.

A. Sasic Kalagasidis. International building physics toobox - block documentation. Technical report, Chalmers Institute of Technology, 2003.

A. Sasic Kalagasidis. *HAM-Tools - An integra Simulation Tool for Heat, Air and Moisture Trasnfer Analyses in Building Physics*. PhD thesis, Chalmers University of Technology, 2004.

H. Satio. Simple parameters for moisture buffering effect to predict indoor humidity variation. Technical report, IEA Annex 41, 2005.

C.J. Simonson, M. Salonvaara, and T. Ojanen. Heat and mass transfer between indoor air and a permeable and hygroscopic building envelope: Part i - field measurements. *Journal of Thermal Envelope and Building Science*, 28(1):63–101, 2004.

C.J. Simonson, M. Salonvaara, and T. Ojanen. Moisture performance o fan air tight, vapor-permeable building envelope in a cold climate. *Journal of Thermal Envelope and Building Science*, 28(3):205–226, 2005.

H.J. Steeman, A. Janssens, J. Carmeliet, and M. De Paepe. Modeling indoor air and hygrothermal wall interaction in building simulation: Comparison between cfd and well-mixed zonal model. *Building and Environment*, 44 (3):572–583, 2009.

J. Straube and E. Burnett. Overview of hygrothermal (ham) analysis methods. In *ASTM Manual 40 - Moisture Analysis and Condensation Control in Building Envelopes*, chapter 5. American Society of Testing and Materials, 2001.

K. Svennberg, L. Hedegaard, and C. Rode. Moisture buffering performance of a fully furnished room. In *Proceedings of the 9th Conference on Thermal Performance of the Exterior Envelopes of Whole Buildings*, 2004.

K. Svennberg, K. Lengsfeld, L.E. Harderup, and A. Holm. Previous experimental studies and field measurements on moisture buffering by indoor surface materials. *Journal of Building Physics*, 30(3):261–274, 2007.

C. Teodosiu, G. Rusaouen, and R. Hohota. Influence of boundary conditions uncertainties on the simulation of ventilated enclosures. *Numerical Heat Transfer*, 44:483–504, 2003.

J. Toftum, A.S. Jorgensen, and P.O. Fanger. Upper limits of air humidity for preventing warm respiratory discomfort. *Energy and Buildings*, 28:15–23, 1998.

UNI EN ISO 12570. Uni en iso 12570:2013: Prestazione igrotermica dei materiali e dei prodotti per edilizia - determinazione del contenuto di umidità mediante essiccamento ad alta temperatura, 2013.

UNI EN ISO 12571. Uni en iso 12571:2013: Prestazione igrotermica dei materiali e dei prodotti per edilizia - determinazione delle proprietà di assorbimento igroscopico, 2013.

UNI EN ISO 12572. Uni en iso 12572:2006: Prestazione igrotermica dei materiali e dei prodotti per edilizia - determinazione delle proprietà di trasmissione del vapore d'acqua, 2006.

UNI EN ISO 13791. Uni en iso 13791:2012: Prestazione termica degli edifici - calcolo della temperatura interna estiva di un locale in assenza di impianti di climatizzazione.

M. Woloszyn and C. Rode. Iea annex 41 whole building heat air and moisture response. modeling principles and common exercises. Technical report, K.U. Leuven, Belgium, 2008a.

M. Woloszyn and C. Rode. Tools for performance simulation of heat, air and moisture conditions of whole buildings. *Building Simulation*, 1:5–24, 2008b.

Y Wu, P. Fazio, and M. Kumaran. Moisture buffering capacities of five north american building materials. *Journal of Testing and Evaluation*, 36 (1):34–40, 2008.

S. Yang, X. ans Vera, J. Rao, H. Ge, and P. Fazio. Full-scale experimental investigation of moisture buffering effect and indoor moisture distribution. In *Proceedings of the 10th Conference on Thermal Performance of the Exterior Envelopes of Whole Buildings*, 2007.

X. Yang. *Investigation on moisture buffering of hygroscopic materials by full-scale experiments and HAM simulations.* PhD thesis, Concordia University, 2010.

X. Yang, P. Fazio, J. Rao, and H. Ge. Experimental evaluation of transient moisture buffering of interior surface materials in a full-scale one-room setup. In *Proceedings of the 3rd International Building Physics Conference*, 2009.

X. Yang, P. Fazio, H. Ge, and J. Rao. Evaluation of moisture buffering capacity of interior surface materials and furniture in a full-scale experimental investigation. *Building and Environment*, 47:188–196, 2012.

Z.L. Zhang. Combined heat, air, moisture and pollutants transport in building environmental systems. *JSME International Journal, Series B: Fluids and Thermal Engineering*, 48:182–190, 2005.